

MinD-DEPENDENT CONFORMATIONAL CHANGES IN MINE REGULATE
THE MIN OSCILLATION

BY

Kyung-Tae Park

Submitted to the graduate degree program in Microbiology,
Molecular Genetics and Immunology and the
Graduate Faculty of the University of
Kansas in partial fulfillment of the
requirements for the Degree of
Doctor of Philosophy.

Dissertation Committee:

Joe Lutkenhaus, Ph.D., Chairperson

Joseph Fontes, Ph.D.

Philip Hardwidge, Ph.D.

Kee Jun Kim, Ph.D.

Jianming Qiu, Ph.D.

Date Defended: December 6, 2011

The Dissertation Committee for Kyung-Tae Park certifies that this is the approved version of the following dissertation:

MinD-DEPENDENT CONFORMATIONAL CHANGES IN MINE REGULATE
THE MIN OSCILLATION

Joe Lutkenhaus, Ph.D., Chairperson

January 25, 2012

ABSTRACT

The *min* system comprised of MinC, MinD, and MinE in *Escherichia coli* ensures that cell division occurs at the midcell position by preventing the assembly of FtsZ into a Z-ring at the poles. MinD is a member of the deviant walker A motif family that dimerizes on the membrane in an ATP-dependent fashion. MinC forms an inhibitory complex with MinD on the membrane to antagonize Z-ring formation. MinE functions as a spatial regulator that displaces MinC from MinD and activates MinD ATPase. The dynamic interplay of the Min proteins culminates in a pole to pole oscillation by which a time-averaged MinCD concentration is the lowest at mid cell, thus allowing Z ring assembly there.

MinD is at the heart of the Min system since MinD-ATP on the membrane recruits both MinC and MinE. In this study, MinD^{D40A}Δ10, an ATP hydrolysis-deficient MinD truncated for the C-terminal amphipathic helix involved in membrane binding, was crystallized in the presence of ATP. The structure resolved at 2.4Å resolution showed that MinD-ATP is a dimer. Furthermore, our mutagenesis studies demonstrate that the MinC and MinE binding sites form upon MinD dimerization and that MinE has a higher affinity for MinD than MinC.

Prior to this study, *E. coli* MinE was thought to consist of two functionally autonomous domains. The N-terminal domain called anti-MinCD (MinE^{CD}) that suppresses MinCD activity is a nascent α helix. The C-terminal domain, known as the topological specificity domain (MinE^{TSD}) required for cell division at midcell, exists as a 4 β -stranded structure. However, recently determined structures of *H. pylori* and *Neisseria gonorrhoeae* MinE revealed that MinE exists as

a 6 β stranded form and part of MinE^{CD} is sequestered at the dimeric interface as a β strand, thus raising question on how MinE interacts with MinD.

We isolated MinE suppressor mutants that overcome some MinD mutants. These MinE mutants have substitutions at I24 position. Through a series of genetic and biochemical approaches we demonstrated that these substitutions for I24 release the sequestered part of MinE^{CD}, thereby converting the 6 β to a 4 β structure. The structures of MinD^{D40A} Δ 10-MinE^{I24N} and MinD^{D40A} Δ 10-MinE peptide¹²⁻³¹, resolved at 4.2 \AA and 2.6 \AA resolution respectively, verified that MinE releases the β strand upon MinD binding which is stabilized as an α helix at the MinD dimeric interface. In addition, we show that the N-terminal region of MinE^{CD} is a membrane targeting sequence (MTS) that is released during MinD-induced conformational alteration of MinE. Finally, we propose the Tarzan of the jungle model to explain how MinE can sequentially interact with multiple MinDs.

MinE binding to MinD-ATP on the membrane triggers MinD ATPase activation, however, the mechanistic basis of the activation is still elusive. To get a sense of how MinE induces ATP hydrolysis in MinD, we compared the structure of MinD^{D40A} Δ 10 with MinD^{D40A} Δ 10 complexed with MinE¹²⁻³¹ peptide. Our analysis shows that MinE binding to MinD causes alterations in switch regions and conformational changes in some residues constituting MinDE binding interface.

The MinD ATPase activation by MinE requires the binding of MinE^{CD} to the dimeric interface of a MinD dimer. Nonetheless, it was unknown whether MinE^{CD} binding to one side of the two dimeric interfaces is sufficient to stimulate MinD ATPase. To test this possibility, we created a MinD heterodimer composed of wild type MinD and a mutant form of MinD deficient in MinE

binding. Our results show that both ATP molecules bound to a MinD heterodimer are hydrolyzed, suggesting that MinE^{CD} binding to one side of a MinD dimer induces ATP hydrolysis in both MinD subunits. Moreover, ATP hydrolysis was also observed in a heterodimer of the hydrolytic-deficient MinD^{D40A} mutant and the MinD mutant deficient in MinE binding. Taken together, we propose an asymmetric activation model where MinD hydrolyzes ATP upon MinE^{CD} binding to one side of the MinD dimer.

ACKNOWLEDGEMENTS

I would like to sincerely thank my advisor Dr. Joe Lutkenhaus for his support and academic guidance throughout my graduate study here in the University of Kansas Medical Center. His passion for science and dedication to the education of graduate students has set a stellar example for me in pursuing scientific career. I would also like to appreciate professors Jianming Qiu, Joseph Fontes, Kee Jun Kim, and Philip Hardwidge for serving on both comprehensive examination and dissertation committees. I thank all the current and past members of the Lutkenhaus laboratory for their support and creating an intellectually stimulating environment.

TABLE OF CONTENTS

| | |
|--------------------------|------|
| Acceptance Page | ii |
| Abstract | iii |
| Acknowledgement | vi |
| Table of Contents | vii |
| List of Figures | v |
| List of Tables | viii |
| Abbreviation | |

| | |
|-------------------------------|----|
| Chapter I Introduction | 1 |
| Bacterial cell division | 1 |
| Divisome assembly | 6 |
| Division site selection | 10 |
| Min system | 14 |

Chapter II The structure of MinD-ATP complex reveals the orientation of MinD on the membrane and the relative location of the binding sites for MinC and MinE

| | |
|--------------|----|
| Abstract | 40 |
| Introduction | 41 |
| Results | 44 |

The bacterial two-hybrid system for assessment of the MinD-MinE

| | |
|---------------------------------------------------------------------|----|
| Interaction | 44 |
| Isolation of MinD mutants unresponsive to MinE | 46 |
| Structure of MinD | 55 |
| Site-directed mutagenesis to further characterize the binding sites | |
| Discussion | 76 |
| Experimental Procedures | 85 |

Chapter III The Min oscillator uses MinD-dependent MinE conformational changes in MinE to spatially regulate cytokinesis

| | |
|----------------------------------------------------------------------------------------------------|-----|
| Abstract | 92 |
| Introduction | 92 |
| Results | 96 |
| Mutations altering MinE residue I24 restore interaction with some MinD mutants | 96 |
| The MinE ^{I24N} mutation reduces the β strand content of MinE | 106 |
| The N-terminal helix of MinE is a MTS responsible for promiscuous membrane binding of MinE mutants | 108 |
| The MinE I24N mutation also rescue some MinE mutants defective in interaction with MinD | 114 |
| Structure of the MinD-MinE ^{I24N} complex | 119 |
| Discussion | 129 |
| Experimental Procedures | 137 |

Chapter IV Asymmetric binding of MinE stimulates MinD ATPase Activity

| | |
|------------------------------------------------------------------------------------------------|-----|
| Abstract | 146 |
| Introduction | 146 |
| Results | 151 |
| Comparison of the MinD ^{D40A} Δ10 and the MinD ^{D40A} Δ10-MinE Structures | 151 |
| MinE activation of the MinD heterodimer ATPase | 152 |
| ATP hydrolysis is not required for the coupled MinD activation | 153 |
| The activation of a MinD subunit bound to R21 of MinE independent of the other subunit | 154 |
| Discussion | 165 |
| Experimental Procedures | 178 |
| Chapter V Discussion | 182 |
| Bibliography | 197 |

LIST OF FIGURES

| | |
|---------------------------------------------------------------------------------------------------------------------------------|-----|
| Figure 1. The bacterial cell cycle | 4 |
| Figure 2. Schematic representation of septal ring assembly in <i>E. coli</i> | 12 |
| Figure 3. The structure of <i>T. maritime</i> MinC | 19 |
| Figure 4. Three MinE structures | 26 |
| Figure 5. Oscillation of the Min proteins in <i>E.coli</i> | 31 |
| Figure 6. Structure of <i>P. furiosus</i> MinD and model for MinE interaction with MinD | 33 |
| Figure 7. MinD-M193L does not respond to MinE | 48 |
| Figure 8. MinD-M193L recruits MinC to vesicles and is unresponsive to MinE | 50 |
| Figure 9. Bacterial 2 hybrid analysis of MinD mutants that fail to respond to MinE but activates MinC | 52 |
| Figure 10. Characterization of MinD-D40A | 57 |
| Figure 11. MinD ^{D40A} Δ10 structure | 59 |
| Figure 12. Example of tests of mutants obtained by site-directed mutagenesis of MinD | 77 |
| Figure 13. Model of interaction of Min proteins and FtsZ | 82 |
| Figure 14. Structures of MinE and location of critical residues | 98 |
| Figure 15. Analysis of the ability of MinE mutants to bind to MinD mutants and suppress MinC/MinD inhibitory activity | 100 |
| Figure 16. Location of MinD residues important for MinE binding | 102 |
| Figure 17. Inhibitory activity and secondary structure of N-terminal truncated MinEs | 109 |
| Figure 18. Oligomerization of MinE ²¹⁻⁸⁸ | 111 |
| Figure 19. Effect of <i>minE</i> mutations on membrane localization of MinE and its ability to counter MinC/MinD | 115 |

| | |
|----------------------------------------------------------------------------------------------------------------------------------------------------------------------------------------------------|-----|
| Figure 20. The N-terminal hydrophobic amino acids of MinE are highly conserved and form an amphipathic helix that can function as a MTS (membrane targeting sequence) | 117 |
| Figure 21. The structure of the MinD-MinE complex | 121 |
| Figure 22. Demonstration that MinE ^{I24N} -h interacts with MinD | 123 |
| Figure 23. The fit of MinE to the electron density map in the MinD-MinE peptide and MinD-MinE complex | 125 |
| Figure 24. Tarzan of the jungle model for the interaction between MinD and MinE | 133 |
| Figure 25. Comparison for the ATP binding region for MinD-MinE(12-31) peptide complex and the MinD dimer | 155 |
| Figure 26. Comparison for the ATP binding region for MinD-MinE(12-31) peptide complex and the MinD dimer at residue Glu-146 | 157 |
| Figure 27. Hydrogen bonding interaction between a MinD dimer and MinE peptide molecule at the dimer interface | 159 |
| Figure 28. Overall scheme for the generation of a MinD heterodimer composed of MinD ^{WT} -MinD ^{E53A/N222A} | 161 |
| Figure 29. MinD ^{WT} and MinD ^{E53A/N222A} form a heterodimer that is activated by MinE to hydrolyze ATP | 163 |
| Figure 30. Activity of a MinD heterodimer composed of MinD ^{WT} -MinD ^{E53A/N222A} is not affected by excess of MinD ^{E53A/N222A} mutant protein in the reaction | 166 |
| Figure 31. MinE stimulates the MinD ^{D40A} -MinD ^{E53A/N222A} heterodimer | 168 |
| Figure 32. ATP bound to MinD ^{WT} dimerized with MinD ^{D40A/E53A/N222A} undergoes hydrolysis independent of the activation of MinD ^{D40A/E53A/N222A} ATPase | 170 |
| Figure 33. A sequential model for MinE activation of heterodimeric MinD ATPase | 176 |

LIST OF TABLES

| | |
|-----------------------------------------------------------------------------------------------------------------------------------|-----|
| Table 1. Bacterial two hybrid system for analysis of MinD-MinE interaction | 47 |
| Table 2. ATPase activity of MinD-D40A | 67 |
| Table 3. Crystallographic data and model statistics for the 2.4 Å structure of the MinD Δ 10-D40A-Mg-ATP complex | 68 |
| Table 4. Summary of MinD mutations | 71 |
| Table 5. Rescue of MinD mutants by MinE mutants | 104 |
| Table 6. Crystallographic data for MinD-MinE complexes | 127 |

ABBREVIATIONS

| | |
|------------------|---------------------------------------------------------|
| Amp ^R | ampicillin resistance |
| ADP | adenosine diphosphate |
| AMPPCP | adenosine 5'-[beta, gamma-methylene] triphosphate |
| ATP | adenosine triphosphate |
| ATP γ S | adenosine 5'-O-(3-thiotriphosphate) |
| CD | circular dichroism |
| Cm ^R | chloramphenicol resistance |
| DEAE | diethylethanolamine |
| dNTP | deoxyribonucleotide |
| DTT | dithiothritol |
| EDTA | ethylenediaminetetraacetic acid |
| g | gravity |
| GFP | green fluorescence protein |
| HEPES | N-(2-Hydroxyethyl)piperazine-N'-(2-ethanesulfonic acid) |
| h | hour |
| His | hexahistidine affinity tag |
| IPTG | isopropyl- β -thiogalactopyranoside |
| Kan ^R | kanamycin resistance |
| Kb | kilobase pair |
| LB | luria-bertani |
| LMV | multilamella large vesicles |
| min | minute |

| | |
|------------------|------------------------------------|
| OD | optical density |
| PAGE | polyacrylamide gel electrophoresis |
| PMSF | phenylmethylsulfonyl fluoride |
| rpm | revolution per minute |
| s | second |
| SDS | sodium dodecyl sulfate |
| Spc ^R | spectinomycin resistance |
| Tris | tris (hydroxymethyl) aminomethane |

Chapter I

Introduction

I. Bacterial Cell Division

The importance of cell division is highlighted by cell dogma which states that the only way to generate more cells is to divide existing cells. Even if the regulatory mechanisms and the machinery involved in cell division vary from prokaryotes to eukaryotes, the vital theme that duplicated genetic materials and cellular components are allocated to functionally viable daughter cells is universal. Cell division, so called cytokinesis, is the terminal stage in the cell cycle that leads to daughter cells via a series of intricately coordinated events. The cell cycle in eukaryotic cells is in general comprised of two disparate stages, interphase and mitosis. During interphase cell growth and chromosomal replication occur whereas karyokinesis and cytokinesis is accomplished in mitosis. Interphase can further be subdivided into three phases, G₁, S, and G₂. During G₁ phase where the G stands for gap, biosynthetic activities of the cell resume to increase its size and to prepare for S phase, in which DNA replication takes place. Following S phase, the cell continues to grow in G₂ phase. During mitosis or M phase, the separation of chromosomes occurs in conjunction with cytokinesis. Regulation of the cell cycle is critical for the survival of a cell and an organism. Hence, uncontrolled cell division is prevented by a set of regulatory checkpoints that ensures orderly progression of the cell cycle (Elledge, 1996).

In eukaryotic cells, the morphological alterations of the nucleus and chromosomes have been used as landmarks for distinct phases of the cell division cycle, whereas most prokaryotic species

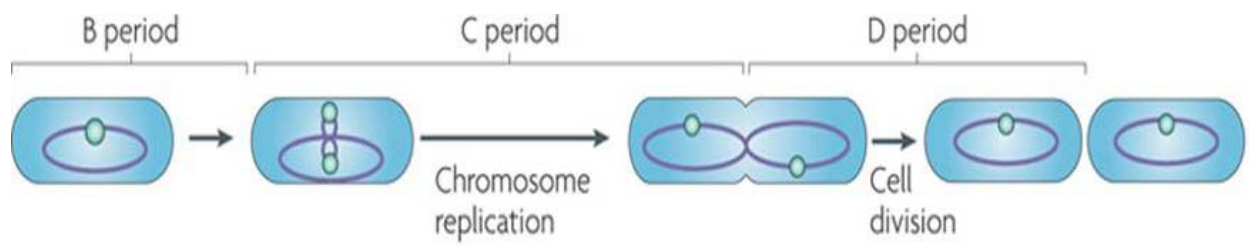
undergo morphologically simplistic binary fission in which various processes such as increase of cell size and biomass, chromosomal replication, and segregation occur simultaneously (Nordstrom, Bernander, & Dasgupta, 1991). Despite this overlap, the bacterial cell cycle can broadly be subdivided into three phases (J. D. Wang & Levin, 2009) (Fig.1). The B period, where B stands for birth, refers to a period between the completion of cytokinesis and the initiation of a new round of DNA replication. Hence, this period is analogous to G1 phase in eukaryotic cells. The C period, in which C highlights chromosome, indicates an interval from replication initiation to termination. Thus, it is equivalent to S phase. The subsequent time span between the end of replication and division is called the D period wherein D symbolizes division. Studies on the model gram-negative bacterium *E. coli* and the gram-positive bacterium *B. subtilis* suggest that achievement of a specific mass to origin ratio triggers the initiation of chromosome replication at the end of the B period (Donachie, 1968; Donachie & Blakely, 2003; Schaechter, Maaloe, & Kjeldgaard, 1958). This idea has recently been challenged and it is believed that the factors controlling the initiation of DNA replication differ depending on cellular growth rate (Boye & Nordstrom, 2003; Weart et al., 2007). Synthesis and increase in the activity of DnaA initiator protein is responsible for triggering initiation (Atlung & Hansen, 1993; Lobner-Olesen, Skarstad, Hansen, von Meyenburg, & Boye, 1989; Moriya, Imai, Hassan, & Ogasawara, 1999; Ogura, Imai, Ogasawara, & Moriya, 2001). So, DnaA expression is regulated by the above-mentioned factors. In fast growing cells in which the mass doubling time of a cell is shorter than the C period, new rounds of chromosomal replication are initiated even before the completion of a previous one, thus resulting in 'multifork replication' (Cooper & Helmstetter, 1968; Yoshikawa, O'Sullivan, & Sueoka, 1964). This mechanism makes sure that at least one round of chromosome replication is completed per division.

Once DNA replication commences in the C period, the duplicated portions of the chromosome begin to segregate toward opposite poles even before the completion of replication. It has been suggested that the initiation of chromosome replication dictates the position of the assembly of the cytokinetic machinery (E. J. Harry, Rodwell, & Wake, 1999; Regamey, Harry, & Wake, 2000). In this model, the replication machinery or replisome drives the duplicated origin regions away from the mid cell position, hence unmasking a site for assembly of the cytokinetic ring. In this scenario, the temporal and spatial regulation of divisome formation is related to the progress of chromosome replication. In *E. coli*, however, cytokinesis has been detected in anucleated cells, excluding a mandatory role for DNA replication in divisome assembly (Sun, Yu, & Margolin, 1998).

The separation of two sister chromosomes poses a challenge due to the circular nature of bacterial chromosomes. Two kinds of physical linkages stand in the way of septation. One is intercatenated links of two chromosomes that are resolved by topoisomerase IV, which is activated at the last stage of the cell cycle. The other less common link is chromosome dimers formed during replication by homologous recombination (in ~10 % of cells). The resolution of chromosome dimers is catalyzed by a tyrosine recombinase complex called XerCD that acts on a specific site, dif, in the terminus region of chromosomes. It is now well-established that the activities of both systems above depend on FtsK, a multifunctional DNA translocase (Bigot, Sivanathan, Possoz, Barre, & Cornet, 2007). Emerging evidence further indicates that FtsK might modulate the activity of the cytokinetic ring and serve as a checkpoint for D to B transition (Dubarry, Possoz, & Barre, 2010; Lesterlin, Pages, Dubarry, Dasgupta, & Cornet, 2008).

Fig.1. The bacterial cell cycle [From Wang, JD et al. (J. D. Wang & Levin, 2009)]

The bacterial cell cycle is traditionally divided into three stages: the period between division (birth) and the initiation of chromosome replication (B period); the period required for chromosome replication (C period); and the time between the completion of chromosome replication and the completion of cell division (D period). The bacterial cells (in this case, *Escherichia coli*) are outlined in black and contain highly schematic chromosomes (purple ovals) with *oriC* regions shown as green circles. This occurs in slow growing cells ($T < 60$ min). In fast growing cells (where $C > D$) new rounds of replication start before the previous round is finished resulting in multifork replication.



II. Divisome Assembly

Cell division in *E. coli* is mediated by a macromolecular complex called the divisome that coordinates invagination of three layers of the envelope, the outer membrane, a peptidoglycan layer in the periplasm, and the inner membrane. Pioneering studies undertaken in the 1960s on conditional temperature sensitive mutations yielded a collection of *E. coli* strains that are defective in cell division and accordingly exhibit a characteristic long filamentous phenotype at an elevated temperature. For this historic reason, a set of genes involved in bacterial cell division was named *fts* to signify a filamentous temperature-sensitive phenotype (Lutkenhaus & Addinall, 1997; Rothfield, Justice, & Garcia-Lara, 1999; Taschner, Huls, Pas, & Woldringh, 1988). The divisome consists of the products of these essential *fts* genes and all others required for cell division. The tubulin homologue FtsZ assembles into a ring-like structure called the Z ring beneath the surface of the cytoplasmic membrane and serves as a scaffold for the divisome (E. F. Bi & Lutkenhaus, 1991; P. de Boer, R. Crossley, & L. Rothfield, 1992; Erickson, Anderson, & Osawa, 2010; Goehring & Beckwith, 2005).

The vital function of FtsZ in bacterial cell division is illustrated by the fact that it is a highly conserved protein found in all bacteria with few exceptions (Margolin, 2005; Vaughan, Wickstead, Gull, & Addinall, 2004). Even eukaryotic organelles such as chloroplast and mitochondria believed to have originated from cyanobacteria and α -proteobacteria, respectively, use FtsZ to divide. However, in many eukaryotes such as yeast, plant, and animal species a dynamin-related protein has replaced the function of FtsZ in mitochondrial fission (E. Harry, Monahan, & Thompson, 2006; Margolin, 2005; Vaughan et al., 2004). The existence of a myriad

of positive and negative regulators of Z ring assembly further testifies to the importance of FtsZ in the division of prokaryotic cells (D. W. Adams & Errington, 2009; Goehring & Beckwith, 2005).

Amino acid sequence analysis indicates that tubulin and FtsZ form a distinct GTPase family (P. de Boer et al., 1992; Lowe & Amos, 1998; Nogales, Downing, Amos, & Lowe, 1998). FtsZ, like tubulin, undergoes GTP-dependent assembly into filaments (Erickson, Taylor, Taylor, & Bramhill, 1996; Lowe & Amos, 1999; Mukherjee & Lutkenhaus, 1994; Oliva, Cordell, & Lowe, 2004). The nucleotide binding site and the region interacting with the nucleotide of the next subunit show the highest degree of conservation whereas the surfaces supposedly involved in lateral contact between protofilaments are rather different (Erickson, 1995; Nogales et al., 1998). The GTPase stimulation caused by FtsZ polymerization can be explained by a sandwich of catalytic residues between the base of one subunit and the GTP-binding site of the other subunit (Oliva et al., 2004; Scheffers, de Wit, den Blaauwen, & Driessen, 2001). It has been proposed that GTP hydrolysis generates a constrictive force (Lu, Reedy, & Erickson, 2000; Osawa, Anderson, & Erickson, 2008). This idea, however, remains controversial since the cells expressing a FtsZ mutant defective in GTPase activity can still divide (Mukherjee, Saez, & Lutkenhaus, 2001). Given the difference in lateral surfaces mentioned above, it is unlikely that FtsZ generates a structure similar to a microtubule. Instead, the lateral interaction of FtsZ protofilaments promoted by several factors in vitro is known to produce various types of higher order structures such as bundles, sheet, ribbons, and helical tubes (Bramhill & Thompson, 1994; Erickson et al., 1996; Gonzalez et al., 2003; Lowe & Amos, 1999, 2000; Oliva et al., 2003). Likewise, some division proteins such as ZipA and ZapA cause FtsZ filament bundling in vitro (Gueiros-Filho & Losick, 2002; RayChaudhuri, 1999), which supports the idea that those

structures are somehow relevant *in vivo*, Nevertheless, the molecular basis of the lateral interaction of FtsZ protofilaments and their arrangement within the Z ring are still elusive.

The Z ring marks the site of division and serves as a scaffold for subsequent recruitment of over two dozen downstream components that includes FtsA, ZipA, ZapA, FtsK, FtsQ, FtsL, FtsB, FtsW, FtsI, FtsN, and AmiC. Recruitment of these proteins to the divisome appears to be linear and sequential, which means that each protein depends on upstream proteins to localize to the divisome (de Boer, 2010; Goehring & Beckwith, 2005; E. Harry et al., 2006). For instance, FtsA and ZipA are indispensable for the localization of FtsK that is required for the targeting of all downstream proteins to the divisome.

A growing body of evidence suggests that formation of the divisome occurs in two steps since there is a notable delay between the Z ring assembly and the recruitment of FtsQ, a FtsK-dependent downstream protein (Aarsman et al., 2005; Gamba, Veening, Saunders, Hamoen, & Daniel, 2009) (Fig. 2). The early divisome complex is composed of FtsZ, FtsA, ZipA, ZapA, ZapB, and ZapC (Fig. 2) that localize almost simultaneously to the division site. Formation of the late divisome complex coincides with the initiation of constriction at the division site.

Therefore, the mature form of the Z ring is sometimes called the septal ring (SR) to contrast with the early divisome, the Z ring (ZR) (de Boer, 2010) (Fig.2). Once the SR is formed, the switch of peptidoglycan synthesis takes place from the lateral axis of a cell to the central position concomitant with the commencement of septation (Aarsman et al., 2005; den Blaauwen, de Pedro, Nguyen-Disteche, & Ayala, 2008).

The precise function of most proteins involved in divisome assembly has been under intense investigation but still remains unanswered. Either FtsA or ZipA is sufficient to tether FtsZ

polymers to the inner surface of the cytoplasmic membrane by interacting with the C-terminal tail of FtsZ (Hale, Rhee, & de Boer, 2000; Pichoff & Lutkenhaus, 2002, 2005). Nevertheless, both proteins are essential for the recruitment of the downstream SR components (Pichoff & Lutkenhaus, 2002). ZapA and ZapB are targeted to the ZR by interacting with FtsZ and ZapA, respectively, and are believed to enhance stability of the ZR (Ebersbach, Galli, Moller-Jensen, Lowe, & Gerdes, 2008; Gueiros-Filho & Losick, 2002; Low, Moncrieffe, & Lowe, 2004) since the two proteins appear to induce the bundling of FtsZ protofilaments in vitro (Gueiros-Filho & Losick, 2002). The more recently discovered ZapC is recruited to the ZR by directly interacting with FtsZ and may also contribute to the stability of the Z ring (Hale et al., 2011).

FtsEX, a component of the SR and an ABC transporter complex where FtsE is an ATPase and FtsX is a membrane protein (de Leeuw et al., 1999), is considered dispensable, because growth defect due to loss of the genes can be easily suppressed by increased osmolarity of the culture medium (Ricard & Hirota, 1973). However, FtsEX is speculated to mediate the transition from ZR to the late divisome or septal ring (SR) since in salt-free medium the targeting of FtsK to the divisome requires FtsEX (Schmidt et al., 2004). Although FtsE is reported to interact with FtsZ, it is only recruited to the septum if FtsX is present (Corbin, Wang, Beuria, & Margolin, 2007).

FtsK, an ATP-driven DNA translocase, has two or three distinct functional domains. The N-terminal domain is essential and necessary for the assembly of the late divisome complex whereas the C-terminal region constitutes a hexameric translocase that activates chromosome dimer resolution (Bigot et al., 2007; Dubarry et al., 2010). FtsQ, FtsL, FtsB are known to form a complex that plays a role in linking septal peptidoglycan synthesis machinery to the Z ring (Buddelmeijer & Beckwith, 2004; Daniel, Harry, & Errington, 2000). FtsW recruits PBP3 also called FtsI that has peptidoglycan transpeptidase activity, which causes cell wall synthesis to

shift from the lateral to the septal region undergoing constriction (Henriques, Glaser, Piggot, & Moran, 1998; Mercer & Weiss, 2002). FtsN whose arrival to the divisome leads to constriction initiation (Addinall, Cao, & Lutkenhaus, 1997; Gerding et al., 2009) is believed to coordinate the action of the SR and peptidoglycan-shaping machinery (Derouaux et al., 2008; Muller et al., 2007; Ursinus et al., 2004). It is required for the recruitment of all nonessential proteins that process the septal peptidoglycan at the septum and cause ingression of the outer membrane (Gerding, Ogata, Pecora, Niki, & de Boer, 2007; Lutkenhaus, 2009). AmiA, AmiB, and AmiC are peptidoglycan amidases that hydrolyze peptidoglycan chains and that are tightly controlled by cognate activators (Peters, Dinh, & Bernhardt, 2011; Priyadarshini, Popham, & Young, 2006; Uehara, Parzych, Dinh, & Bernhardt, 2010). Therefore, despite completion of inner membrane constriction and fusion, an *E. coli* mutant deficient in these amidases remains connected via peptidoglycan that interferes with outer membrane ingression (Bernhardt & de Boer, 2003; Heidrich et al., 2001).

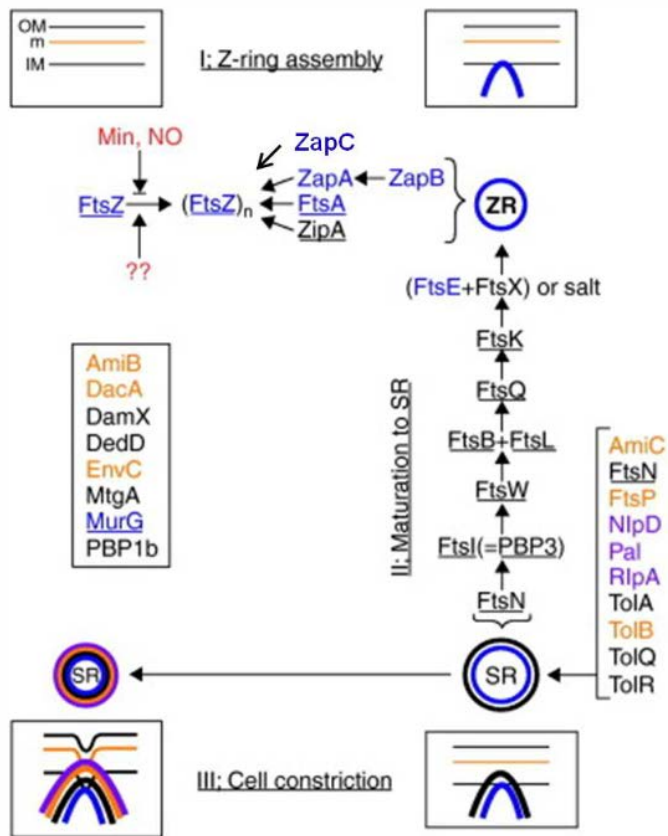
III. Division Site Selection

Both in *B. subtilis* and *E. coli* the position of Z ring assembly is influenced by two systems that prevent the Z rings from forming at inappropriate places in a cell. The first example of a negative regulatory system is nucleoid occlusion which describes a phenomenon where cell division is inhibited over the nucleoid (Mulder & Woldringh, 1989; Woldringh, Mulder, Huls, & Vischer, 1991). The proteins responsible for nucleoid occlusion are SlmA in *E. coli* (Bernhardt & de Boer, 2005) and Noc in *B. subtilis* (L. J. Wu & Errington, 2004). They bind their cognate sequences that are scattered around the chromosome except for the replication terminus region

(Cho, McManus, Dove, & Bernhardt, 2011; Tonthat et al., 2011). SlmA and Noc, members of ParB and TetR families, respectively, share almost no sequence homology, however, they appear to function similarly (Bernhardt & de Boer, 2005). In vitro SlmA disrupts FtsZ polymers or alters the bundling pattern of FtsZ filaments by a direct interaction. The binding of SlmA to its cognate DNA sequence drastically potentiates the activity of SlmA (Cho et al., 2011). However, hitherto, the exact molecular mechanisms by which SlmA is activated by DNA and disassembles FtsZ polymers are unknown. It has been speculated that Noc might also directly antagonize FtsZ polymerization.

The second regulator is the Min system that blocks cell division at the poles. In *E. coli* the oscillatory behavior of the Min system results in the residence time of an inhibitory complex of the Z ring that is highest at the poles and lowest at mid cell (Hale, Meinhardt, & de Boer, 2001). On the other hand, in *B. subtilis*, instead of oscillation, the inhibitory complex of the Min system is targeted to the poles by interacting with a polar scaffold protein called DivIVA (Marston, Thomaidis, Edwards, Sharpe, & Errington, 1998). The cooperative relationship between nucleoid occlusion and the Min system is manifested by the synthetic lethal phenotype when the two systems are simultaneously disrupted (Bernhardt & de Boer, 2005). In the double mutant, a functional Z ring is not formed and FtsZ is present in structures that are dispersed throughout the cell. The lack of Z ring maturation highlights the importance of the two negative systems in restricting FtsZ to a certain subcellular location. Taken together, the gradients of the two negative regulators, one on the chromosome and one emanating from the poles, only allow Z ring assembly at mid cell once the two daughter chromosomes begin to separate, thereby orchestrating bacterial growth and chromosomal replication with cell division (Bramkamp & van Baarle, 2009; Lutkenhaus, 2007; Rothfield, Taghbalout, & Shih, 2005).

Fig. 2 Schematic representation of septal ring assembly in *E. coli* [From de Boer, PA, (de Boer, 2010)]. Indicated are three stages in development of the septal ring, known proteins, and the approximate step at which they become associated with the apparatus. Proteins that are essential for viability are underlined. Proteins assembling at the cytoplasmic face of the inner membrane are in blue, trans-membrane inner-membrane proteins are in black, periplasmic proteins in orange, and outer membrane (lipo-) proteins are in purple. Regulators of Z ring positioning are in red. Some septal ring components (listed in box) were left out of the recruitment pathway for clarity.



IV. Min System

i) The Min Phenotype

The Min mutants in *E. coli* and *B. subtilis* were discovered decades ago and are characterized by the presence of small cells deficient in chromosomes called minicells that are produced by polar cell division at the expense of division at the central position (Adler, Fisher, Cohen, & Hardigree, 1967; Reeve, Mendelson, Coyne, Hallock, & Cole, 1973). The outcome of polar division is the generation of a mixture of heterogeneous populations ranging from minicells to long nucleated cells. A study on the nonessential *min* locus designated *minB* in *E. coli* led to the isolation of an operon that consists of three genes, *minC*, *minD*, and *minE*, whose coordinated actions prevent polar cell division (de Boer, Crossley, & Rothfield, 1988, 1989). MinC and MinD are well-conserved across the broad spectrum of prokaryotes while MinE and DivIVA are preferentially distributed in gram-negative and gram-positive species, respectively (E. Harry et al., 2006; Lutkenhaus, 2007; Rothfield et al., 2005). Even in plant cell chloroplasts, putatively originated from cyanobacteria, MinD and MinE regulate division although a homologue of MinC has not been discovered (Aldridge, Maple, & Moller, 2005). Studies in *E. coli* revealed that MinC and MinD act in concert to block division throughout the cell while MinE regulates MinC and MinD activity such that their action is directed away from midcell. Intriguingly, in a Δ *minB* mutant MinD overexpression alone did not affect division, however, a forty fold excess of the MinC suppressed cell division (P. A. de Boer, R. E. Crossley, & L. I. Rothfield, 1992). Introduction of MinE into the latter strain did not rescue the cells. These findings suggest that MinD potentiates or activates MinC, the authentic inhibitor of cell division, and that MinD is the

protein through which MinE exerts specificity to confine MinC activity to the poles (P. A. de Boer et al., 1992). Concomitant with the development above, a series of compelling results indicated that MinC specifically targets FtsZ (E. Bi & Lutkenhaus, 1990, 1993; de Boer, Crossley, & Rothfield, 1990; Hu & Lutkenhaus, 2000; Hu, Mukherjee, Pichoff, & Lutkenhaus, 1999). The results included that the introduction of additional copies of FtsZ in wild type causes mini cells (de Boer et al., 1990; Ward & Lutkenhaus, 1985), that MinC and MinD-mediated cell division inhibition can be relieved by excess FtsZ (de Boer et al., 1990; P. A. de Boer et al., 1992), that certain FtsZ mutants are resistant to the activity of MinC and MinD (Pichoff & Lutkenhaus, 2001; Shen & Lutkenhaus, 2009, 2010), and that FtsZ assembly in vitro is antagonized by MinC (Dajkovic, Mukherjee, & Lutkenhaus, 2008; Hu & Lutkenhaus, 2000).

ii) The Min Oscillation

The application of GFP technology in which GFP or its variant fluorescence proteins are fused with the Min proteins unveiled a stunning dynamicity of the Min system. At first, GFP-MinD was shown to undergo a rapid pole-to-pole oscillation during which MinD alternatively occupies polar zones, one-half of a cell extending from a pole toward midcell (Raskin & de Boer, 1999b). This oscillatory behavior of MinD requires MinE which forms a mobile ring-like structure, the MinE ring, near midcell (Fu, Shih, Zhang, & Rothfield, 2001; Hale et al., 2001; Raskin & de Boer, 1997). A study using YFP-MinD and MinE-CFP together demonstrated that the MinE ring was at the edge of the MinD polar zone near midcell and migrated towards the pole removing MinD which assembled at the opposite pole (Shih, Fu, King, Le, & Rothfield, 2002). In contrast

to MinE, MinC does not appear to modulate the MinD dynamicity. Instead, it seems to be a passenger through association with MinD (Hu & Lutkenhaus, 1999; Raskin & de Boer, 1999a). The period of the MinD oscillation is dictated by temperature and the ratio of MinD to MinE, both of which as will be discussed later are critical determinants of the MinD enzymatic reaction. In addition, rather than a geometric cue at the pole, inherent biochemical parameters, as will be discussed later, probably play a more crucial role in MinD oscillation. The oscillation of MinD occurs in a stripe pattern in long filamentous cells (Hale et al., 2001; Raskin & de Boer, 1999a) and is seen in round-shaped cells that are less than symmetric (Corbin, Yu, & Margolin, 2002; Ramirez-Arcos, Szeto, Dillon, & Margolin, 2002). Together, the results suggest that the Min oscillator is a geometric sensor that finds the longest axis of the cell.

v) MinC

MinC is a dimer and is comprised of two distinct functional domains. The N-terminal domain (MinC^N) is primarily responsible for antagonizing Z ring assembly, shown in vivo and in vitro (Dajkovic, Lan, Sun, Wirtz, & Lutkenhaus, 2008; Hu & Lutkenhaus, 2000; Hu et al., 1999), whereas the C-terminal domain (MinC^C) is responsible for dimerization and MinD binding (Hu & Lutkenhaus, 2000; Szeto, Rowland, & King, 2001) (Fig.3). In the absence of MinD, a significant overexpression of MinC or MinC^N is required to suppress Z ring formation (P. A. de Boer et al., 1992; Hu & Lutkenhaus, 2000; Hu et al., 1999). Thus, it has been argued that MinD activates MinC by concentrating MinC on the membrane (Hu, Saez, & Lutkenhaus, 2003; Johnson, Lackner, Hale, & de Boer, 2004; Szeto, Rowland, Habrukowich, & King, 2003). This

idea is consistent with an *in vivo* concentration of MinC of merely 400 molecules per cell (T. H. Szeto et al., 2001) and an affinity of MinC for FtsZ monomer that is relatively modest (Hu et al., 1999; Shen & Lutkenhaus, 2010).

A recent study revealed that MinC^C antagonizes Z ring assembly by competing with FtsA and ZipA for the C-terminal tail of FtsZ (Shen & Lutkenhaus, 2009). *In vitro*, MinC^C does not prevent the sedimentation of FtsZ filaments. Instead, it prevents the lateral association of FtsZ filaments (Dajkovic, Mukherjee, et al., 2008). The lateral interaction of FtsZ filaments is rather a downstream event of the FtsZ-tethering by FtsA, so the significance of FtsZ filament debundling by MinC^C should be further clarified.

MinC^N shortens the length of FtsZ protofilament *in vitro* without affecting the GTPase activity of FtsZ (Hu et al., 1999), which excludes the possibility that MinC sequesters FtsZ molecules as SulaA does. A puzzling observation is that FtsZ polymerized with non-hydrolytic GTP analogues is completely resistant to MinC (Dajkovic, Mukherjee, et al., 2008). With this in mind and based on a FtsZ mutant recalcitrant to MinC^N, a model was proposed. In this model, MinC^N weakens the longitudinal bonds of FtsZ in a filament following GTP hydrolysis by attacking α helix 10 of FtsZ located at the FtsZ subunit interface (Shen & Lutkenhaus, 2010). Consistent with this, previously isolated FtsZ mutants deficient in GTPase activity are resistant to MinC (Dai, Mukherjee, Xu, & Lutkenhaus, 1994; Pichoff & Lutkenhaus, 2001). However, more direct structural and biochemical evidence is needed for this model. Taken together, MinC^C binding to both MinD and the C-terminal tail of FtsZ positions MinC^N close to FtsZ.

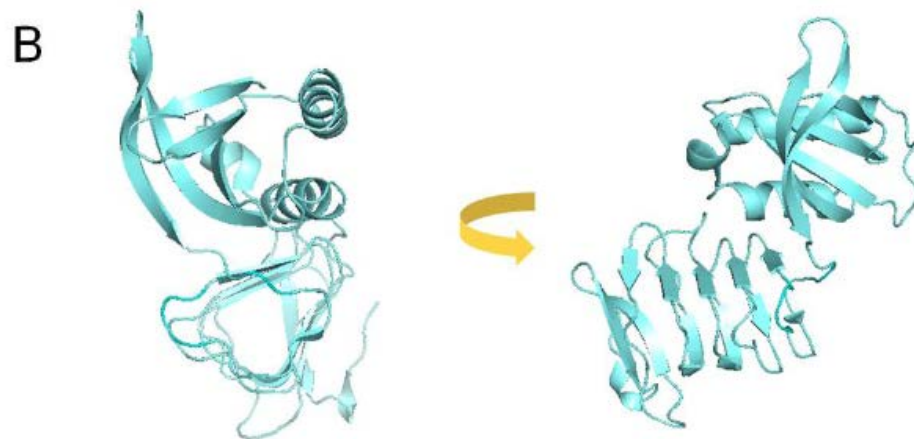
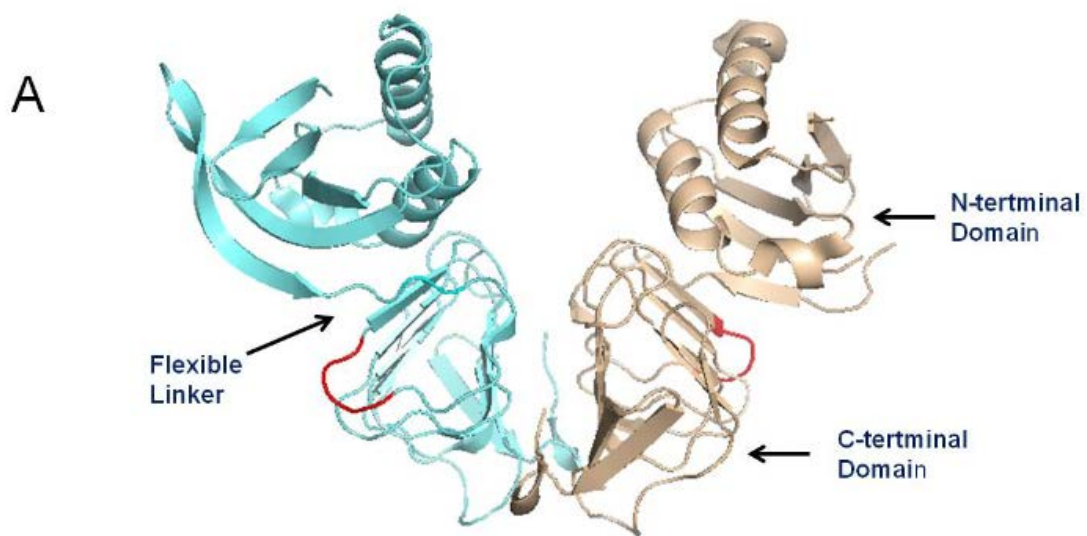
vi) MinC Structure

The crystal structure of MinC from *Thermotoga maritima* was obtained to 2.2 Å resolution (Cordell, Anderson, & Lowe, 2001). In the asymmetric unit four MinC molecules are arranged in two dimers where the C-terminal domain of MinC forms the dimeric interface and is connected to the N-terminal domains via a flexible linker that allows the two N-terminal domains to be in different orientations. In the C-terminal part, a series of β strands are packed into a triangular right-handed β helix configuration where one face of the triangle forms a dimeric interface (Fig. 3). Since a very hydrophobic surface is extensively involved in dimerization, it is presumed that MinC always exists as a dimer in vivo. The N-terminal region of MinC consists of two α helices and five β strands in which the overall organization of the secondary structural elements are distantly related to those of the 1A domain of FtsA. It was this structural similarity that led to a suggestion that MinC and FtsA share a common binding site on FtsZ.

iii) MinD

MinD is a member of the deviant walker A motif family of ATPases that shares the basic structural architecture and nomenclature of G proteins such as Ras (de Boer, Crossley, Hand, & Rothfield, 1991; Koonin, 1993). The MinD ATPase likewise contains the three motifs critical for ATP catalysis, switch I, switch II, and a deviant walker A motif often called the P-loop. The deviation of the walker A motif [xKGGxxK(T/S)] from a classic P-loop [GxxGxGK(T/S)] has been used as a characteristic marker of the MinD-related superfamily of proteins that mediate diverse biological functions (Koonin, 1993).

Fig. 3 The structure of *T. maritima* MinC (PDB 1HF2) dimer (A) and monomer (B). Residues critical for MinD binding are highlighted in red (A).



Typical examples of these proteins include ParA/Soj, NifH, and ArsA that catalyze DNA segregation, electron transfer in the nitrogenase complex, and anion efflux respectively. These deviant Walker A motif superfamily proteins have similar structures even though the primary sequences of the proteins only share 25 % identity (Lutkenhaus & Sundaramoorthy, 2003). A close examination of the structures of NifH and Soj revealed a unique signature lysine in the P-loop that contacts an ATP bound to the opposite monomer, suggesting that the signature lysine mediates ATP-dependent dimer formation (Leipe, Wolf, Koonin, & Aravind, 2002; Lutkenhaus & Sundaramoorthy, 2003).

Among the superfamily members listed above, a group of more closely related proteins such as MinD and Soj has been referred to as WACA (walker A cytomotive ATPase) proteins that share a few distinctive features (Michie & Lowe, 2006). The ATP-bound proteins of the WACA family adhere to specific surfaces such as DNA for Soj and membrane for MinD on which they appear to form polymers (Hu, Gogol, & Lutkenhaus, 2002; Leonard, Butler, & Lowe, 2005; Suefuji, Valluzzi, & RayChaudhuri, 2002). In addition, with a partner that stimulates ATP hydrolysis these proteins show dynamic oscillation patterns on the surfaces. So far, MinDs from archaea species have been crystallized and are present as monomers (Cordell & Lowe, 2001; Hayashi, Oyama, & Morikawa, 2001; Sakai et al., 2001). Nevertheless, evidence indicates that *E. coli* MinD bound with ATP exists as a dimer (Hu et al., 2003). Also, two copies of the membrane targeting motif of *E. coli* MinD are required to target GFP to the cytoplasmic membrane (Szeto et al., 2003). In addition, in vitro *Neisseria gonorrhoeae* MinD dimerized in the absence of the membrane (J. Szeto et al., 2001) and a self-association of *E. coli* MinD and *N. gonorrhoeae* MinD can easily be detected in the yeast two hybrid system (L. Ma, King, & Rothfield, 2004; J. Szeto et al., 2001). Consistent with these evidence, the aforementioned

MinD-related proteins such as NifH-ATP and a hydrolytic mutant type of Soj-ATP have all been crystallized as dimers (Leonard et al., 2005; Schindelin, Kisker, Schlessman, Howard, & Rees, 1997). Hence, the monomeric MinD crystallized with AMPPCP (Hayashi et al., 2001), an ATP analogue, does not represent biologically active structure, considering that WACA family proteins do not respond to ATP analogues (Hu et al., 2002) and have basal ATPase activity making it challenging to crystallize in ATP-bound forms (Leonard et al., 2005; Lutkenhaus & Sundaramoorthy, 2003).

iv) MinD Structures

To date, three MinD structures from archaea species have been determined using X-ray crystallography. A nucleotide-free and monomeric form of MinD-1 from *Archaeoglobus fulgidus* was solved to 2.6 Å resolution (Cordell & Lowe, 2001). The secondary structure of MinD-1 is characterized by a twisted arch of stacked β strands surrounded by α helices. Amino acids around the nucleotide binding surface are highly conserved. In this structure, the C-terminal tail of MinD-1, believed to mediate the membrane binding of MinD, was unstructured. Next, the structure of MinD-2 monomer bound with ADP from hyperthermophilic *Pyrococcus horikoshii* OT3 was determined (Sakai et al., 2001). Except for the phosphate binding region the overall fold of MinD-2, like MinD-1, is distinct from those of ATP-dependent motor protein domains of kinesin and myosin, hence illustrating a unique position of MinD-related proteins amongst other ATPase families. Thirdly, *Pyrococcus furiosus* MinD homologue complexed with an ATP analogue, AMPPCP, or ADP was crystallized (Hayashi et al., 2001) (Fig. 6A). Surprisingly, no structural differences between the two monomeric structures were detected around the γ -

phosphate of the adenosine nucleotide. Even though this study demonstrated the importance of some MinD residues involved in ATP and MinC binding, the essence of MinD dimerization and membrane binding was not grasped since AMPPCP is not a true mimic of ATP for MinD-related proteins (Hu et al., 2002; Hu et al., 2003) and this homologue lacks the C-terminal tail involved in membrane binding.

vii) MinE

MinE, a small protein of only 88 amino acids, exists as a dimer and consists of two modular domains in which the N-terminal region (MinE^{CD}, residues 1-31) constitutes an anti-MinCD domain whereas the C-terminal domain (MinE^{TSD}, residues 32-88) has been referred to as a topological specificity domain (Pichoff, Vollrath, Touriol, & Bouche, 1995; Zhang, Rowland, King, Braswell, & Rothfield, 1998; Zhao, de Boer, & Rothfield, 1995). As will be discussed below, the C-terminal domain is involved in dimerization and the regulation of the N-terminal MinE^{CD}. MinE^{CD} alone, if overexpressed, is sufficient to counteract the activity of MinCD. MinE^{CD} can displace MinC from MinD and stimulate the MinD ATPase causing MinD to dissociate from the cytoplasmic membrane (Ghasriani et al., 2010; L. Y. Ma, King, & Rothfield, 2003; Pichoff et al., 1995; Zhao et al., 1995). However, due to lack of the C-terminal domain, Z ring assembly is not confined to the midcell position and mini cells are formed. In addition, a general consensus is that MinE^{CD} forms a nascent helix and exists as a monomer (King et al., 1999). It is much less efficient than the dimeric full-length MinE protein in counteracting MinCD (Pichoff et al., 1995). This indicates that linking the N-terminal MinE^{CD} to the C-terminal segment MinE^{TSD} significantly enhances the anti-MinCD reaction through dimerization.

The fact that expressing various levels of the MinE^{CD} alone does not restore a wild-type phenotype ((Pichoff et al., 1995) indicates that MinE^{TSD} is required for topological specificity.

The dimerization of MinD-ATP causes MinD to bind the membrane and recruit MinC and MinE (Hu et al., 2003; Lackner, Raskin, & de Boer, 2003). What sets MinE apart from MinC is that MinE seems to have a cryptic property to localize on the membrane independent of MinD (L. Y. Ma et al., 2003). MinE^{CD} and particular mutants such as MinE^{L22D} and MinE^{I25R} are targeted to the membrane when expressed in cells devoid of the Min system. These discoveries signify an intimate relationship between MinE^{CD} and MinE^{TSD} (Ghasriani et al., 2010; Kang et al., 2010; Ramos et al., 2006) and suggest that the cytoplasmic MinE protein might undergo structural conversion upon MinD binding which reveals a membrane targeting motif in the MinE^{CD} that is masked by the MinE^{TSD} (Park et al., 2011).

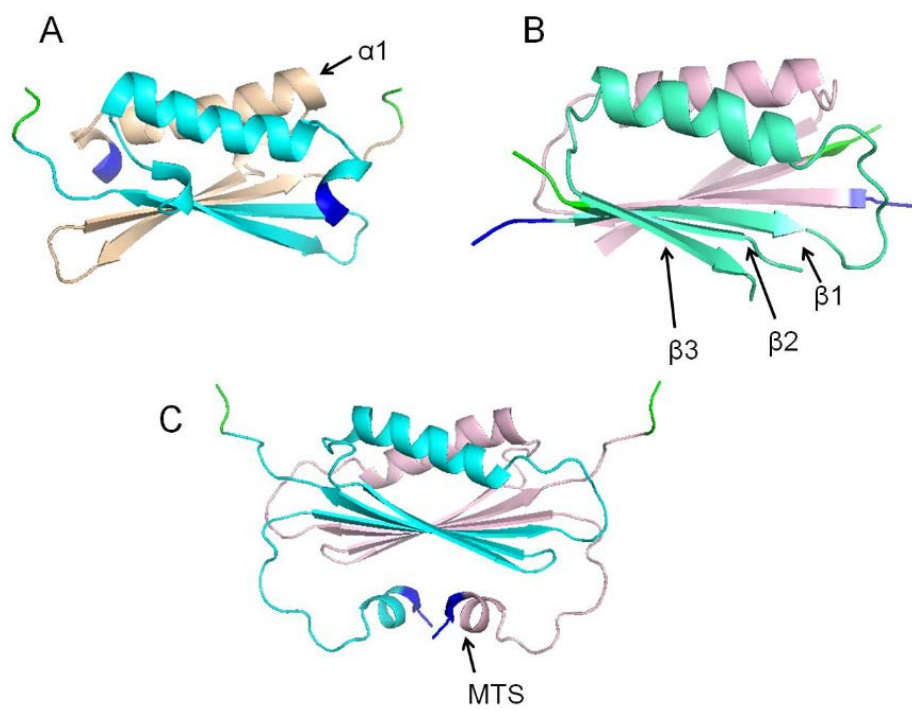
viii) MinE Structures

The structure of the topological specificity domain of *E. coli* MinE (MinE^{TSD}, residues 32-88) that is resistant to trypsin digestion was determined using heteronuclear NMR spectroscopy (King et al., 2000). The MinE^{TSD} structure reveals a well-defined region (residues 32-82) which forms an extensive hydrophobic dimeric interface. Each monomer of the MinE^{TSD} consists of a long α helix (α 1) followed by a large antiparallel β hairpin encompassing two consecutive β strands (β 2, β 3). In the dimeric form, the α 1s from each monomer generate an antiparallel coiled coil by packing against one another. Each monomer in addition contributes two β strands to the dimer to form a four β stranded antiparallel β sheet in which the β 3s form a dimeric interface

(Fig.4A). The coiled coil created by the two α 1s is primarily stabilized by hydrophobic interactions that are also responsible for the packing of the coiled coil against the β strands. The extensive conservation of amino acid residues involved in the coil-coil and the α 1- β strand interaction supports the relevance of the MinE^{TSD} structure.

The crystal structure of *Helicobacter pylori* MinE (HpMinE, residues 19-77) disproved the very model that the MinE N-terminal region (MinE^{CD}, residues 1-31) is rather disordered and might exist as a nascent helix. Instead, part of the MinE^{CD} (residues 19-26) exists as a β strand (β 1) at the dimeric interface. Each monomer of HpMinE donates three β strands to the dimer to create a six β stranded antiparallel β sheet in which the β 1 strands form a dimeric interface (Kang et al., 2010) (Fig.4 B). The β 1s from each monomer form an anti-parallel interface that packs against the coiled coil (α 1s) via hydrophobic interactions. The presence of part of the MinE^{CD} as a β strand at the dimeric interface raises the question of how it could interact with MinD. Consistent with this finding is the recently determined NMR structure of the full-length MinE dimer from *Neisseria gonorrhoeae* (NgMinE, residues 1-87) (Ghasriani et al., 2010). The region corresponding to β 1 (residues 19-26) of HpMinE does indeed exist as a β strand (β 1, residues 18-29) and is an integral part of the dimeric interface in NgMinE. A strikingly unique feature of the NgMinE structure is the presence of the N-terminal region (residues 1-18) which is disordered in the HpMinE structure. It included N-terminal helices (residues 3-8) that pack against the β - sheet through hydrophobic side chains, consequently further masking the residues putatively critical for MinD binding (Fig.4C). The implications of the sequestration of the part of the MinE^{CD} in a β 1 strand at the dimer interface masked by the N-terminal helices will be addressed in this thesis. Finally, the finding that the tertiary structures of the HpMinE and NgMinE are

Fig. 4 Three MinE structures. The MinE^{TSD} (residues 32-88, PDB: 1EV0) of *E. coli* (A), MinE (residues 19-77, PDB: 3MCD) of *H. pylori* (B), and MinE of *N. gonorrhoeae* (residues 1-88, PDB: 2KXO)



almost identical suggests that MinE from *E. coli* exists as a 6 β stranded form.

ix) The Biochemical Basis of Min Dynamics

The dynamic behavior of the Min proteins has been under intense study for years and some of the biochemical factors critical for the oscillation have emerged. It is now well accepted that MinD, a peripheral membrane ATPase, forms a dimer upon binding ATP and localizes to the plasma membrane using C-terminal membrane targeting sequences (MTS) that insert in the membrane as an amphipathic helix (de Boer et al., 1991; Hu & Lutkenhaus, 2001, 2003; Hu et al., 2003; Mileykovskaya et al., 2003; Szeto et al., 2003; Szeto, Rowland, Rothfield, & King, 2002). It is possible that dimerization of MinD is aided by lipid vesicles by averting the MTS from the dimerization interface at physiological pH. The reports that MinD binding to anionic lipid vesicles is a cooperative process (Lackner et al., 2003; Mileykovskaya et al., 2003) and that MinD-ATP can tubulate lipid vesicles by wrapping around in a helical structure (Hu et al., 2002; Suefuji et al., 2002) suggest that MinD molecules in a polar zone might form polymers during the oscillation (Fig.5). However, the cooperative property could arise from other factors such as a physical change in the membrane. Also, MinD in the absence of MinE is seemingly evenly dispersed on the cytoplasmic membrane (Raskin & de Boer, 1999b; Rowland et al., 2000), questioning whether MinD exists as polymer on the membrane.

MinD dimerization on the membrane is required for the MinD ATPase stimulation by MinE, an activator protein for the MinD ATPase (Hu & Lutkenhaus, 2001; Hu et al., 2003; Lackner et al., 2003). This stimulation explains why MinE causes MinD to come off the membrane. MinC by

itself does not stimulate the MinD ATPase (Hu & Lutkenhaus, 1999; Raskin & de Boer, 1999a). Genetic evidence indicates that MinC and MinE compete for overlapping binding sites on the surface of a MinD dimer (L. Ma et al., 2004; W. Wu, Park, Holyoak, & Lutkenhaus, 2011b). In vitro evidence indicates that MinE displaces MinC from MinD in a step that precedes ATP hydrolysis (Hu et al., 2003; Lackner et al., 2003). However, the observation that introduction of extra copies of MinC in a wild type strain yields a filamentous phenotype (de Boer et al., 1989; Hu et al., 1999) suggests that MinC can compete with MinE.

Mutational studies of MinE confirm that the MinE activity, the ability to stimulate MinD ATPase, is a principal parameter that governs the frequency of Min oscillation (Hu & Lutkenhaus, 2001). Therefore, as the ratio of MinD to MinE increases, the frequency and speed decreases while the period of the oscillation increases (Hale et al., 2001; Lutkenhaus, 2007; Raskin & de Boer, 1999b) (Fig. 5). Intriguingly, even if the Min protein ratio is constant, the oscillation only occurs within a narrow window of Min protein concentrations (Hale et al., 2001). The Min oscillation is also controlled by temperature. A study showed that the period of MinD oscillation in rod-shaped and filamentous *E.coli* cells decreases as temperature elevates from 20 °C to 40 °C, while the characteristic wavelength remains constant (Touhami, Jericho, & Rutenberg, 2006). The quantitative analysis agrees with the idea that the MinE-dependent MinD ATPase activation is enhanced by the temperature increase.

MinE stimulates the MinD ATPase activity ten fold over the basal MinD ATPase activity (Hu & Lutkenhaus, 2001) and the MinE-dependent MinD ATPase stimulation is of cooperative nature (Hu & Lutkenhaus, 2001; Suefuji et al., 2002). The basis of the cooperative activation is, however, unknown. A model to explain the chemistry of the MinD ATPase activation by MinE

was proposed (L. Ma et al., 2004). In the structure of the *Pyrococcus furiosus* MinD, K11 interacts with D152 in helix $\alpha 7$ (Fig. 6B). In this model, the MinE^{CD} of MinE out-competes K11 for helix $\alpha 7$, so that K11 can interact with the oxygens of the α and γ -phosphate of ATP to stimulate hydrolysis. The stabilization of the leaving γ -phosphate by the basic amino acid lysine is asserted to be what makes the ATP hydrolysis energetically favorable (Fig. 6C). Inconsistent with this model, the D152A mutation, which releases K11, led to dimerization but not constitutive ATPase activity.

One of the outstanding issues is that there is no concrete data or model to clarify the ring-like structure generated by MinE during the oscillation and why the C-terminal domain of MinE (MinE^{TSD}) is so crucial to the formation of the mobile MinE ring near midcell (King et al., 2000; Rowland et al., 2000; Shih et al., 2002). When all the available evidence is combined so far, the MinE^{TSD} action seems to be somehow due to the intrinsic property of MinE^{TSD} interacting with MinE^{CD} and the MTS (residues 3-8) (Ghasriani et al., 2010; Kang et al., 2010; Park et al., 2011; Ramos et al., 2006).

x) The Theoretical Models of Min Oscillation

The phenotypic patterns routinely observed in biological organisms such as zebra, butterfly and clams are known to be caused by the differential regulation that is selectively responsive to certain thresholds of gradients of morphogens (Kondo & Miura, 2010). At the molecular level, for example, signal transduction cascades involved in the insulin release cycle depend on a series

Fig. 5 Oscillation of the Min proteins in *E. coli* [From Lutkenhaus, J (Lutkenhaus, 2007)]. MinD-ATP binds to the membrane and recruits MinC. MinE displaces MinC and stimulates MinD ATPase, causing release of proteins from the membrane. Whereas released MinE can immediately rebind to MinD on the membrane, the released MinD must undergo nucleotide exchange to regenerate MinD-ATP. In this model by Huang et al. (Huang, Meir, & Wingreen, 2003), the concentration of MinD-ATP in the vicinity of the old pole is lowered because it binds cooperatively to the membrane already containing bound MinD. In contrast, the MinD-ATP concentration increases at other pole, which lacks bound MinD. As the concentration rises, it eventually binds, forming a new polar zone. As MinE is released from the old pole, it binds to the ends of the MinD polar zone.

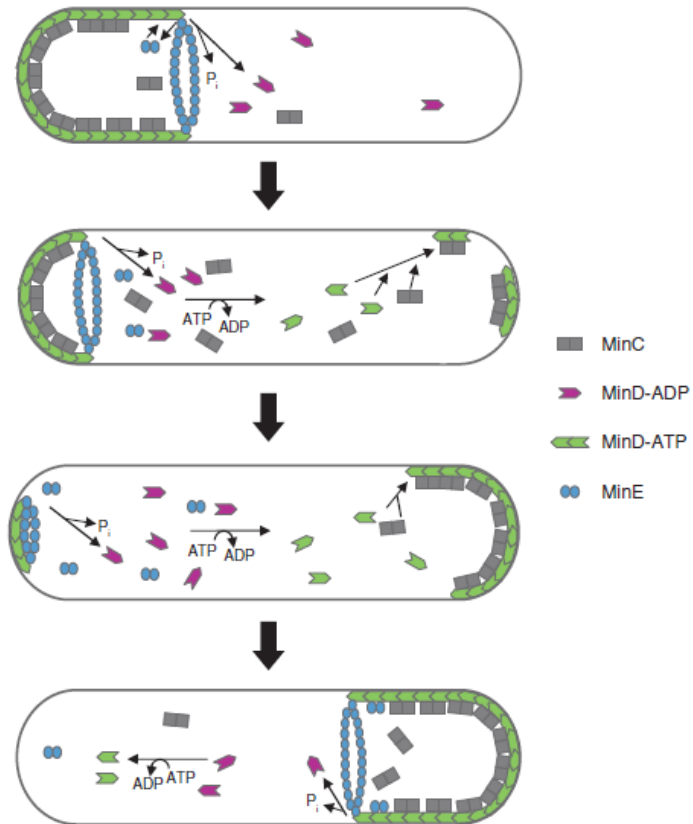
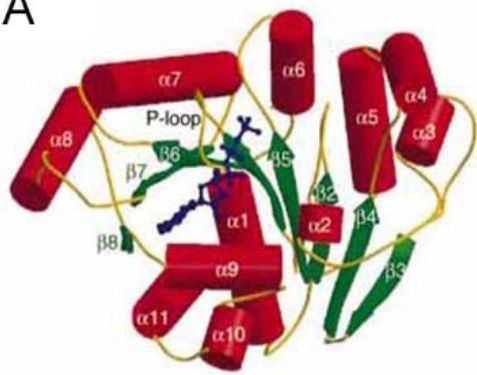
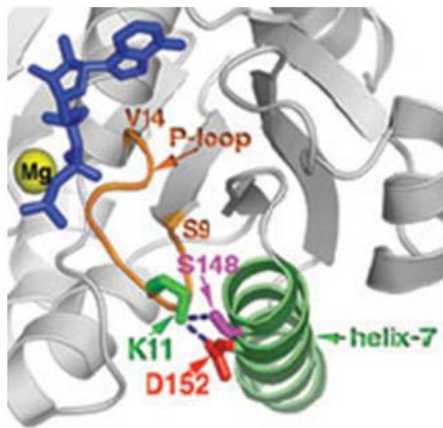


Fig. 6 Structure of *P. furiosus* MinD and model for MinE interaction with MinD. (A) Monomeric MinD in complex with AMPPCP. The α helices are in red and the β strands are in green. (B) The region of MinD putatively involved in the interaction with MinE^{CD}. AMPPCP and divalent magnesium are in blue and yellow, respectively. The side chain of K11 residue is highlighted in green. It is located within the P-loop and interacts with D152 in red and S148 in pink of the α 7 helix colored in green. (C) Binding of MinE^{CD} in yellow to the α 7 helix is proposed to disrupt the ionic interaction between K11 and D152 and the hydrogen bond between K11 and S148, releasing K11.

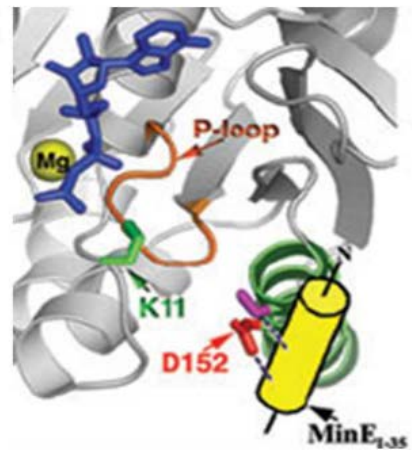
A



B



C



of biochemical reactions that periodically oscillate to coordinate insulin secretion and glucose uptake (Ravier, Gilon, & Henquin, 1999). Unique sets of enzymes and co-factors appear to have co-evolved to form modular feedback loops for biologically important functions. In *E. coli*, the spatiotemporal oscillation of the Min proteins that provides accurate positional information for cell division has been the subject of several mathematical models whose theoretical framework suggests that only a few key properties of the Min proteins can account for the oscillatory dynamics. The idea that Min oscillation is a self-organized event, not requiring other proteins, has been demonstrated by reconstitution of an in vitro system containing only Min proteins, membrane surface, and ATP (Ivanov & Mizuuchi, 2010; Loose, Fischer-Friedrich, Herold, Kruse, & Schwille, 2011; Loose, Fischer-Friedrich, Ries, Kruse, & Schwille, 2008). Most models thus include only MinD and MinE for the analysis. They are based on a reaction-diffusion style mechanism in which a dynamic instability, a spontaneous fluctuation originating from the homogenous distribution of the Min proteins, combined with differences in diffusion of the Min proteins in the cytoplasm and on the membrane, triggers a series of self-organized events and leads ultimately to ordered pattern formation (Howard & Kruse, 2005).

The inherent properties of the Min proteins that culminate in the oscillatory pattern, however, are different in each of those models: That is, protein synthesis and turnover, binding constant, negative and positive cooperativity on the membrane localization, diffusion rate in the cytoplasm and on the membrane, nucleotide hydrolysis and exchange rate, polymerization and depolymerization were selectively and preferentially weighed in each regime (Cytrynbaum & Marshall, 2007; Derr, Hopper, Sain, & Rutenberg, 2009; Drew, Osborn, & Rothfield, 2005; Fange & Elf, 2006; Howard & Rutenberg, 2003; Howard, Rutenberg, & de Vet, 2001; Huang et al., 2003; Kerr, Levine, Sejnowski, & Rappel, 2006; Kruse, 2002; Meacci & Kruse, 2005;

Meinhardt & de Boer, 2001; Tostevin & Howard, 2006). For instance, the persistent MinE retention on the membrane indispensable for the oscillation is achieved in one model by the cytoplasmic MinDs that inhibit MinE dissociation from the membrane (Howard et al., 2001), while in another scheme MinE dissociated into the cytoplasm after peeling MinD off the membrane has a low diffusion rate in solution and hence rapidly rebinds to MinDs on the membrane (Derr et al., 2009; Huang et al., 2003; Meacci & Kruse, 2005). Despite the lack of solid experimental data for certain parameters and the disparities among those regimes, ironically, most differential equations that incorporate aforementioned sets of properties and simulate the concentration changes of the Min oscillator in the cytoplasm and on the membrane have been able to generate the oscillations in their respective models.

Even within the reaction-diffusion schemes, the various models can be divided into two classes. Some theoretical models referred to as a stochastic or a probabilistic take the relatively small numbers of the Min proteins in vivo into consideration (Fange & Elf, 2006; Howard & Rutenberg, 2003; Kerr et al., 2006; Tostevin & Howard, 2006). A deterministic or a mean field model captures local concentration changes from a fixed averaged rate over time and does not need a detailed specification of an elementary event (Cytrynbaum & Marshall, 2007; Drew et al., 2005; Huang et al., 2003; Meacci & Kruse, 2005; Meinhardt & de Boer, 2001). In a stochastic regime an inherent randomness or noise can be essential for pattern formation. For example, in the deterministic scheme, the depletion of the Min proteins in the cytoplasm during oscillation is required, but in the stochastic regime it is not necessary. Since the realization that the diffusion rate of the Min proteins and ATP hydrolysis are not sufficient to recapitulate the oscillation (Howard et al., 2001; Kruse, 2002; Meinhardt & de Boer, 2001), nonlinear types of interaction among components has been incorporated into some models, which can be further categorized

into two classes (Kruse, Howard, & Margolin, 2007). One is cooperative attachment (CA) models where cooperative attachment of MinD molecules to the membrane is taken into account (Howard et al., 2001; Huang et al., 2003; Loose et al., 2008). The other type is aggregation current (AC) models in which attractive interactions between membrane-bound MinD molecules are considered important (Cytrynbaum & Marshall, 2007; Drew et al., 2005; Kruse, 2002; Meacci & Kruse, 2005). Both types of models simulate general properties of MinD dynamics and are supported by certain experimental evidence. Nonetheless, they did not incorporate detailed molecular interactions into their respective schemes.

The Min oscillation mechanism surely demands more concrete data for the properties of the Min oscillator as recent adoption of MinE membrane binding exemplifies. So far among all the reaction-diffusion schemes a deterministic CA model has been well-accepted which takes into account the ATP nucleotide exchange rate and, arguably, linearly cooperative MinD localization to the existing MinD on the membrane (Huang et al., 2003). Recently, however, an AC style model has been put forward, where some of the important parameters employed in all the reaction-diffusion style models such as the depletion of Min proteins in the cytoplasm has been called into question (Ivanov & Mizuuchi, 2010). This new scheme involved the initiation and inhibition of centers for MinD binding on the membrane, by a yet-to-be clarified mechanical membrane stress.

xi). The Aims and Significance of Our Study

The three MinD structures obtained from archaea species were all crystallized as monomers (Cordell & Lowe, 2001; Hayashi et al., 2001; Sakai et al., 2001). Nonetheless, the structures of the WACA family member proteins available hitherto have been shown to exist as dimers (Leonard et al., 2005; Schindelin et al., 1997; T. Zhou, Radaev, Rosen, & Gatti, 2001). Likewise, both the in vivo and in vitro evidence suggests that MinD dimerizes in an ATP-dependent manner (Hu et al., 2003; Szeto et al., 2003). So, solving the structure of *E. coli* MinD in the presence of ATP is imperative to confirm that MinD-ATP indeed exists as a dimer and to understand why the ATP-dependent dimerization is a pre-requisite for the interaction with MinC and MinE. To this end, it was already shown that a WACA family protein Soj can be crystallized as a dimer if an ATP hydrolysis-deficient catalytic mutant is used (Leonard et al., 2005). Therefore, we will try to determine the MinD-ATP structure using a catalytic mutant. Our laboratory has already isolated and characterized a few catalytic mutant forms of MinD such as D152A, N45A, and D40A that are highly soluble when the C-terminal MTS comprised of 10 amino acids is removed. This version, labeled as MinD delta10 ($\Delta 10$), is capable of interacting with MinC and MinE in solution even in the absence of any membrane phospholipids. Moreover, several conditions where these mutant forms of MinD-ATP are readily crystallized have been catalogued through preliminary screening processes.

A pilot study in our laboratory revealed that MinD mutants such as M193L and E53K can activate MinC but cannot interact with MinE. Importantly, these residues (each on a different subunit) come together upon dimerization based on homology model using Soj-ATP as a template for the dimer. We will adopt an extensive site-directed mutagenesis strategy to test our hypothesis that the ATP-dependent dimerization of MinD creates the MinE binding sites at the dimeric interface. Testing this idea is important in that as discussed earlier a model proposed

using the structure of the *Pyrococcus furiosus* MinD-AMPPCP monomer emphasized only the role of the α -7 helix of MinD in MinE binding (L. Ma et al., 2004). The same is true for MinC, so using the strategy adopted for studying MinE binding we will create a map for the residues critical for the interaction with MinC. Once we identify MinD residues involved in MinE interaction from the study above, we will employ a random mutagenesis methodology to obtain MinE mutants that regain interaction with the MinD mutants. Hopefully, those MinE mutants will provide information concerning the orientation of the N-terminal MinE^{CD} binding to the MinD-ATP dimer.

In our preliminary investigation, we found that mutations in position I24 of MinE rescue MinD^{M193L} but not MinD^{E53K}. Considering that a previous genetic study excluded an involvement of the I24 residue in MinD binding (L. Y. Ma et al., 2003), we postulate that the I24 mutations release the β 1 strand to interact with MinD. In this regard, the MinD^{M193L} mutant is deficient in sensing MinE and causing the release of the β 1 strand whereas the MinD^{E53K} mutant is defective in MinE binding. Hence, our hypothesis that EcMinE undergoes a conformational switching from 4 β to 6 β strand to interact with MinD will be further tested with biochemical and genetic analysis. The crystallization of a catalytic mutant form of MinD with MinE is conceivable.

In the light of the previous report that the MinE mutants such as MinE^{L22D} and MinE^{I25R} are localized to the membrane in a MinD-independent manner (L. Y. Ma et al., 2003), we hypothesize that the N-terminal α helix (residues 3-8) that interacts with the β sheet in the NgMinE structure (Ghasriani et al., 2010) could be a MTS that is released by mutations such as L22D and I25R in MinE. Accordingly, we will use the MinE mutants such as MinE^{I25R}-GFP to

examine if the introduction of the mutations intended to disrupt the MTS prevents the membrane targeting of those MinE mutants. If it is confirmed that the helix is a de facto MTS, we will look into the significance of the MinE membrane binding through phenotypic characterization.

Chapter II

Determination of the structure of the MinD-ATP complex reveals the orientation of MinD on the membrane and the relative location of the binding sites for MinE and MinC

Abstract

The three Min proteins, which spatially regulate *Z* ring positioning in *E. coli*, are dynamically associated with the membrane. MinD binds to vesicles in the presence of ATP and can recruit MinC or MinE. Biochemical and genetic evidence indicates the binding sites for these two proteins on MinD overlap. Here we solved the structure of a hydrolytic-deficient mutant of MinD truncated for the C-terminal amphipathic helix involved in binding to the membrane. The structure solved in the presence of ATP is a dimer and reveals the face of MinD abutting the membrane. Using a combination of random and extensive site-directed mutagenesis additional residues important for MinE and MinC binding were identified. The location of these residues on the MinD structure confirms that the binding sites overlap and reveals they are at the dimer interface and exposed to cytosol. The location of the binding sites at the dimer interface offers a simple explanation for the ATP-dependency of MinC and MinE binding to MinD.

Introduction

Cell division in bacteria such as *E. coli* occurs precisely at midcell due to spatial regulation of the positioning of the Z ring, which dictates the location of the divisome and thus, where division will occur (Lutkenhaus, 2007; Rothfield et al., 2005). Two negative effector systems, Min and Noc, cooperate to ensure placement of the Z ring at midcell. The Min system, consisting of MinC, MinD and MinE, prevents Z rings from forming near the poles and the Noc system prevents assembly of the Z ring over the nucleoid (Bernhardt & de Boer, 2005; E. Bi & Lutkenhaus, 1993; de Boer et al., 1989; L. J. Wu & Errington, 2004). The Min proteins undergo a coupled oscillation that produces a time-averaged gradient of MinC, an antagonist of FtsZ assembly, on the membrane that is highest at the poles and lowest at midcell (Fu et al., 2001; Hale et al., 2001). The oscillation is driven by interaction between MinD and MinE (Raskin & de Boer, 1999b). MinC is not required for the oscillation but is a passenger through interaction with MinD (Hu & Lutkenhaus, 1999; Raskin & de Boer, 1999a). Underlying the oscillation is the dynamic association of the Min proteins with the membrane. MinD binds to the membrane through the C-terminal 10 amino acids, which form an amphipathic helix that inserts into the membrane bilayer (Hu & Lutkenhaus, 2003; Szeto et al., 2002; H. Zhou & Lutkenhaus, 2003). The binding is thought to require dimerization of MinD since one copy of the amphipathic helix is insufficient to tether GFP to the membrane whereas a tandem repeat of the helix is sufficient (Szeto et al., 2003). Although MinD undergoes ATP dependent dimerization in solution (Hu et al., 2003), it is not clear if MinD dimerizes in the cytoplasm before binding to the membrane since FRET data suggests that MinD oligomerization is promoted by the presence of vesicles (Mileykovskaya et al., 2003).

MinE is a small protein of only 88 amino acids. It has been divided into two functional domains by deletion analysis (Pichoff et al., 1995; Zhao et al., 1995). Residues approximately 1-31 (MinE¹⁻³¹) constitute an anti-MinCD domain. Investigation of MinE mutations that affect MinD binding suggest a model in which the anti-MinCD domain forms an α -helix and residues from ~9-30 lying on one side of the helix contact MinD (Hu & Lutkenhaus, 2001; L. Y. Ma et al., 2003). The other domain consists of residues 32-88 (MinE³²⁻⁸⁸) and constitutes the topological specificity domain (Pichoff et al., 1995; Zhao et al., 1995). Although MinE¹⁻³¹ can counteract the inhibitory activity of MinC/MinD to prevent filamentation, it cannot spatially regulate division unless fused to MinE³²⁻⁸⁸. The recent structures of full-length MinE reveal that critical residues in the MinE¹⁻³¹ domain (around position 21) involved in MinD binding are buried in the structure, suggesting that MinE must undergo a conformational change to bind MinD (Ghasriani et al., 2010; Kang et al., 2010).

MinC consists of two functional domains (Cordell et al., 2001; Hu & Lutkenhaus, 2000). The C-terminal domain (MinC^C) is responsible for dimerization, binding to MinD and, in the presence of MinD binding to the extreme C-terminal tail of FtsZ (Hu & Lutkenhaus, 2000; Shen & Lutkenhaus, 2009). The MinC^C domain consists of a triangular α -helix with a hydrophobic face involved in dimerization (Cordell et al., 2001). The MinD binding site is located at the vertex of the triangular α -helix opposite the dimer interface (H. Zhou & Lutkenhaus, 2005). In a MinC dimer the two MinD binding sites are far apart and cannot be in contact with the same MinD dimer. The N-terminal domain of MinC is connected to the C-terminal domain through a flexible linker. This domain contacts an FtsZ subunit in the filament and may fragment the filament (Shen & Lutkenhaus, 2010).

MinD is at the center of the Min system and binds both MinE and MinC. Biochemical and genetic studies indicate that the binding sites for MinE and MinC overlap. In vitro MinD binds to vesicles in the presence of a nonhydrolyzable analog of ATP and recruits MinC (Hu & Lutkenhaus, 2001). If MinE is added, MinC is displaced consistent with the possibility that the binding sites overlap (Hu et al., 2003; Lackner et al., 2003). Stronger evidence for overlap of the binding sites comes from genetic studies (L. Ma et al., 2004). Mutations altering residues in helix 7 of MinD affect either MinC or MinE binding or both (L. Y. Ma et al., 2003). Residues S148, D154 and I159 are involved in binding to both MinC and MinE, whereas D152 is specifically required for MinE binding and L157, G158 and A161 are specifically required for MinC binding. D152 and D154 are highly conserved within the MinD subfamily, but are not conserved within the larger ParA family, consistent with a role unique to MinD.

The structures of three MinD proteins from various archaeal species have been determined (Cordell & Lowe, 2001; Hayashi et al., 2001; Sakai et al., 2001). Although two of them lack a C-terminal amphipathic helix, they contain several signature sequences indicating they are MinD homologues. The structures are monomers, even in the presence of a nonhydrolyzable analogue of ATP (Hayashi et al., 2001). In the monomer structure, D152 is one of three residues that interacts with residue K11, the signature lysine in the deviant Walker A motif. Based upon the observation that D152 is critical for MinE binding a model was proposed in which the anti-MinCD domain of MinE competes with K11 for interaction with D152, freeing K11 to interact with ATP (L. Y. Ma et al., 2003). Nevertheless, in the dimer structure of other proteins in the ParA family obtained in the presence of ATP, including Soj, the lysine corresponding to K11 interacts with ATP bound to the other monomer (Leonard et al., 2005; Schindelin et al., 1997). If MinD is similar, then the K11-D152 interaction is disrupted when MinD binds ATP and

dimerizes, a step preceding MinE binding. Consistent with this, MinD-D152A dimerizes with ADP suggesting that disrupting the K11-D152 linkage by mutation frees up K11, which promotes dimerization by interacting with ADP bound to the other monomer. Also, the MinD-D152A mutant is able to recruit MinE to lipid vesicles indicating residue D152 is not essential for MinE binding (H. Zhou et al., 2005). It should be noted, however, that the interaction of the signature lysine with an aspartic residue in the monomer is unique to MinD and is not observed in the ADP form of Soj or the iron protein of nitrogenase.

Although some residues in helix 7 of MinD have been implicated in binding to MinC and MinE, the results were largely interpreted on a MinD monomer structure (L. Y. Ma et al., 2003; H. Zhou et al., 2005). Since the binding site for MinE on MinD is not well characterized and it is now known that MinD dimerizes (Hu et al., 2003) we set out to further explore the region of MinD that is involved in binding both MinE and MinC. We started out with a random mutagenesis of MinD and followed this up with extensive site-directed mutagenesis while pursuing the structure of MinD. Determining the structure of a hydrolysis-deficient derivative of MinD, along with the mutagenesis, confirms that the binding sites for MinC and MinE overlap and reveals that they are at the MinD dimer interface, offering a simple explanation for the ATP-dependency of binding. The structure also allowed determination of the orientation of MinD on the membrane.

Results

The bacterial 2-hybrid system for assessment of the MinD – MinE interaction The region of

MinE that interacts with MinD is defined by deletion to residues 6-30 of MinE (Hu & Lutkenhaus, 2001; Pichoff et al., 1995; Zhao et al., 1995); however, the region of MinD involved with MinE is not well defined. One study indicated residue D152 of MinD was a critical residue specifically required for interaction with MinE (L. Y. Ma et al., 2003). This conclusion was based upon elimination of the strong interaction observed between MinD and MinE¹⁻³¹ in the yeast 2-hybrid system by the MinD-D152A mutation. MinE¹⁻³¹, rather than full length MinE, was used in that study since it displayed a strong interaction with MinD, whereas the interaction between MinD and full length MinE was barely detectable. Why that is the case is not completely clear since full length MinE is better than MinE¹⁻³¹ in competing with MinC for MinD in this system. This latter result suggests that full length MinE has higher affinity for MinD than MinE¹⁻³¹ or is more effective at removing MinC. In contrast to the elimination of the interaction between MinD and the MinE¹⁻³¹ by the MinD-D152A mutation we found in a previous study that full length MinE interacted with the MinD-D152A mutant in an in vitro assay involving lipid vesicles in vitro (H. Zhou et al., 2005). We observed that the MinD-D152A mutant bound to lipid vesicles and recruited MinE, even though the ATPase activity of this mutant was not stimulated by MinE. In addition, we observed that MinC displaced MinE bound to a MinD-D152A vesicle complex. This was unusual since MinE displaces MinC bound to a WT MinD-vesicle complex. Support for an interaction between MinD-D152A and MinE was also obtained from in vivo studies, which revealed that the MinD-D152A protein recruited MinE to the membrane, although not as effectively as wild type MinD (H. Zhou et al., 2005). These results were somewhat at odds to those obtained with the yeast 2-hybrid system so we investigated this further using the bacterial 2-hybrid system.

A strong interaction between MinD and MinE¹⁻³¹ was observed in this system (Table 1). A similar strong interaction was also observed between MinD and full length MinE. Why these two interactions are nearly equivalent in the bacterial 2-hybrid system and yet vastly different in the yeast 2-hybrid system is not known. The MinD-D152A mutation reduced the interaction between MinD and MinE by ~50% and the interaction between MinD and MinE¹⁻³¹ by 90%. Thus, the MinD-D152A mutation reduces the binding of MinE but has a stronger affect on the interaction between MinD and MinE¹⁻³¹ than on the interaction with full length MinE. In addition, these results indicate that the bacterial 2-hybrid system is more useful than the yeast 2-hybrid system in examining the interaction between MinD and MinE.

Isolation of MinD mutants unresponsive to MinE The above studies revealed that the MinD-D152A mutation reduced but did not eliminate the interaction between MinD and MinE. To obtain more information about the region of MinD involved in the interaction with MinE we screened for MinD mutants that fail to respond to MinE while retaining the ability to activate MinC. This approach should eliminate MinD mutants that do not fold properly since interaction with MinC is required. To do this screen pSEB104CDE ($P_{ara}::minC\ minD\ minE$) was mutagenized by passage through the mutagenic strain XL-1 Red and transformed into the *min* deletion strain JS964 ($\Delta min::kan$). With no mutation on the plasmid this strain displays a minicell phenotype in the absence of arabinose whereas in the presence of arabinose it displays a wild type morphology due to expression of the *min* operon. Colonies were patched onto plates containing 0.1% arabinose and those that did not grow were candidates.

Table 1. Bacterial two-hybrid system for analysis of MinD–MinE interaction.

| | |
|----------------------------------|-------------------------|
| MinE–MinD | 100% (330) ^a |
| MinE ^{1–31} –MinD | 120% (398) |
| MinE–MinD-D152A | 44% (145) |
| MinE ^{1–31} –MinD-D152A | 8% (28) |

a. The numbers in parentheses are units of β -galactosidase activity.

Fig. 7 MinD-M193L does not respond to MinE. JS964 (Δ min) containing pSEB104CD (Para::minC minD) carrying WT MinD or MinD-M193L was transformed with a plasmid carrying MinE (pJPB216 [Plac::minE]) or the corresponding vector. A colony from each transformation was picked into 500 μ l of LB, serially diluted tenfold and 2.5 μ l of each dilution was spotted on plates containing 0.1% arabinose (to induce MinCD) and 100 μ M IPTG (to induce MinE).

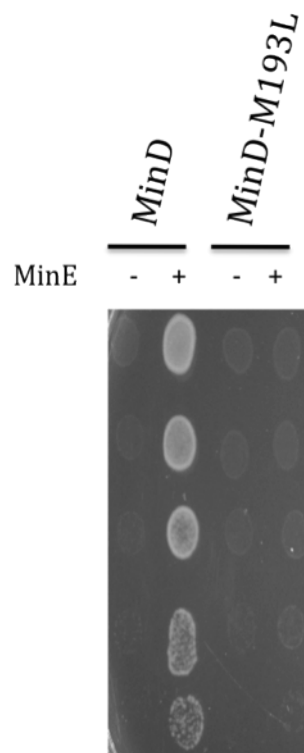


Fig. 8 MinD-M193L recruits MinC to vesicles and is unresponsive to MinE. MinD or MinD-M193L was mixed with Male-MinC^c in the presence of ADP or ATP and vesicles. MinE was added as indicated. Vesicles were collected by centrifugation and the bound proteins analyzed by SDS-PAGE.

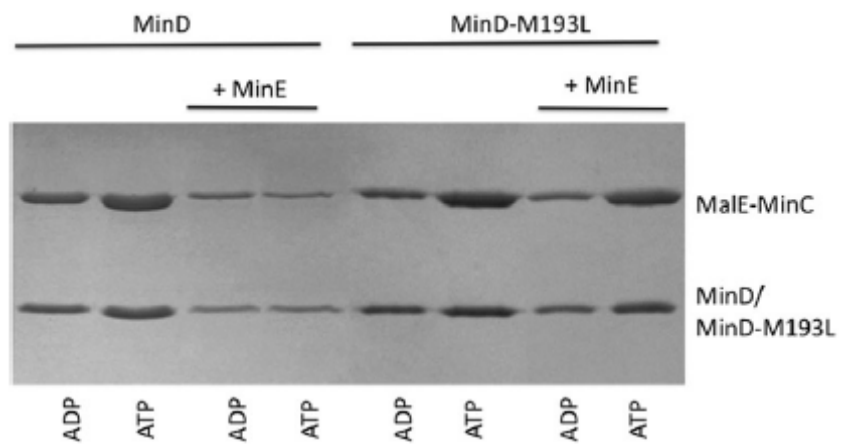
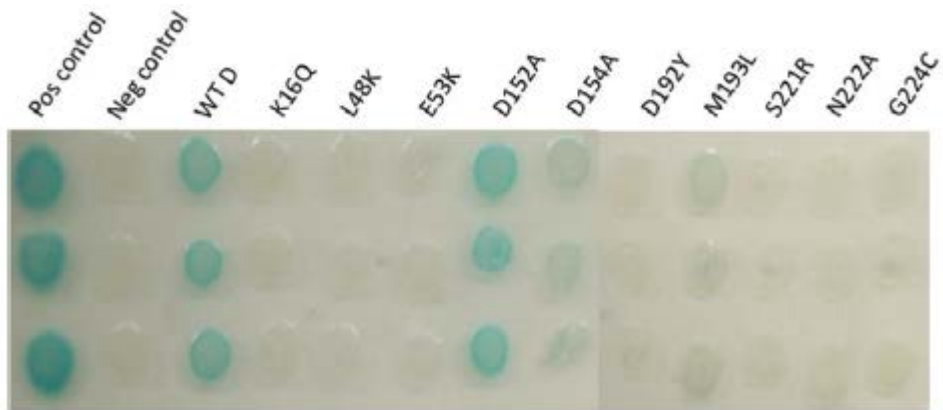


Fig. 9 Bacterial 2 hybrid analysis of MinD mutants that fail to respond to MinE but activate MinC. MinD and MinE were fused to the C-termini of the T18 and T25 fragments of adenyl cyclase. Plasmids containing these fusions were cotransformed into BTH101 (Δ min). Three transformants for each were picked into media and spotted on LB plates supplemented with X-gal and antibiotics. The appearance of blue color indicates a positive reaction. The positive control were fusions to bZIP and the negative control contained plasmids expressing T25-MinD and the T18 vector. The plates were incubated overnight at 30°C.



Out of approximately 500 colonies screened 30 were obtained that did not grow when the *min* operon was induced. The inability to grow under inducing conditions correlated with filamentation and could be due to: 1) mutations that inactivate MinE, or 2) mutations that alter MinD such that it does not respond to MinE even though it must still interact with MinC. To differentiate between these two possibilities a compatible plasmid (pJPB216 [$P_{lac}::minE$]) carrying MinE was introduced into each of the candidates to determine if it could rescue growth. Of the 30 candidates 13 could be rescued by expressing MinE in trans indicating they contained a mutation in MinE. Sequencing these candidates confirmed mutations in MinE including A15T, R21W, R31A, P36S and stop codons at codons 20, 23, 35, 55 and 65. The stop codon mutations are likely to produce a nonfunctional MinE due to truncation and A15T mutant was previously shown to result in a reduced interaction with MinD. R21 is conserved in all bacterial MinEs and is likely to be important for MinD-MinE interaction.

The mutants that could not be rescued by MinE in trans were expected to have mutations in MinD. Sequence analysis revealed that several of the mutants contained multiple mutations and others that contained single mutations. The latter included MinD-E53K, -D192Y, -M193L, and -G224C. To confirm these mutations they were introduced by site-directed mutagenesis into a plasmid containing MinC/MinD under arabinose promoter control (pSEB104CD [$P_{ara}::minC minD$]). The resultant plasmids were transformed into JS964 (Δmin) along with a compatible plasmid (pJPB216 [$P_{lac}::minE$]) carrying MinE. Although MinE rescued the lethality due to expression of WT MinD (along with MinC) it could not rescue the lethality caused by the four MinD mutants (Fig. 7, results with MinD-M193L, but results were the same for all four; immunoblots revealed all four were stable).

To check these results in vitro we attempted to purify the four mutants. Since MinD-M193L and MinD-G224C could be readily purified they were tested in a vesicle-binding assay. Similar to MinD, MinD-M193L and MinD-G224C bind to vesicles in an ATP-dependent manner and recruit MinC (Fig. 8; only MinD-M193L is shown). The addition of MinE removes wild-type MinD and MinC from the vesicles, however, MinE is unable to displace MinD-M193L and MinC from the vesicles. These results confirm that MinD-M193L binds MinC but is unable to respond to MinE. The same results were obtained with MinD-G224C (data not shown).

Since the other two MinD mutants were more difficult to purify we checked if the failure of MinE to rescue these MinD mutants was due to loss of interaction in the bacterial 2-hybrid system. MinD-E53K, -D192Y, -M193L and -G224C all showed a dramatic decrease in interaction with MinE (Fig. 9). The controls included MinD-D152A, which was positive (also Table 1), MinD-D154A, which was only very weakly positive, and MinD-K16Q, which cannot bind ATP, and served as a negative control. Thus, all four of the MinD mutants we isolated failed to bind to MinE even though they activate MinC.

Structure of MinD The structures of three MinD-like proteins from several archaeal species have been determined. Although all three contain several signature motifs that characterize them as MinD homologues, two lack the C-terminal amphipathic helix for binding to the membrane. The structures of all three are monomers with ADP or no nucleotide, and one was a monomer in the presence of a nonhydrolyzable analogue of ATP (Cordell & Lowe, 2001; Hayashi et al., 2001; Sakai et al., 2001). However, it is known that the *E. coli* MinD does not respond to most nonhydrolyzable analogues of ATP (Hu et al., 2002). MinD dimerizes in the presence of ATP but is not soluble at high concentrations (Hu et al., 2003). In contrast, a truncated version of MinD

(MinD Δ 10) missing the carboxy 10 amino acids is very soluble (Hu et al., 2003). This protein is only missing the amphipathic helix so it is possible that the structure might still give information about how the protein is positioned on the membrane. Since several ATP analogues (ATP γ S and AMPPCP) were unable to support MinD dimerization (Hu et al., 2002), two approaches were used to try and capture MinD in the dimeric state. The first involved crystallization of MinD Δ 10-D152A in the presence of ADP, since ADP promotes dimerization of this mutant as well as the binding of both MinC and MinE (H. Zhou et al., 2005). One condition was found in which crystals were obtained, however, they did not diffract well. Nonetheless, this condition proved useful for obtaining crystals of a second hydrolysis-deficient mutant of MinD. This mutant was obtained by introducing a D40A mutation. Mutating the equivalent residue in the closely related Soj protein produced a hydrolysis-deficient version of the protein that was crystallized as a dimer (Leonard et al., 2005).

A MinD mutant deficient in ATP hydrolysis would be expected to bind the membrane, MinC and MinE but would not be able to undergo oscillation and spatially regulate division. To determine if MinD-D40A behaved as expected we checked if it was able to activate MinC and respond to MinE. The growth of JS964 (Δ min) containing pSEB104CD ($P_{ara}::minC\ minD\text{-}D40A$) was inhibited by arabinose indicating MinD-40A activated MinC (Fig. 10A). Addition of MinE (pJPB216[$P_{lac}::minE$]) allowed growth and prevented filamentation indicating that MinD-D40A also responded to MinE, nonetheless, the morphology was heterogeneous indicating a defect in spatial regulation of division. Checking the oscillation revealed that gfpMinD-D40A was on the membrane but did not undergo oscillation in the presence of MinE (data not shown).

Fig. 10 Characterization of MinD-D40A. (A) The ability of MinD-D40A to activate MinC and respond to MinE was determined. JS964 (Δ min) containing pSEB104CD carrying WT MinD or MinD-D40A was transformed with a plasmid carrying MinE or the corresponding vector. A colony from each transformation was picked into 500 μ l of LB, serially diluted tenfold and 5 μ l of each dilution was spotted on plates containing 0.1% arabinose (to induce MinCD) and 5 μ M IPTG (to induce MinE). (B) MinD-D40A binds MinC and MinE in vitro. MinD-D40A was incubated with vesicles in the presence of ATP or ADP. MinE, MalE-MinC^c or both were added and vesicles recovered by centrifugation. Bound proteins were determined by analyzing the pellets on SDS-PAGE.

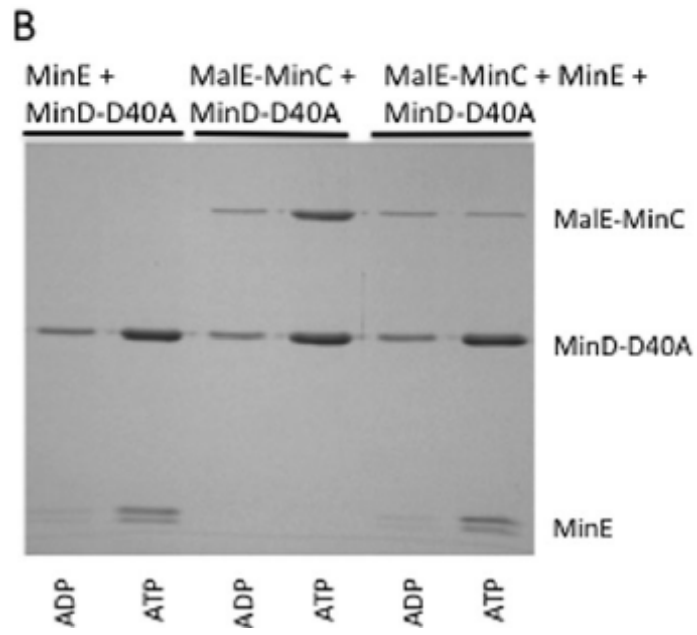
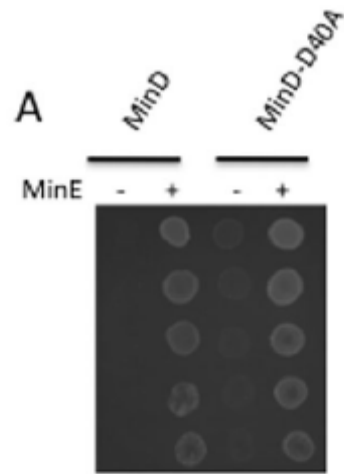
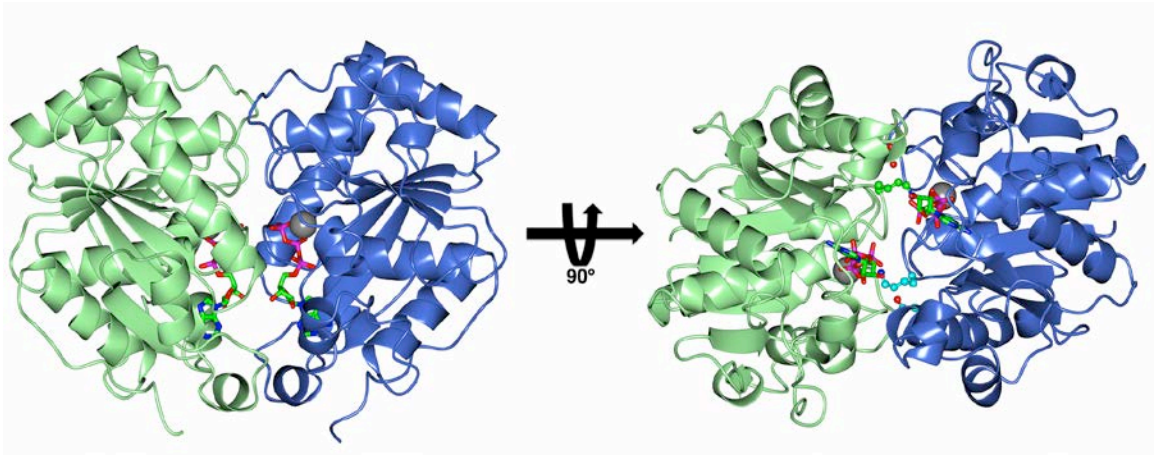


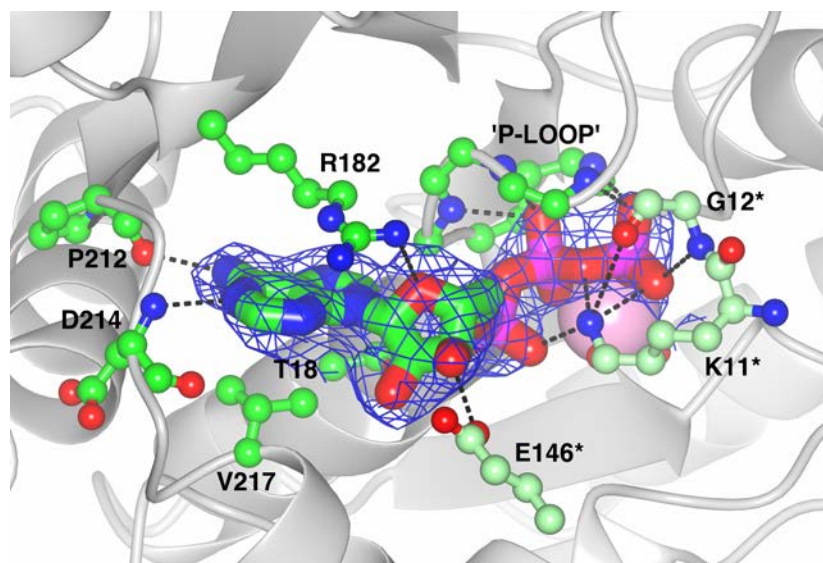
Fig. 11 MinD^{D40A}Δ10 structure.

A. The dimeric structure of MinD. Each monomer is indicated by different coloring and the ATPs and Mg ion are indicated.

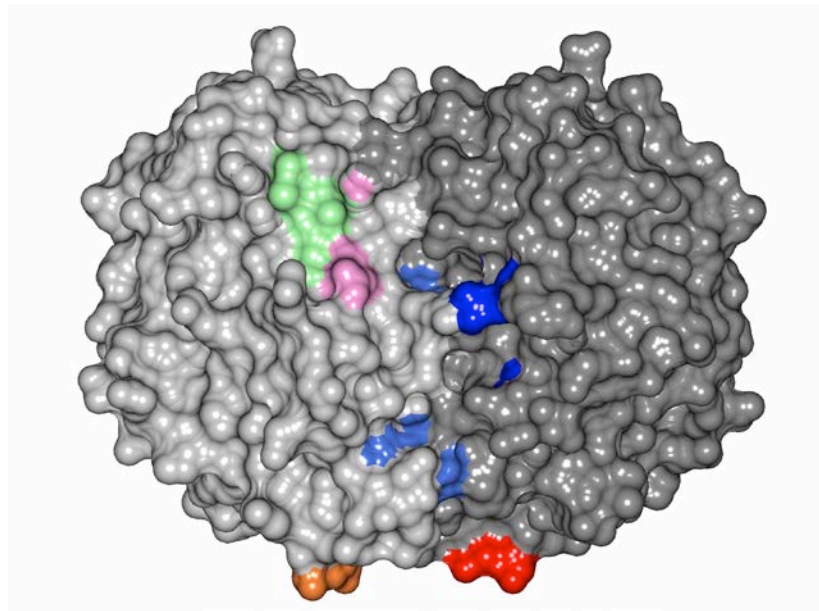


B. Residues interacting with ATP. Residues important for ATP binding are indicated in green.

The three residues reaching across the dimer interface are light green and have an *.



C. Location of the 4 residues identified in the random screen that are important for MinE interaction but not for MinC (indicated in blue). The location of D152 (blue), D154 and I159 (pink; involved in both MinC and MinE interaction) and L157, G158 and A161 (green; specifically required for MinC interaction) are also indicated. The C-terminal glutamate residues are colored red and orange.



D. Location of residues involved in interaction with MinE and MinC. The structure is of the MinD dimer with residues colored as in B. For all residues the lighter shade is the monomer to the left and the darker shade is the monomer to the right. Residues not involved in binding MinC or MinE are colored yellow. Three types of residues important for binding are indicated. Those specifically involved in MinE binding are blue, those specifically involved in MinC binding are green and those involved in both MinC and MinE binding are pink. The C-terminal glutamates are colored red and orange.

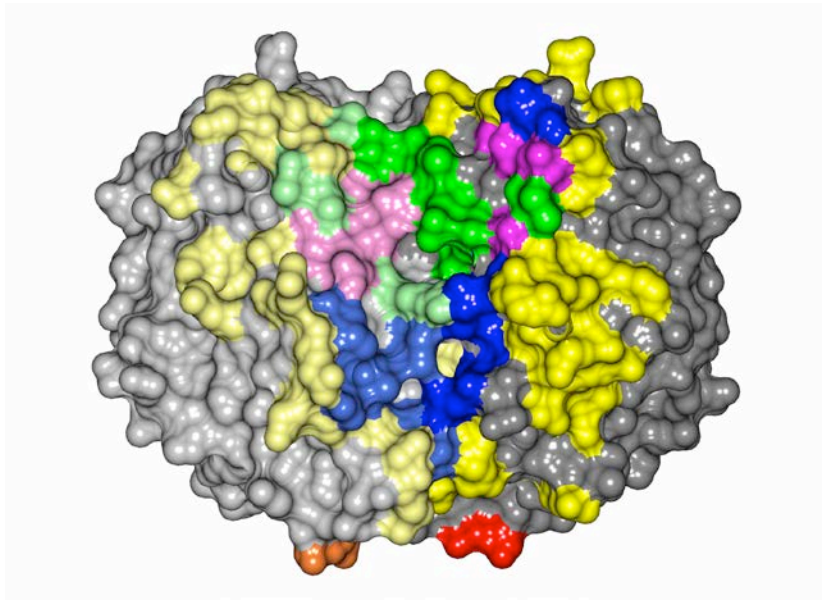


Table 2. ATPase activity of MinD-D40A.^a

| | - MinE | + MinE |
|-----------|--------|--------|
| MinD | 0.9 | 18.6 |
| MinD-D40A | 0.5 | 2.1 |

a. The ATPase activity is nmoles of Pi released $\text{mg}^{-1} \text{min}^{-1}$.

Table 3. Crystallographic data and model statistics for the 2.4 Å structure of the MinDΔ10-D40A-Mg-ATP complex.

| Data statistics | | Model statistics | |
|----------------------------------|-----------------------------------------------|------------------------------------------------------------|----------------------|
| Wavelength (Å) | 0.9 | Resolution range | 68.2–2.34 |
| Space group | P2 ₁ 2 ₁ 2 ₁ | Completeness % (after LTD correction) | 96 (92) ^a |
| Unit cell | <i>a</i> = 83.7 Å | No. of ASU molecules | 2 |
| | <i>b</i> = 86.6 Å | <i>R</i> _{free} | 30.7 (43.3) |
| | <i>c</i> = 110.7 Å | <i>R</i> _{work} | 26.6 (35.3) |
| | $\alpha = \beta = \gamma = 90.0^\circ$ | Estimated co-ordinate error based on maximum likelihood, Å | 0.4 |
| Resolution limits, Å | 100–2.35 | Bond length rmsd, Å | 0.01 |
| No. of unique reflections | 33 366 | Bond angle rmsd | 1.35 |
| Completeness, % (all data) | 96.8 (94.6) | Ramachandran Statistics (preferred, allowed, outliers) % | 95, 4, 1 |
| Redundancy | 3.8 (3.6) | Average B factors (Å ²) Protein | 37.4 |
| <i>I</i> / σ (<i>I</i>) | 10.4 (2.0) | Water | 37.9 |
| <i>R</i> _{merge} | 0.04 (0.34) | ATP | 27.3 |
| | | Magnesium ions | 25.7 |
| | | Refined residues/waters/ATP/magnesium ions | 516/240/2/2 |

a. The values in parentheses represent the statistics for the highest resolution shell (2.43-2.34 angstroms).

Purification of the full length version of MinD-D40A revealed that it bound to vesicles in ATP-dependent fashion. It was able to recruit MinC to the vesicles and the MinC was displaced by MinE. Importantly, MinE was unable to cause release of MinD-D40A from the vesicles but bound to the MinD-40A-vesicle complex (Fig. 10B). Although MinE was recruited to vesicles by MinD-40A it was unable to stimulate its ATPase activity (Table 2). Thus, MinD-D40A interacts with its partners and behaved as expected for a hydrolysis-deficient mutant. A C-terminal truncated version (MinD Δ 10-D40A) was purified and size exclusion chromatography confirmed it underwent ATP-dependent dimerization (data not shown).

MinD Δ 10-D40A crystallized in the presence of ATP using the same conditions that allowed MinD Δ 10-D152A to crystallize (Table 3). Determination of the structure at a resolution of 2.4 \AA confirmed that MinD formed a nucleotide sandwich dimer similar to Soj and nitrogenase (Fig. 11A). Examination of the structure confirms that the signature lysine in the deviant Walker A motif no longer interacts with D152 but reaches across the interface to interact with the phosphates of ATP bound to the other monomer (Fig. 11A and 11B). Thus dimerization, and not MinE, is responsible for breaking the D152-K11 interaction ruling out the previous model for the role of MinE in the activation of the MinD ATPase.

Three residues, D152, S148, and E146, interact with K11 in the monomer (Hayashi et al., 2001). In the dimer S148 interacts with N45A in the other monomer and E146 makes contact with the ribose ring of ATP bound to the other subunit. These two contacts are not essential for dimer formation since MinD-S148A and MinD-E146A mutants still dimerize (H. Zhou et al., 2005), although the ATPase activity of MinD-E146A is not stimulated by MinE. In contrast, the K11-

ATP interaction is important since MinD-K11A does not dimerize (H. Zhou et al., 2005). G12 also makes contact with the γ -phosphate of ATP across the dimer interface (Fig 11B).

Although the C-terminal 10 amino acids constituting the amphipathic helix were removed to obtain a more soluble version of MinD, the structure still gives information about the orientation of MinD at the membrane surface. MinD is ~20 residues longer than Soj or the archeal MinD-like proteins that lack the amphipathic helix. The structures of Soj and these latter proteins terminate in a helix that angles away from the bottom of the structure (as drawn in Fig. 11A) towards the top. In the MinD Δ 10 structure the final 10 amino acids, including the three glutamates (colored red and orange in Fig. 11D) that precede the alpha helix, are visible and extend from the terminal helix to the bottom of the structure as drawn in Fig. 11. Since only the residues comprising the amphipathic helix, which would be embedded in the membrane bilayer (H. Zhou & Lutkenhaus, 2003), are missing the bottom face of the dimer must be near the membrane (Fig 11C).

The mutations isolated earlier (L. Ma et al., 2004) that affect MinC and or MinE binding are located in helix 7 and map to the monomer on the left (colored green and pink in Fig. 11C with D152 colored blue in the middle of the structure). In contrast, the residues altered by the four mutations isolated in the random mutagenesis in this study are located near the dimer interface; two residues from each monomer (Fig. 11C). This result suggests that the MinE binding site is at the MinD-dimer interface and is formed upon dimerization. To further test this possibility we performed site directed mutagenesis.

Table 4. Summary of MinD mutations

| Residue | MinC Activation ¹ | Rescue by MinE ² | Interaction with MinE (B2H) ³ | Self-Dimerization (B2H) ⁴ |
|---------|------------------------------|-----------------------------|------------------------------------------|--------------------------------------|
| G42D | 0 | N/A | 0 | ++ |
| L43D | 0 | N/A | 0 | ++ |
| R44G | 0 | N/A | +++++ | ND |
| D47R | 0 | N/A | 0 | + |
| L48K | +++++ | + | 0 | |
| G51D | +++++ | +++++ | | |
| C52A | +++++ | +++++ | | |
| C52R | +++++ | +++++ | | |
| E53A | +++++ | 0 | ND | |
| E53K | +++++ | 0 | 0 | |
| R54E | +++++ | +++++ | | |
| R55E | +++++ | +++ | +++++ | |
| V56E | + | N/A | 0 | +++++ |
| V57E | + | N/A | +++++ | |
| Y58D | + | N/A | + | +++++ |
| D59R | 0 | N/A | 0 | 0 |
| V61E | + | N/A | 0 | +++++ |
| N62K | ++ | N/A | + | +++++ |
| Q65R | +++++ | +++ | +++++ | |
| D67R | +++++ | ++ | ++ | |
| Q72R | +++++ | +++++ | | |
| I75D | +++++ | +++++ | | |
| K76D | +++++ | +++++ | | |
| K78A | +++++ | ++++ | | |
| R79D | +++++ | +++++ | | |
| Q90A | ++ | N/A | +++++ | |
| T91K | 0 | N/A | +++++ | |
| R92A | 0 | N/A | +++++ | |
| D93R | +++++ | +++++ | | |
| K94D | 0 | N/A | ++ | +++++ |
| D95R | +++++ | +++++ | | |
| T98D | +++++ | ++++ | | |
| R99D | +++++ | +++++ | | |
| E100K | +++++ | +++++ | | |
| K104E | +++++ | ++++ | | |
| E146K | 0 | N/A | 0 | 0/+ |
| V147E | +++++ | 0 | 0 | |
| S148E | 0 | N/A | 0 | +++ |
| V150E | 0 | N/A | 0 | 0 |

| | | | | |
|-------|-------|-------|-------|-------|
| R151A | + | N/A | +++++ | |
| D154A | + | N/A | + | +++++ |
| R155E | + | N/A | 0 | +++ |
| L157D | + | N/A | 0 | + |
| G158R | + | N/A | +++++ | |
| I159D | ++++ | +++++ | | |
| A161R | ++ | N/A | +++++ | |
| S162K | +++++ | ++++ | ++++ | |
| K163D | +++++ | +++++ | +++++ | |
| A167K | +++++ | ++++ | | |
| E168A | +++++ | ++++ | | |
| N169R | +++++ | +++ | | |
| G170R | +++++ | +++++ | | |
| E172K | +++++ | +++++ | | |
| P173R | 0 | N/A | +++++ | |
| K175D | +++++ | +++++ | | |
| E176K | +++++ | +++++ | | |
| R187A | +++++ | +++++ | | |
| V188E | +++ | N/A | 0 | 0 |
| R190A | +++++ | +++++ | | |
| G191E | +++++ | +++++ | | |
| G191R | +++++ | +++++ | | |
| D192Y | +++++ | 0 | 0 | |
| M193L | +++++ | + | + | |
| L194D | +++++ | + | 0 | |
| S195R | +++++ | +++++ | | |
| E197K | +++++ | +++++ | | |
| D198R | +++++ | 0 | + | |
| E201A | +++++ | +++++ | | |
| I202D | +++++ | 0 | 0 | |
| R204A | +++++ | +++++ | | |
| K206E | +++++ | +++++ | | |
| D214A | +++++ | +++++ | | |
| Q215E | +++++ | +++ | | |
| L218E | ++++ | ++ | 0 | |
| R219A | +++++ | +++++ | | |
| S221A | +++++ | +++++ | | |
| S221R | +++++ | + | 0 | |
| N222A | +++++ | 0 | 0 | |
| N222E | +++++ | + | | |
| N222R | +++++ | + | | |
| G224C | +++++ | 0 | 0 | |
| E225K | +++++ | +++++ | | |
| L229K | +++++ | +++++ | | |

| | | | | |
|-------|-------|-------|--|--|
| N232A | +++++ | ++++ | | |
| I246D | +++++ | +++++ | | |
| F253D | +++++ | +++++ | | |

Note

For all assays the tests were scored qualitatively. N/A, not applicable.

¹MinC activation was scored as follows: 0 = no activation, cells grow fine; +++++ = no growth; in cases where there was some growth it is indicated by + to ++++

²Rescue from MinC/MinD killing. 0 = no rescue; +++++ = complete rescue; partial rescue was scored from + to ++++.

³Interaction between MinD and MinE assayed by growth with X-gal. 0 = no color development; +++++ = dark blue; lighter colors were scored from + to ++++.

⁴MinD self-interaction assayed by growth with X-gal. 0 = no color development; +++++ = dark blue; lighter colors were scored from + to ++++.

Site-directed mutagenesis to more fully characterize the binding sites With the availability of the MinD structure we carried out additional site-directed mutagenesis to further characterize the MinE binding site. For this analysis, we used the two-plasmid system (pSEB104CD [$P_{ara}::minC$ $minD$] and pJB216 $P_{lac}::minE$) used above to confirm the mutations from the random mutagenesis. Mutations were introduced into *minD* on pSEB104CD and their effect was determined by examining the ability of the plasmid to prevent the growth of JS964 (Δmin) when induced. If the mutant MinD was able to activate MinC, pJPB216 was introduced to determine if the mutant was able to respond to MinE. Using this approach we found the following nine MinD mutants that were able to activate MinC but were unable to respond to MinE: L48K, D67R, V147E, L194D, D198R, I202D, L218E, S221R and N222A (Table 4). This response was tested at two levels of MinE, the basal level of expression and that produced by 100 μ M IPTG. None of the mutants, including the four from the random mutagenesis, were rescued by the basal expression of MinE, which is sufficient to overcome lethality caused by wild type MinD. In addition, most of the mutants were not rescued with the higher level of MinE induced by 100 μ M IPTG (Fig. 13, MinD-M193L). Only the MinD-D67R mutant was rescued by the induced level of MinE suggesting it binds MinE weakly. Examination of these mutants with the bacterial 2-hybrid system revealed a reduction in interaction with MinE; D67R produced pale blue colonies whereas the others produced white colonies (data not shown, and Fig. 9, L48K and S221R are shown). The weak interaction observed between D67R and MinE is consistent with it responding to a high level of MinE.

A number of other MinD mutants were generated that activated MinC and responded to MinE: MinD-G51D, -C52A, -C52R, -R54E,R55E -Q65R, -Q72R, -I75D, -K76D,K78A,R79D -D95R, -T98D, -R99D, -E100K, K104E, -S162K, -K163D, -A167K, E168A, -N169R, -G170R, -E172K, -K175D, -E176K, -R187A, -R190A, -G191E, -S195R, -E197K, -E201A,-R204A-K206E, -D214A, -Q215R, -R219A, -E225K, -L229K, -N232A, -I246D, F253D (Table 4). Since these residues surround those that are required for MinE binding, a more complete picture of the surface of MinD involved in the interaction with MinE emerges (Fig. 11D; residues required for binding are in blue and those not required are yellow; note residues on the left monomer are a lighter shade). From this result it is clear that residues required for MinD binding come together upon dimerization. During the above mutagenesis we also isolated several mutants in which the activation of MinC was lost but MinE binding, determined by the bacterial 2-hybrid system, was not affected (Table 4). These included MinD-R44A, -V57E, -Q90A, -T91K, -R92A, -R151A, -G158R, -I159D, -A161R and -P173R. Locating these residues on the MinD structure (Fig. 11D; residues in green), as well as those not required for MinC activation (Fig. 11D; residues in yellow), gives a more complete picture of the region of MinD involved in MinC binding. It is clear that the MinC binding site is also composed of residues coming together upon MinD dimerization.

During the site directed mutagenesis we isolated several mutations that affected the interaction of MinD with both MinE and MinC. This was ascertained by the inability of the MinD mutant to kill JS964 (Δmin) when expressed from pSEB104CD and the inability of the mutant to interact with MinE in the bacterial 2-hybrid system. Such mutations included MinD-L43D,-D47R, -

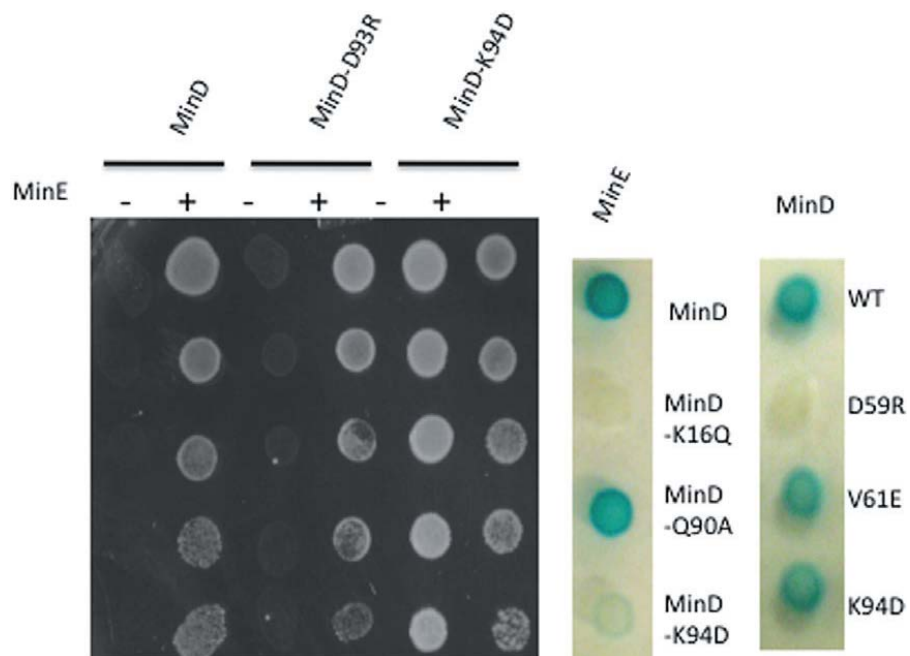
V56E, -Y58D, -D59R, -V61E, -K94D, E146K, V150E, -L157D and -V188E. D154A and I159R, isolated earlier, also fall into this class. Since the new mutations affect the interaction of MinD with both MinC and MinE it was possible that they affect MinD dimerization.

The ability of these mutants to dimerize was assessed with the bacterial 2-hybrid system. MinD-K16Q, a mutant defective in interaction with ATP was used as a control. Surprisingly, we detected a strong interaction between MinD and MinD-K16Q, however, we did not detect an interaction between MinD-K16Q and MinD-K16Q (data not shown). Therefore, in testing the other mutants we used constructs carrying the relevant mutation in both components of the system. Using this approach we found five mutants that displayed no self-interaction (MinD-D47R, -D59R, -E146K, -V150E, and -V188E) and therefore are probably defective in dimerization or folding. However, five of the mutants (MinD-V56E, -Y58D, -V61E, N62K, -K94D; Fig.12, Table 4), displayed strong self-interaction. D154A, previously shown to be deficient in interaction with both MinC and MinE, but able to self interact, served as a control (L. Ma et al., 2004). These mutations are unlikely to affect the folding of MinD suggesting that the corresponding residues are required for interaction with both MinC and MinE (Fig. 11D, pink residues).

Discussion

The interaction of MinD with MinE is essential to achieve Min oscillation whereas the interaction of MinD with MinC is essential to effectively antagonize FtsZ assembly

Fig 12 Example of tests of mutants obtained by site-directed mutagenesis of MinD. Spot test were used to determine if MinD mutants activate MinC (no growth in the absence of MinE). Mutants, such as MinD-D93, activated MinC and responded to MinE, whereas K94D did not activate MinC. To see if MinD-K94D interacts with MinE it was tested in bacterial 2-hybrid system (MinD alleles are shown to the right of the test strip). If, like *minD-K94D*, they did not interact with MinE, they were tested for self-interaction (*minD-K94D* and *V61E* did self-interact whereas *minD-D159R* did not). Results for all mutations were summarized in Table 4.



(P. A. de Boer et al., 1992; Hu et al., 2002; Raskin & de Boer, 1999b; Shen & Lutkenhaus, 2009). In this study we determined the structure of MinD lacking the C-terminal amphipathic helix and found that it formed a nucleotide sandwich dimer similar to Soj. This structure, along with the extensive site-directed mutagenesis, confirmed that the binding sites for MinE and MinC on MinD overlap and revealed that the sites are at the MinD dimer interface. The binding site for MinE appears more extensive and runs all along the dimer interface whereas the binding site for MinC is limited to the upper half of the dimer. The finding that the binding sites involve the dimer interface offers a simple explanation for the ATP-dependent binding of MinC and MinE to MinD; the complete binding sites are only present upon dimerization of MinD, a process known to be ATP-dependent. In the model of the MinD the dimer bound to the membrane the binding sites for MinE and MinC are exposed to the cytosol.

MinD structure

MinD Δ 10-D40A formed a nucleotide sandwich dimer in the presence of ATP as expected based upon its known ability to dimerize in solution and homology to Soj. Nonetheless, several important features of MinD were revealed by solving the structure that are unique to MinD. The role of MinE in stimulating the ATPase activity of MinD was previously postulated to arise from MinE disrupting the K11-D152 interaction freeing K11 to bind to ATP and stimulate ATP hydrolysis (L. Ma et al., 2004). An argument against this is that the residue equivalent to K11 interacts with ATP in the dimer structures of Soj and the iron protein of nitrogenase indicating that ATP binding and/or dimerization disrupts the K11-D152 interaction (Leonard et al., 2005; Schindelin et al., 1997). Since Soj and nitrogenase do not have residues equivalent to D152, this remained a possibility for MinD. However, the MinD dimer structure obtained in this study

confirmed that K11 interacts with ATP leading to the conclusion that dimerization, not MinE, disrupts the D152-K11 interaction. The interaction between K11 and ATP probably stabilizes the dimer since a K11A mutant does not dimerize (H. Zhou et al., 2005). Comparison of the structure of the monomer of MinD from *Pyrococcus furiosus* (Hayashi et al., 2001) with the *E. coli* MinD dimer did not reveal significant structural changes indicating that dimerization may be primarily due to the K11-ATP interaction. This possibility is consistent with ADP promoting dimerization of the MinD-D152A mutant (H. Zhou et al., 2005).

. The MinD structure also revealed the likely orientation of MinD on the membrane. In the dimer of MinD Δ 10 the C-terminal 10 residues of each monomer are fixed in position, extending from the C-terminal helix towards the bottom of the MinD dimer (Fig. 11A). Since both C-termini end up on the same face of the dimer it suggests that this face of the MinD dimer comes near the membrane. Furthermore, the absence of only the amphipathic helix from the structure suggests that this face of MinD is in close contact with the membrane surface. Interestingly, this face of MinD is analogous to the face of Soj that is involved in nonspecific DNA binding (Hester & Lutkenhaus, 2007). Thus, these two similar proteins bind to completely different substrate surfaces with the same face of the protein. In this orientation the binding sites for MinE and MinC on MinD are fully exposed and available for interaction. This is especially important for MinC, which is a relatively large molecule. One complication is that there is some evidence that MinD forms larger oligomers and it is possible that the binding sites could be occluded in the oligomer (Hu et al., 2002).

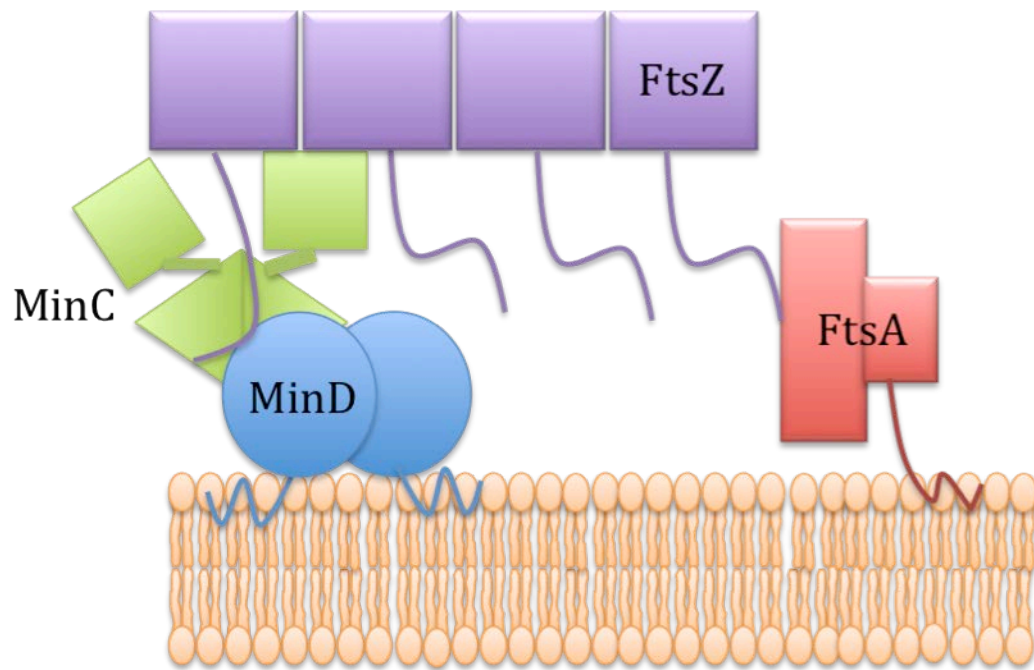
MinC-MinD

Each MinC dimer consists of a C-terminal dimerization domain fused through a flexible linker to an N-terminal domain responsible for disrupting FtsZ filaments (Cordell et al., 2001). The extensive mutagenesis in this study limits the MinC binding site to the top half of the MinD dimer. Thus, it is likely that the C-terminal domain of MinC binds near the top of MinD in such an orientation that the N-terminal domain is extending away from the membrane (Fig. 13). In this orientation MinC would be in position to make the two known contacts with FtsZ filaments. The MinD/MinC^C complex on the membrane would be in position to compete with membrane bound FtsA and ZipA for the carboxy tail of FtsZ subunits present in polymers (Dajkovic, Lan, et al., 2008; Shen & Lutkenhaus, 2009). MinC^N would extend further out away from the membrane where it would be in position to contact the body of FtsZ subunits in the filament (Fig. 13). Previous mutagenesis of the MinC C-terminal domain indicated the MinD binding sites on the MinC dimer (containing the conserved sequence RSGQ) are located far apart on opposite ends of the dimer (Ramirez-Arcos et al., 2004; H. Zhou & Lutkenhaus, 2005). Each C-terminal domain consists of a triangular beta helix with one of the faces involved in dimerization (Cordell et al., 2001). The MinD interaction site is at a vertex of the triangular beta helix farthest away from the dimer interface. Thus, it is possible that a MinD dimer could be sandwiched between two MinC dimers and/or a MinC dimer could be sandwiched between two MinD dimers.

MinD-MinE

Mapping the four mutations isolated from the random mutagenesis that are deficient in MinE binding but proficient in MinC activation was the first indication that the binding site for MinE forms upon dimerization. More extensive site-directed mutagenesis indicates the MinE binding

Fig. 13 Model of interaction of Min proteins and FtsZ. MinD and FtsA bind to the membrane through an amphipathic helix. MinC binds to MinD through its C-terminal domain whereas the N-terminal domain is free to contact FtsZ. The tail of FtsZ binds to FtsA and to the MinD-MinC^C complex.



site on MinD extends from the bottom of the MinD dimer interface (i.e. membrane proximal) to the top of the structure. The residues that are involved in MinE binding line a cleft that extends along the side of the MinD dimer interface (Fig. 11D). The anti-MinCD domain of MinE, composed of residues ~6-30, is proposed to assume an alpha helix that would fit into this cleft (L. Ma et al., 2004). However, the recent structure of full-length MinE reveals that a portion of the anti-MinCD domain is occluded and unavailable for interaction suggesting that for this model to be true, MinE would have to undergo major rearrangement (Ghasriani et al., 2010; Kang et al., 2010).

The structure of MinD is similar to the iron protein of the nitrogenase complex (Hu & Lutkenhaus, 2003; Lutkenhaus & Sundaramoorthy, 2003). Notably, the cleft in the iron protein is occupied by a helix that arises from the carboxy domain of the iron protein itself. The structure of Soj is similar to MinD with a cleft running along each side of the dimer interface (Leonard et al., 2005). Similar to MinD the ATPase activity of Soj is stimulated by a partner protein containing an unstructured N-terminal domain (SpoOJ for Soj). It is likely that this unstructured region of SpoOJ also assumes an alpha helix upon contact with Soj that fits in the cleft and that this is common theme among ParA/MinD family members.

Experimental procedures

Bacterial strains and growth conditions

E. coli strains JS964 (MC1061 malP::lacI^q Δmin::kan) and its isogenic parental strain JS219 (minCDE⁺) have been described previously (Pichoff et al., 1995). BTH101 Δmin strain (F⁻ *cydA*-99, *araD*139, *galE*15, *galK*16, *rpsL*1 (Str^r), *hsdR*2, *mcrA*1, *mcrB*1) (Karimova, Ullmann, & Ladant, 2000) has entire minB operon consisting of three genes, minC, minD, and minE, deleted and replaced with a kan-resistance cassette. It was made by P1 transduction with P1 grown on JS964 (Dmin::kan). LB (Luria-Bertani) medium containing 0.5% NaCl and relevant antibiotics at 37°C was used for most experiments unless otherwise indicated.

Plasmid constructions

Plasmid pSEB104CD (P_{BAD}::minCD) and pJB216 (P_{lac}::minE) were described earlier (H. Zhou et al., 2005). SEB104CDE (P_{BAD}::minCDE) was created by ligation of the small BstXI/HindIII fragment from pJBP210 (Pichoff et al., 1995) into BstXI/HindIII-digested pSEB104CD. pZH115 (pJF118EH [Ptac::minD]) has been described before (Hu & Lutkenhaus, 2001). The same strategy that yielded pZH115 was employed to construct pZH115-10 (pJF118EH Ptac::minD Δ10) in which MinD deleted of the C-terminal 10 codons (Hu & Lutkenhaus, 2003). The MinD-D40A or MinD-D152A mutations were introduced into this plasmid by site-directed mutagenesis to give pZH115-40 and pZH115-152, respectively. The construction of pZH112 (P_{BAD}::MalE-MinC¹¹⁶⁻²³¹) was detailed in an earlier study (Hu et al., 2003). pKT25 and pUT18 were described before (Karimova et al., 2000). pCT25 (Cm^R) was constructed by ligating the PvuII/HindIII

fragment of pKT25 (Km^R) with the HincII/HindIII fragment of pACYC184. pCT25 MinD (cya^{T25} -MinD) was generated by ligating PCR-amplified MinD from pSEB104CD into BamHI/KpnI-digested pCT25 (cya^{T25}). The PCR amplification of MinE followed by digestion with BamHI /KpnI and ligation into BamHI/KpnI site of pUT18 vector (cya^{T18}) yielded pUT18 MinE (cya^{T18} -MinE). Various *minE* and *minD* mutations were introduced into these plasmids by site-directed mutagenesis.

Bacterial two-hybrid analysis

A *cya*-null strain BTH101 Δ min was transformed with plasmids pCT25MinD and pUT18MinE, respectively carrying wild-type or mutant *minD* and *minE* alleles, and grown overnight at 37°C on LB plates containing 0.2% glucose, chloramphenicol (20 mg/ml) and ampicillin (100 mg/ml). For plate-based assay, colonies from the LB plate were diluted in 300 ml volume of LB broth and spotted onto fresh LB plates supplemented with chloramphenicol (20 mg/ml), ampicillin (100 mg/ml), 5-bromo-4-chloro-3-indoyl- β -D-galactopyranoside (X-Gal) at 40 mg/ml, and 0.5 mM IPTG. Observation was usually made after 14-18 hours of incubation at 30°C.

For the quantitative β -galactosidase assay, three colonies were picked from each plate and cultured overnight at 30°C in LB medium containing 0.2% glucose, 20 μ g/ml chloramphenicol, and 100 μ g/ml ampicillin. The overnight cultures were then diluted 1/100 into fresh LB medium containing 0.5 mM IPTG, 20 mg/ml chloramphenicol, and 100 mg/ml ampicillin and cultured for 3-4 h at 30°C followed by measurement of OD₆₀₀. Cells were permeabilized with the addition of 0.0016% SDS [w/v] and 2.5% chloroform [v/v]) and vigorously vortexed. Then 0.4 ml of permeabilized cells were mixed with 0.6 ml of Z buffer (60 mM Na₂HPO₄, 40 mM NaH₂PO₄

[pH 7.5], 1 mM MgSO₄, 50 mM β-mercaptoethanol) and 0.25 ml of ONPG (o-nitrophenyl b-D-galactopyranoside, 4 mg/ml) (Sigma) was added, the reactions were incubated for additional 20 min at 30°C and stopped with 400 mM Na₂CO₃. OD₄₂₀ values were recorded and converted into Miller activity units as described.

Mutagenesis using XL-Red strain

Plasmid pSEB104CDE was transformed into *E. coli* XL1-Red strain (F- endA1 gyrA96 (nal^R) thi-1 relA1 lac glnV44 hsdR17 (r_K⁻ m_K⁺) mutS mutT mutD5 Tn10) (Stratagene) containing 25 mM β-mercaptoethanol and plated onto LB plates containing 0.2% glucose, spectinomycin (100 mg/ml), and kanamycin (50 mg/ml). The colonies from the LB plates were pooled and the plasmid DNAs were isolated using a Plasmid Miniprep Kit (Qiagen). This mutagenized plasmid library was then transformed into JS964 strain (Δ *min*) and grown in LB plates containing 0.2% glucose, spectinomycin (100 mg/ml), and kanamycin (50 mg/ml). To look for mutations affecting min function, approximately 500 colonies were picked and streaked onto LB plates containing 0.2% arabinose and spectinomycin (100 mg/ml) to induce expression of MinCDE. The colonies manifesting filamentous phenotypes were selected and cultured prior to plasmid DNA isolation and sequencing confirmation. Additional information is available in the main text.

Site-directed mutagenesis

The specific mutations within MinD and MinE ORFs were introduced into the various plasmids using the QuickChange site-directed mutagenesis kit according to the manufacturer's instruction (Stratagene). The plasmids used as templates and primers are available upon request.

Protein purification

MinD Δ 10-D40A and MinD Δ 10-D152A were purified from JS964 (Δ *min*) containing pZH115-40 and pZH115-152, respectively. Cells were collected from 1 liter cultures grown in LB with ampicillin (100 mg/ml), resuspended in buffer A (25 mM Tris-HCl [pH 7.5]), 20 mM NaCl, 1mM EDTA, 2 mM DTT and 10 % glycerol) and lysed with a French press. The clarified lysate as loaded on a DEAE column and MinD Δ 10 eluted with a 60-120 mM NaCl gradient in bufferA. The peak fractions were pooled and ran over a HiLoad Superdex 200 column in buffer. The peak fractions were collected and concentrated with a Vivaspin 20 (MW cutoff of 10 kDa) to ~20 mg/ml. The purification of full length wild-type and mutant MinD proteins were previously described (Hu & Lutkenhaus, 2001). MalE-MinC^C was purified using the method reported previously (Dajkovic, Lan, et al., 2008).

Vesicle binding assay

The preparation of multilamellar vesicles (MLV) has been described previously (Hu & Lutkenhaus, 2001). MinD, MinD-M193L or MinD-D40A (4 mM) were incubated with vesicles (400 mg/ml) in the presence of ADP or ATP (1 mM) and MinE (4 mM) or MalE-MinC (4 mM)

or both were added. After a 10 minute incubation at room temperature the vesicles were collected by centrifugation and the pellets analyzed by SDS-PAGE.

Crystallization

Crystals of the MinD Δ 10-D40A-Mg-ATP complex were grown by the hanging drop vapor diffusion method at 4°C. 4 μ L MIND-D40A (10 mg/mL) in 10 mM HEPES pH 7.0, 200 mM NaCl 2 mM DTT 5 mM ATP, 10 mM MgSO₄ was mixed with 2 μ L 1.5-1.7 M (NH₄)₂SO₄, 0.1M Hepes, pH 7.4. The crystals were subsequently cryoprotected by transfer to a solution of 60% sodium malonate (Holyoak et al., 2003) and cryocooled by immersion in liquid nitrogen.

Data Collection

Data on the cryo-cooled crystals maintained at 100K were collected at the Stanford Synchrotron Radiation Laboratory, Beamline 11-1, Menlo Park, CA. All data were integrated and scaled with HKL-2000 .

Structure determination and refinement.

The structure of MinD Δ 10-D40A was solved using Se-methionine substituted enzyme and a three-wavelength MAD approach. Incorporation of Se-methionine was carried out using the methionine auxotroph B834(DE3) and near 100% incorporation was verified using mass spectrometry (data not shown). The programs SOLVE and RESOLVE (Terwilliger, 2000, 2003; Terwilliger & Berendzen, 1999) as incorporated into the Phenix program suite (P. D. Adams et

al., 2010) were utilized for the determination of phases from the experimental diffraction data and initial automated model building. Phases were subsequently extended to a native dataset that diffracted to 2.4 Å. All crystals of MinD Δ 10-D40A suffer from a lattice translocation defect that results from the random translocation of some layers in the crystal by a fixed constant with respect to the other layers comprising the crystal. Correction of data suffering from this type of defect has been previously described (Tsai, Sawaya, & Yeates, 2009; J. Wang, Kamtekar, Berman, & Steitz, 2005; J. Wang, Rho, Park, & Eom, 2005). Reflection intensities for the MinD Δ 10-D40A crystals were corrected by these published procedures using the program LTD correct generously provided by Dr. Jimin Wang, Center for Structural Biology, Yale University and an iterative modulation of the defect fraction. Determination of the final defect fraction was performed via inspection of the native Patterson maps for the elimination of the cross peak due to the lattice translocation defect fraction. In the case of the MinD diffraction data, this cross peak is observed at (0,0.3,0) and has a peak height that is ~37% of the origin peak height. The final defect fraction was also verified by minimization of the R_{free} value for a model refined against data corrected with varying defect fractions. Based upon Patterson map inspection and the R_{free} values, the final defect fraction for the 2.4 Å dataset was determined to be 32%. While the correction procedure does not perfectly remove the contribution from the lattice defect fraction, a significant improvement in map quality in the overlap regions is observed allowing for complete model building, and a significant improvement in R and R_{free} is observed. Prior to correction the R/R_{free} is 34.7/39.9, while the corrected data results in a final R/R_{free} of 25.0/30.7 (Table 3). A more complete description of the lattice translocation defect phenomenon as manifest in the MinD Δ 10-D40A crystals and a rigorous description of the correction procedure will be published elsewhere. After data correction, model building and refinement were carried out using COOT

(Emsley & Cowtan, 2004) and Refmac 5 as contained in the CCP4 program suite, respectively. ATP, magnesium, and water addition and validation were also performed in COOT. Medium NCS restraints between the two molecules of MinD were imposed throughout refinement. A final round TLS refinement was performed for the model in Refmac5. A total of 5 groups per chain were used, as refinements using greater than five groups per chain did not significantly improve R/R_{free} . The optimum TLS groups were determined by submission of the PDB file to the TLSMD server [<http://skuld.bmsc.washington.edu/~tlsmd/>] (Painter & Merritt, 2005, 2006a, 2006b). Final data and model statistics are presented in Table 3.

Chapter III

The Min oscillator uses MinD-dependent conformational changes in MinE to spatially regulate cytokinesis

Abstract

MinD recruits MinE to the membrane leading to a coupled oscillation required for spatial regulation of the cytokinetic Z ring in *E. coli*. How these proteins interact, however, is not clear since the MinD binding regions of MinE are sequestered within a 6-stranded b-sheet and masked by N-terminal helices. Here, *minE* mutations are isolated that restore interaction to some MinD and MinE mutants. These mutations alter the MinE structure releasing the MinD binding regions and N-terminal helices that bind MinD and the membrane, respectively. Crystallization of MinD-MinE complexes reveals a 4-stranded b-sheet MinE dimer with the released b strands (MinD binding regions) converted to a-helices bound to MinD dimers. These results suggest a 6 stranded, b-sheet dimer of MinE ‘senses’ MinD and switches to a 4-stranded b-sheet dimer that binds MinD and contributes to membrane binding. Also, the results indicate how MinE persists at the MinD-membrane surface.

Introduction

Prokaryotes contain a family of proteins, designated the WACA family (Walker A cytomotive ATPase; also called ParA), that display oscillatory behavior involved in such diverse processes as spatial regulation of cell division, plasmid and chromosome segregation and regulation of development (Michie & Lowe, 2006). How this oscillatory behavior is achieved is not

completely clear. The best studied member of the WACA family is MinD a component of the Min system involved in the spatial regulation of the positioning of the cytokinetic Z ring (Lutkenhaus, 2007).

In *E. coli* MinD and MinE undergo a rapid pole-to-pole oscillation that produces a time-averaged gradient of MinC, a passenger in the oscillation and an antagonist of FtsZ assembly, that is highest at the poles and lowest at midcell (de Boer et al., 1989; Fu et al., 2001; Hale et al., 2001; Hu & Lutkenhaus, 1999; Meinhardt & de Boer, 2001; Raskin & de Boer, 1999a). During the oscillation MinD, along with MinC, is present in a polar zone flanked near midcell by the MinE ring. Migration of the MinE ring towards the pole of the cell displaces MinD and MinC, which reassemble at the opposite pole, again flanked by a MinE ring near midcell.

Underlying the oscillation is the ATP-dependent interaction of the three Min proteins with each other and with the membrane (Lutkenhaus, 2007). MinD dimerizes in the presence of ATP and binds cooperatively to the membrane through a C-terminal amphipathic helix; dimerization is required for MinD to have sufficient affinity for the lipid bilayer (Hu & Lutkenhaus, 2003; Lackner et al., 2003; Szeto et al., 2003; Szeto et al., 2002; W. Wu et al., 2011b). MinC and MinE are recruited to MinD and bind to overlapping sites located at the MinD dimer interface (L. Ma et al., 2004; W. Wu et al., 2011b). MinC binding produces a potent inhibitor of Z ring assembly, whereas the binding of MinE, displaces MinC, stimulates the ATPase activity of MinD and triggers the release of MinD from the membrane (Hu et al., 2003; Lackner et al., 2003).

The apparent simplicity of the Min system has attracted modelers and experimentalists to determine the basis of dynamic pattern formation (Kruse et al., 2007). An important step was the demonstration that MinD and MinE are able to form travelling waves in vitro on a planar lipid

bilayer in the presence of ATP that have characteristics of the *in vivo* oscillation. One study explained pattern formation by a reaction-diffusion mechanism (Loose et al., 2008) whereas another study emphasized surface-based mechanical stress arising from protein-membrane interactions involving multiple MinD-MinE species (Ivanov & Mizuuchi, 2010). More information is needed about the interaction between MinD and MinE to understand the structural basis of this self-organizing system.

MinE is a dimer of a small protein of 88 residues with two functional domains (Pichoff et al., 1995; Zhao et al., 1995). The N-terminal domain (residues ~6-31) is able to counteract MinCD's division inhibitory activity. Genetic studies suggest that this anti-MinCD domain forms an α helix that binds MinD (L. Y. Ma et al., 2003). The C-terminal domain (residues 32-88) is designated a topological specificity domain because it is required for MinE to spatially regulate cell division, presumably by dimerizing the anti-MinCD domains. Dimerization of these domains is essential as expression of MinE²²⁻⁸⁸, which lacks part of the anti-MinCD domain, blocks cell division due to formation of heterodimers with WT MinE. These heterodimers are less efficient at countering MinCD (Zhang et al., 1998).

There are indications that MinE can interact directly with the membrane, although, recruitment of MinE to the membrane requires MinD (Hu et al., 2002; Raskin & de Boer, 1999b). For example, some MinE mutants, such as MinE^{L22D} and MinE^{I25R}, bind directly to the membrane (L. Y. Ma et al., 2003). The basis or significance of membrane binding by these mutants is not known. More recently, positively charged residues at positions 10-12 were implicated in MinE-membrane interaction (Shih et al., 2011). Also, in one of the models for Min oscillation

formation of the MinE ring was achieved through MinE binding directly to the membrane after being recruited by MinD (Arjunan & Tomita, 2010).

The structures of two intact MinE proteins and one trypsin resistant fragment of MinE have been solved. Surprisingly, these structures differ significantly raising the possibility that they represent different conformational states. A trypsin resistant fragment of the *E. coli* MinE consists of residues 31-88 and is a dimer where each subunit consists of 2 anti-parallel b-strands packed against an α -helix (King et al., 2000). The helices pack together in the dimer to form an anti-parallel coiled coil and the b-strands (b2 & b3) form a 4-stranded, anti-parallel b-sheet (Fig. 14A). The structures of the intact MinE's from *Helicobacter pylori* and *Neisseria gonorrhoeae* are also dimers, but contain a 6-stranded, anti-parallel b sheet in addition to the α helices (Ghasriani et al., 2010; Kang et al., 2010). The additional b-strands (b1) containing part of the anti-MinCD domain are at the dimer interface sandwiched between the b-strands found in the structure of the truncated *E. coli* protein (Fig. 14B). In both of these structures the anti-MinCD domain is not solvent accessible and therefore unavailable for binding MinD. Additionally, in the *N. gonorrhoeae* structure a short N-terminal amphipathic helix (residues 3-8; residues 1-17 are not observed in the *H. pylori* structure) packs against the b-sheet further masking it (Fig. 14B). These structures suggest that the sequestered anti-MinCD domains (b1 strands) must be released to interact with MinD. Our study confirms this and reveals that both structures of the C-terminal domain of MinE (4 and 6-stranded) are physiologically relevant. We suggest that MinE senses MinD and undergoes a dramatic conformational change that releases the anti-MinCD domains and unmasks cryptic membrane targeting sequences

(MTS) in MinE. These results lead to a model for MinD-MinE interaction that has implications for the mechanism of Min oscillation.

Results

Mutations altering MinE residue I24 restore interaction with some MinD mutants

Previously, we identified 13 MinD mutants that are defective in interaction with MinE but still activate MinC (W. Wu et al., 2011b). To explore the MinD-MinE interaction we used the bacterial 2-hybrid system to select MinE mutants that regain interaction with these MinD mutants (Fig. 15A and Experimental Procedures). MinE mutants were isolated that regain interaction with 4 of these 13 MinD mutants. The amino acids altered in these 4 MinD mutants (MinD^{M193L}, MinD^{D198R}, MinD^{G224C} and MinD^{N222A}) are located near each other at the MinD dimer interface close to the membrane (Fig. 16). With MinD^{M193L} we obtained MinE^{I24N}, which retained the ability to interact with WT MinD and also interacted with MinD^{D198R} but not with the other MinD mutants (Fig. 15A, only 5 of the MinD mutants are shown). With MinD^{D198R} we obtained MinE^{I24S/E66G} and MinE^{I24S/D45E} and with MinD^{G224C} we obtained MinE^{I24T/N16K} (data not shown). It was striking that in each of the MinE mutants, which retain the ability to interact with WT MinD, the I24 residue was altered.

The MinE mutants were tested in a physiological assay by assessing rescue of a Δmin strain from the expression of each of the 13 MinD mutants along with MinC. Only the MinD mutants (and WT MinD) that interact with the MinE mutants in the bacterial 2-hybrid system were rescued to some extent by the MinE mutants (Table 5). Further study revealed that the ability to rescue the MinD mutants is due to changes at position I24 as mutations that altered other residues (N16,

D45 and E66) showed little ability to rescue on their own, even though they enhance rescue by mutations that alter I24 (Fig. 15B results with MinD^{M193L}; Table 5 for summary of results).

The isoleucine codon at position 24 is ATT and we obtained all three possible (due to a single nucleotide change) hydrophilic amino acid substitutions (Asn, Thr, Ser), but none of the possible hydrophobic amino acid substitutions (Val, Leu, Phe, Met). We hypothesized that the mutations altered the structure of MinE, which restored interaction with the MinD mutants. To test this further, we made multiple nucleotide changes to the ATT codon to yield arginine, glutamate, tryptophan, cysteine and valine. Consistent with our hypothesis, the hydrophilic substitutions along with the bulky tryptophan substitution resulted in a mutant MinE that was able to rescue MinD^{M193L}. Only MinE^{I24V}, containing a hydrophobic substitution, behaved like WT and was unable to rescue MinD^{M193L} (Fig. 15C).

In the MinE structure from *N. gonorrhoeae* the residue corresponding to I24 is one of 3 large hydrophobic residues in the b1 strand that make hydrophobic interactions with the long a1 helix to generate a hydrophobic interior (Fig. 14B, residue in yellow). The I24 residue occupies the central position in the b1 strand and also makes hydrophobic interactions with itself so that a hydrophilic residue at position 24 would be very unfavorable. Although the I24 residue is also within the anti-MinCD domain, it is not required for binding MinD (L. Ma et al., 2004). One hypothesis to explain the I24 substitutions is that binding of MinE to MinD involves a ‘sensing step’ that leads to the release of the b1 strand (part of the anti-MinCD domain) so that it is available to bind MinD. In this scenario the four MinD mutants, such as MinD^{M193L}, are deficient in ‘sensing’ MinE and inducing the release of the b1 strand. In MinE mutants, such as MinE^{I24N}, the b1 strand is already released so the ‘sensing step’ is bypassed. Another hypothesis is that two

Fig. 14 Structures of MinE and location of critical residues. The structure of the trypsin-treated MinE (residues 31-88) from *E. coli* (A) and two views of the the MinE (residues 1-89) from *N. gonorrhoeae* (B) are shown (PDBs 1EVO and 2KXO, respectively). These structures contain 4-stranded and 6-stranded β -sheets, respectively. The labeling of secondary structural elements follows the labeling of the *N. gonorrhoeae* structure. The N-terminal helices are shown in this study to function as a membrane targeting sequence (MTS). The residue corresponding to I24 of the *E. coli* MinE is colored yellow in this structure and the residue corresponding to I25 is colored green. (C) The structure of MinE^{12-88(I24N)} from the MinD-MinE complex reported in this work (residues 13-83 of MinE are visible). Note that it is a 4-stranded β -sheet and the region corresponding to β 1 in panel B (red) is part of an α helix (the contact helix). The N- and C-termini are indicated. (D) The sequence of MinE from *E. coli* with the secondary structural elements present in free MinE displayed above the sequence and those present in MinE in the complex with MinD displayed below the sequence.

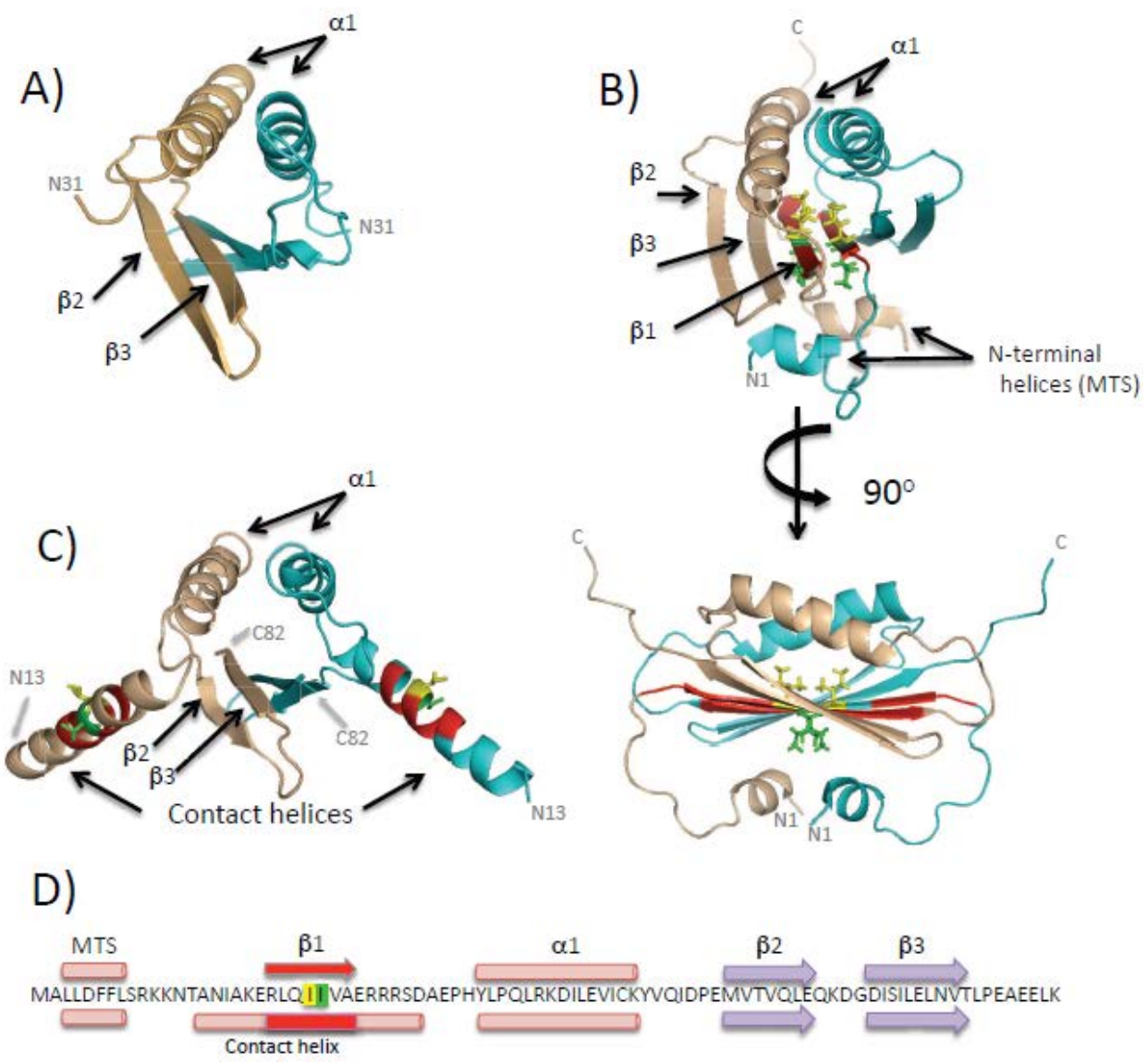


Fig. 15 Analysis of the ability of MinE mutants to bind to MinD mutants and suppress MinC/MinD inhibitory activity. A) Bacterial two-hybrid analysis of the interaction between MinE^{I24N} and several MinD mutants. First row (controls): MinD + MinE, MinD + X and X + MinE^{I24N} (X=empty vector); the second and third row contain MinE^{I24N} in combination with the indicated MinD mutant. B) The ability of various *minE* alleles to suppress killing by MinC/MinD^{M193L}. JS964 (Δmin) /pSEB104CD-193 (P_{ara}::*minC minD*^{M193L}) with pJB216 (P_{lac}::*minE*) derivatives containing the indicated *minE* allele were serially diluted 10 fold and spotted on plates containing 0.1% arabinose and 100 μ M IPTG. C) As in panel B. D) The *minE*^{I24N} mutation suppresses some, but not all, *minE* mutations. pJB216 (P_{lac}::*minE*) derivatives carrying the *minE* alleles indicated were tested for their ability to protect JS964 (Δmin) from the induction of MinC/MinD from pSEB104CD (P_{ara}::*minC minD*).

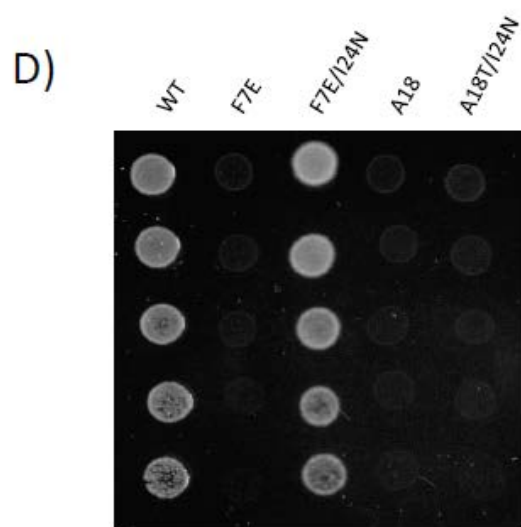
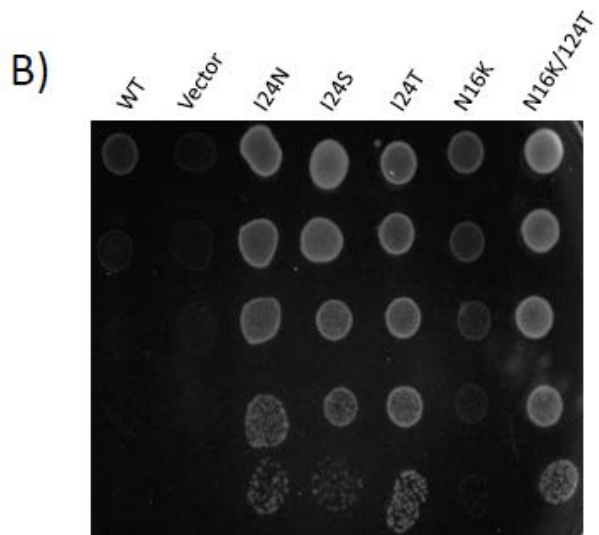
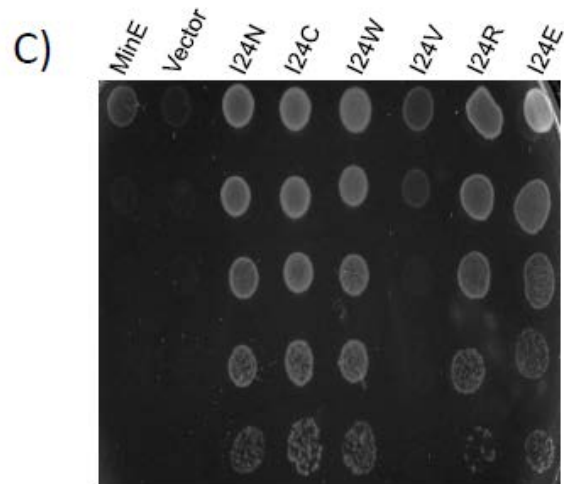
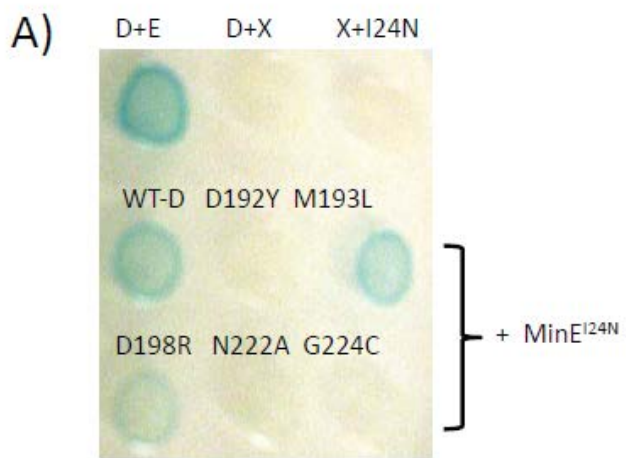


Fig. 16 Location of MinD residues important for MinE binding is related to Figure 15. The residues altered in the 4 MinD mutants that can be rescued by the MinE mutants isolated in this study are colored green. The residues indicated in blue are altered in mutants for which no MinE mutants were obtained.

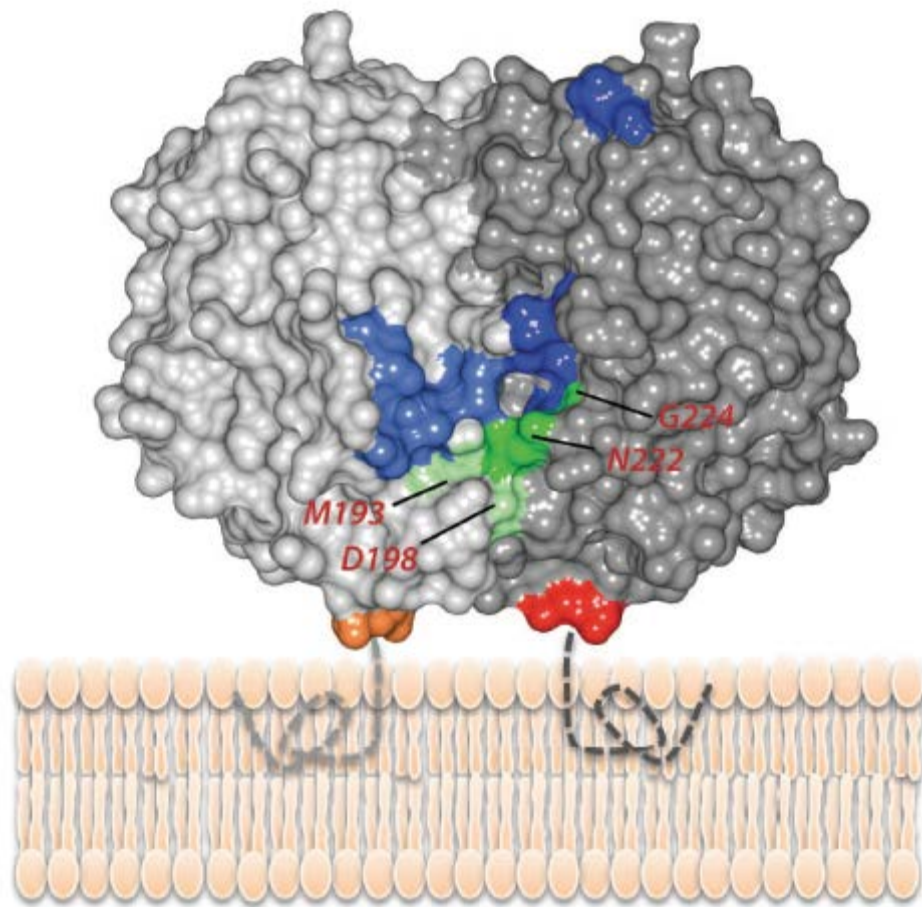


Table 5. Rescue of MinD mutants by MinE mutants is related to figure 15.

A. (-IPTG)

| MinE | WT | I24N | I24S | I24T | I24V | N16K | E66G | N16K/ I24T | I24S/ D45E | I24S/ E66G |
|-------|-----|------|------|------|------|------|------|---------------|---------------|---------------|
| MinD | | | | | | | | | | |
| M193L | - | ++ | ++ | - | - | - | - | +++ | - | - |
| D198R | - | ++ | + | + | - | - | - | - | - | - |
| N222A | - | - | - | - | - | | | | | |
| G224C | - | - | - | - | - | - | | - | - | - |
| MinD | +++ | +++ | +++ | ++ | +++ | +++ | +++ | ND | ND | ND |

B. (+IPTG)

| MinE | WT | I24N | I24S | I24T | I24V | N16K | E66G | N16K/ I24T | I24S/ D45E | I24S/ E66G |
|--------|----|------|------|------|------|------|------|---------------|---------------|---------------|
| MinD | | | | | | | | | | |
| M193L | - | +++ | +++ | ++ | - | + | - | +++ | +++ | +++ |
| D198R | - | +++ | +++ | ++ | - | - | + | +++ | +++ | +++ |
| N222A | - | + | - | + | - | | | ++ | - | + |
| G2224C | - | + | - | + | - | | - | +++ | - | - |

JS964 (Δmin) containing pJB216 ($P_{lac}::minE$) derivatives carrying the *minE* alleles indicated were tested for their ability to protect cells from the expression of MinC/D from pSEB104CD ($P_{ara}::minC minD$) carrying the *minD* alleles indicated. Plates were incubated in the presence or absence of IPTG as indicated.

Legend: -, no rescue; +, some growth at innoculum; ++, growth throughout but cells slightly filamentous; +++, normal growth. ND = not done.

conformations of MinE exist in equilibrium and one is selected by MinD, however, we argue against this alternative based upon the failure of MinE to bind directly to the membrane (see discussion). To examine the first hypothesis we proceeded to determine if I24 substitutions altered the structure of MinE.

The *minE*^{I24N} mutation reduces the b strand content of MinE

To examine the effect of the *minE*^{I24N} mutation on the activity and structure of MinE we took advantage of the observation that ectopic expression of MinE²²⁻⁸⁸ in a WT strain inhibits division and causes cell death due to MinE²²⁻⁸⁸ forming a heterodimer with WT MinE (Pichoff et al., 1995; Zhang et al., 1998). In contrast, MinE³⁶⁻⁸⁸ does not form a heterodimer with WT MinE nor inhibit division. Thus, filamentation offers a simple readout of the ability of N-terminally truncated MinEs to form heterodimers with WT MinE. Furthermore, since MinE²²⁻⁸⁸ has most of the b1 strand intact for heterodimerization whereas MinE³⁶⁻⁸⁸ is missing the b1 strand entirely these heterodimers are likely to be 6 b-stranded dimers (Fig. 14).

To test the 6-stranded heterodimer hypothesis we analyzed additional MinE constructs with an amino acid addition or deletion at the N-terminus of MinE²²⁻⁸⁸. We suspected that these changes would enhance or hinder the ability of the resultant constructs to form heterodimers, respectively. Consistent with this, the inhibitory activity of MinE²¹⁻⁸⁸ was enhanced compared to MinE²²⁻⁸⁸, whereas MinE²³⁻⁸⁸ lacked inhibitory activity and behaved similarly to MinE³⁶⁻⁸⁸ (Fig. 17A). Western blots demonstrated that the various MinEs derivatives had similar stability (data not shown).

We speculated above that the *minE*^{I24N} mutation caused release of the b1 strand from the dimer interface. If so, introducing the I24N substitution into MinE²¹⁻⁸⁸ should interfere with its ability to form heterodimers with WT MinE and inhibit division, and instead cause it to behave like MinE²³⁻⁸⁸ and MinE³⁶⁻⁸⁸. Consistent with this, MinE²¹⁻⁸⁸ with the I24N substitution (MinE^{21-88(I24N)}) did not inhibit division (Fig. 17A).

To examine the structural consequences of the *minE*^{I24N} mutation we analyzed the secondary structure content of MinE²¹⁻⁸⁸ and MinE^{21-88(I24N)}. The purified proteins were oligomers (Fig. 18A & B) and circular dichroism revealed they had similar α -helical content but that MinE^{21-88(I24N)} had significantly reduced β -strand content and an increase in random coil (Fig. 17B and C). The calculated secondary structure content of MinE²¹⁻⁸⁸ from the circular dichroism data is consistent with the 6 β -stranded structure. For MinE^{21-88(I24N)} the calculation is consistent with loss of the b1 strands from the dimer interface and their conversion to a random coil. Since MinE^{21-88(I24N)} is a dimer (Fig. 18) we suggest that it is a 4 β -stranded dimer in which the b3 strands (Fig. 14A) come together to form the dimer interface as observed in the structure of the trypsin treated MinE (King et al., 2000). Based upon this reasoning and the inhibition data, MinE usually folds into the 6-stranded dimer but forms a 4-stranded dimer if formation of the 6-stranded dimer is compromised.

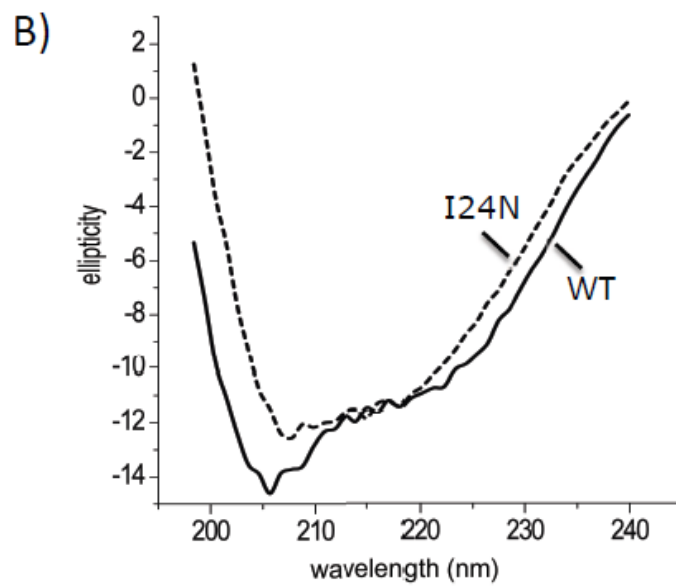
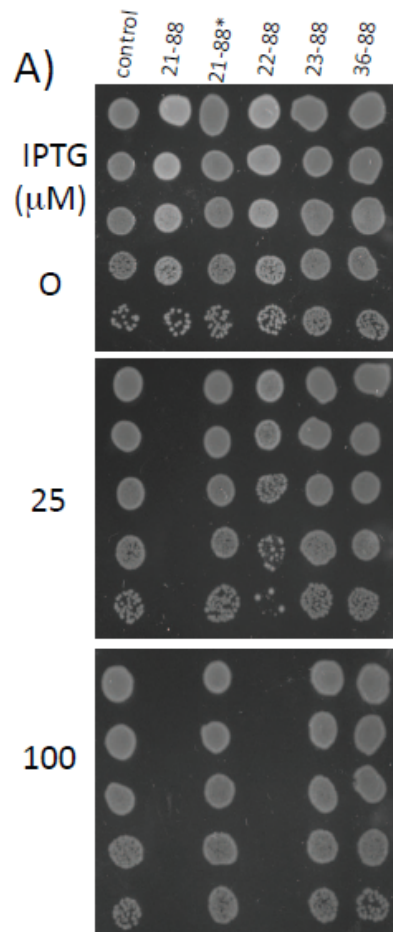
In contrast to the effect of the I24N substitution on the inhibitory activity of MinE²¹⁻⁸⁸, a different result is expected with the I25R substitution. We assume that the *minE*^{I25R} mutation affects MinE structure since MinE^{I25R} binds directly to the membrane (L. Y. Ma et al., 2003), although, it is unlikely to disrupt the MinE β -sheet structure. The I25 side chain, unlike the I24 side chain, is directed away from the large α 1 helix (Fig. 14B, residue in green), and instead

makes hydrophobic contacts with the N-terminal helix, which we designate a membrane targeting sequence (MTS, see below) (Ghasriani et al., 2010). Thus, the *minE*^{I25R} mutation is likely to disrupt this interaction and free the N-terminal helix without disrupting the 6 b-stranded structure. If so, it should not interfere with the ability of MinE²¹⁻⁸⁸ to form heterodimers and inhibit division. Consistent with this expectation, the I25R substitution had no effect on the ability of MinE²¹⁻⁸⁸ to cause filamentation and cell death when expressed in a WT strain (data not shown).

The N-terminal helix of MinE is a MTS responsible for promiscuous membrane binding of MinE mutants

Recruitment of WT MinE to the membrane requires MinD (Hu et al., 2002; Raskin & de Boer, 1999b), however, MinE¹⁻³¹ and several MinE mutants that do not bind MinD, including MinE^{I25R} and MinE^{L22R}, bind directly to the membrane (L. Y. Ma et al., 2003). This result raised the possibility that the N-terminal domain of MinE has a cryptic membrane targeting sequence (MTS) that is unmasked by mutation or possibly by interaction with MinD. Although membrane binding by MinE¹⁻³¹ has been attributed to positive charged residues located at positions 10-12, these residues do not appear to be masked in the most recent MinE structure (Ghasriani et al., 2010; Hsieh et al., 2010). Another possibility is that membrane binding is due to the short N-terminal amphipathic helix, which contains large conserved, hydrophobic residues that could function as a membrane targeting sequence (MTS) (Fig. 14B & 20). If so, mutations that release this amphipathic helix either by releasing the b1 strand (*minE*^{I24N} and *minE*^{L22R}) or interfering with its hydrophobic tethering (*minE*^{I25}) would produce constitutive membrane binding.

Fig. 17 Inhibitory activity and secondary structure of N-terminal truncated MinEs. A) The sensitivity of JS219 (*min*⁺) to N-terminally truncated MinEs was determined by spotting serial (10-fold) dilutions of cultures of JS219 containing plasmids expressing various N-terminal truncated MinE derivatives on plates containing IPTG as indicated. The control is the parent vector without an insert. The presence of the I24N substitution is indicated by the asterisk. B) Circular dichroism spectra of MinE²¹⁻⁸⁸ and MinE^{21-88(I24N)}. C) The % of secondary structure content was estimated from the CD spectra using the K2d prediction program (Andrade, Chacon, Merelo, & Moran, 1993) and is compared to the % of secondary structure content present in the crystal structure of MinE (corresponding to residues 21-88) from *H. pylori*. The asterisk indicates that the value for β content of MinE^{21-88(I24N)} was calculated assuming the β 1 strand is a random coil.

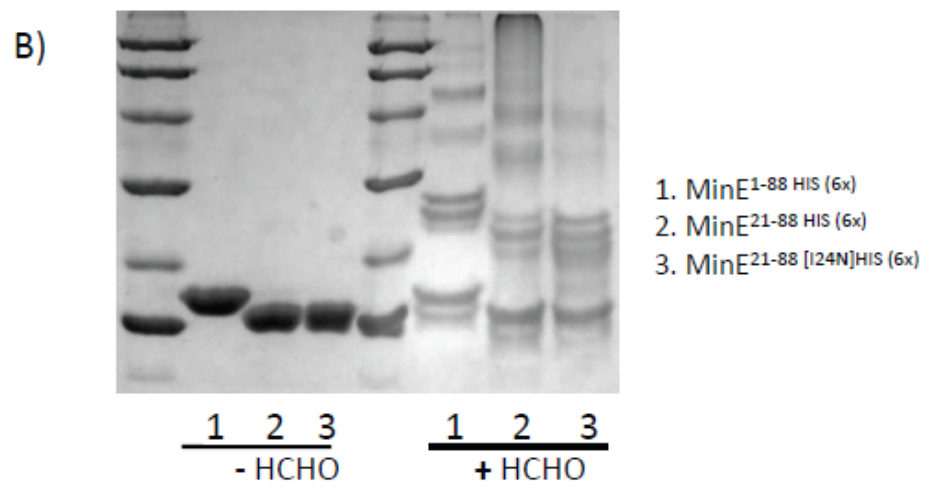
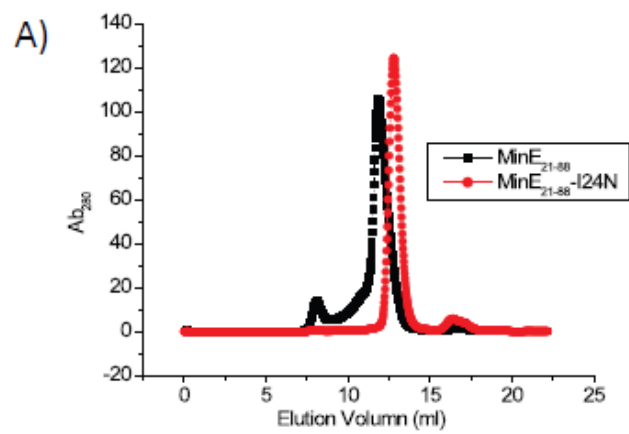


C)

| | | Alpha | Beta | Random |
|------|----------------|-------|------|--------|
| WT | From sequence | 19 | 34 | 48 |
| I24N | From sequence* | 19 | 23 | 58 |
| WT | Calc from CD | 25 | 35 | 40 |
| I24N | Calc from CD | 27 | 15 | 58 |

Fig. 18 Oligomerization of MinE²¹⁻⁸⁸ is related to Figure 17.

- A) Size-exclusion chromatography of MinE²¹⁻⁸⁸. Full length MinE elutes at 12.5 ml (not shown) as does MinE^{21-88(I24N)} consistent with these proteins being dimers. MinE²¹⁻⁸⁸ elutes at 11.8 ml indicating a higher oligomer size, perhaps two dimers interacting through their β -strands as found in the crystal structure of MinE from *H. pylori*. Controls: carbonic anhydrase (31K) elutes at 12.5 ml and bovine serum albumin (66K) elutes at 10.4 ml.
- B) Crosslinking of MinE proteins. Purified MinE proteins were treated with formaldehyde and analyzed by SDS-PAGE. Molecular weight markers were run in the lanes lacking numbers. The MWs of the markers are (from the top) – phosphorylase b (97.4K), bovine serum albumin (66.2K), alcohol dehydrogenase (45K), carbonic anhydrase (31K), soybean trypsin inhibitor (21.5), and lysozyme (14.4K).



To test if this amphipathic helix is responsible for membrane binding in these mutants, we substituted a charged residue for each of the large hydrophobic residues and monitored their effects on membrane binding of MinE^{I25R} tagged with GFP. Whereas MinE^{I25R}-GFP localized to the membrane, the introduction of any of 4 substitutions tested (L3E, L4E, F6E or F7E) abrogated membrane binding of MinE^{I25R}-GFP (Fig. 19A). Since we found that MinE^{I24N} alters the structure of MinE we tested if it also led to membrane binding. Indeed, MinE^{I24N}-GFP was also targeted to the membrane independent of MinD (Fig. 19A). Introduction of any of the above charged substitutions also prevented MinE^{I24N}-GFP from going to the membrane (data not shown). These results demonstrate that the N-terminal amphipathic helix can function as an MTS.

Although the above results revealed that charged substitutions in the MTS of MinE blocked promiscuous membrane binding due to altering the structure of MinE, they did not reveal if this membrane binding was of physiological significance. To try and address this, the charged mutations were introduced into pSEB104CDE ($P_{\text{ara}}::\text{minC minD minE}$) and the resultant plasmids introduced into JS964 (Δmin) to determine if WT morphology was restored under inducing conditions. Surprisingly, the strains containing minE^{L3E} and minE^{F7E} were extremely filamentous and could not form colonies on plates with arabinose (Fig. 19B and data not shown) indicating MinE function was absent. In contrast, strains containing minE^{L4E} and minE^{F6E} formed colonies normally on plates with arabinose but the morphology of the cells were heterogeneous in length with some minicells. The average cell length of an exponential culture of the strain with minE^{WT} was $2.84 \pm 0.89 \mu\text{m}$ compared to $4.68 \pm 2.48 \mu\text{m}$ for the strain lacking Min function. The strains containing minE^{F6E} and minE^{L4E} had average cell lengths of $3.81 \pm 2.67 \mu\text{m}$ and $2.95 \pm$

1.37 μ m, respectively (N~250 for each). In summary, each of the 4 charge substitution mutations eliminated membrane binding of the MinE^{I25R} mutant. However, two of the mutations, *minE*^{L3E} and *minE*^{F7E}, completely eliminated the ability of MinE to counteract MinC/MinD, whereas the other two, *minE*^{L4E} and *minE*^{F6E}, did not, although they did reduce the ability of MinE to spatially regulate division as evidenced by the increases in the average cell length and the standard deviation.

The *minE*^{I24N} mutation also rescues some MinE mutants defective in interaction with MinD

The proposal that the anti-CD domain of MinE (~ residues 6-31) adopts an a helical conformation upon binding to MinD stemmed from a genetic study that revealed that residues important for binding MinD are located on one face of this putative helix (L. Y. Ma et al., 2003). The exact length of this helix is uncertain but it does not appear to extend to position 8, which would be on the same face of the helix, since the L8R substitution did not affect binding to MinD (Ryan & Shapiro, 2003). Although the L8R substitution was tested in the context of MinE¹⁻³¹, we confirmed that MinE^{L8R} was able to bind MinD (data not shown). In contrast, two of the MinE mutants we described above, MinE^{F7E} and MinE^{L3E}, were unable to rescue cells from expression of MinC/MinD (Fig. 19B). This was surprising since these residues lie beyond the putative interacting helix. We reasoned that these residues could play a role in ‘sensing’ MinD and therefore might have a defect in MinD-MinE interaction similar to the MinD^{M193L} mutant. If so, the *minE*^{I24N} mutation should suppress these mutations. As shown in Fig. 15D, the double mutant, MinE^{F7E/I24N}, rescued cells from expression of MinC/MinD demonstrating that the *minE*^{I24N} mutation is an intragenic suppressor of *minE*^{F7E}. It also suppressed *minE*^{3LE} (data not shown).

Fig. 19 Effect of *minE* mutations on membrane localization of MinE and its ability to counter MinC/MinD. A) JS964 (Δmin) containing pJK100 ($P_{trc}::minE-gfp$) derivatives expressing *minE-GFP* fusions with the indicated *minE* mutations were analyzed by fluorescence microscopy. The strains were grown in the presence of 20 μ M IPTG. B) The effect of *minE* mutations on spatial regulation of cell division. JS964 (Δmin) containing pSEB104CDE ($P_{ara}::minC minD minE$) derivatives containing various *minE* mutations (as indicated in the panels) was grown to exponential phase with 0.1% arabinose for 24 hours to induce the *min* operon. The first panel contained the *minC*^{R133A} mutation, which prevents interaction with MinD and inactivates Min function (H. Zhou & Lutkenhaus, 2005).

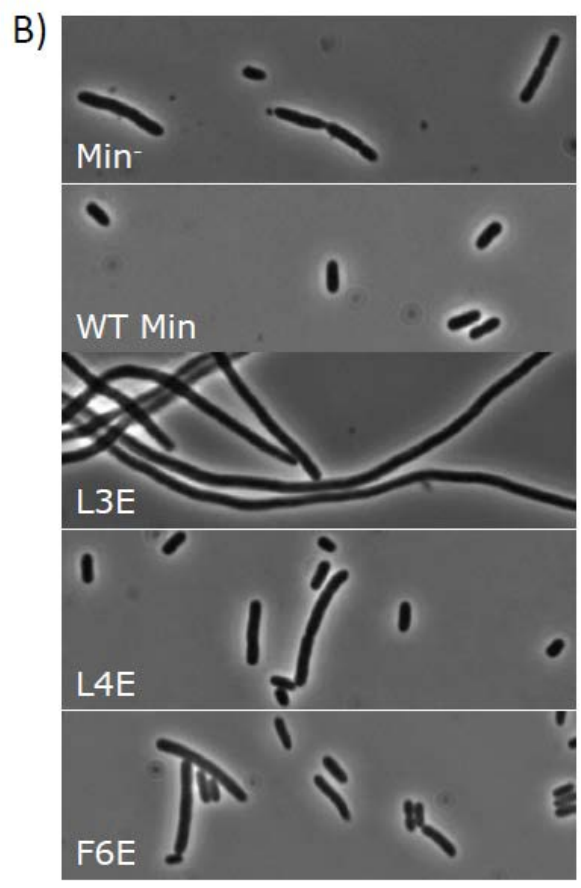
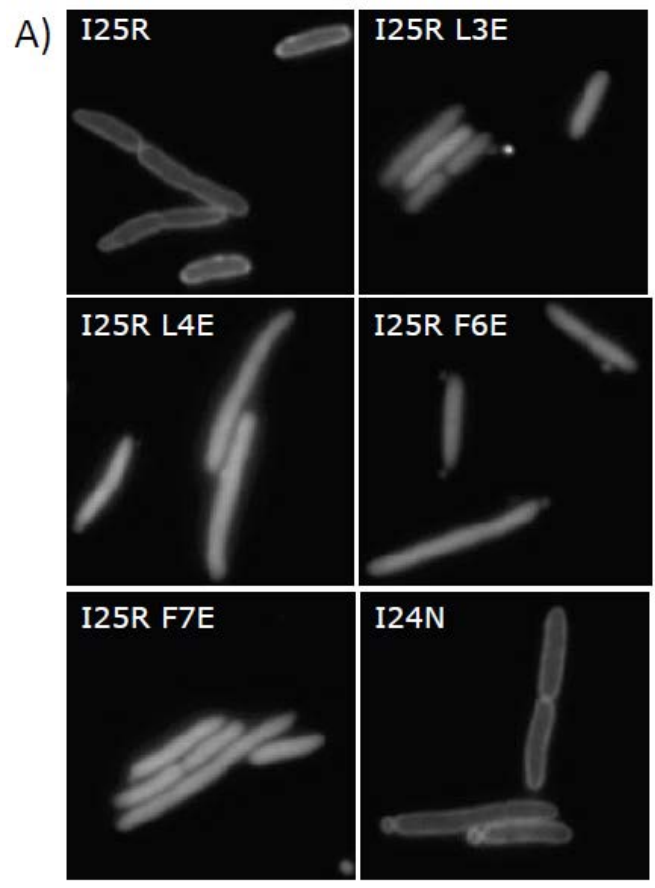
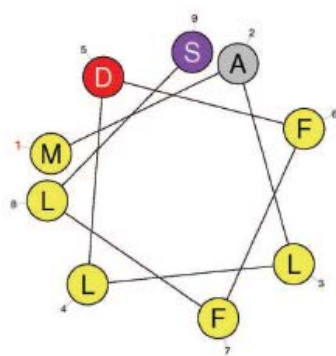


Fig. 20 The N-terminal hydrophobic amino acids of MinE are highly conserved and form an amphipathic helix that can function as a MTS (membrane targeting sequence) is related to Figure 4. MinE sequences are taken from COG0851 and are from a wide variety of Gram-negative organisms. The amphipathic nature of this N-terminal region (line above the sequence alignment) is indicated by the left helical wheel representation. The membrane targeting sequence present at the carboxyl end of MinD is on the right for comparison (large hydrophobic residues are in yellow). MinE sequences from the top: *E. coli*, gi 127098; *Salmonella enterica*, gi 16765157; *Yersinia pestis*, gi 16122315; *Vibrio cholera*, gi 12230283; *Xylella fastidiosa*, gi 12230298; *Agrobacterium tumefaciens*, gi 15891685; *Buchnera aphidicola*, gi 12230240; *Helicobacter pylori*, gi 12230217; *Neisseria meningitidis*, gi 12230269; *Pseudomonas aeruginosa*, gi 15598441; *Sinorhizobium meliloti*, gi 16265100; *Synechocystis species*, gi 6016574.

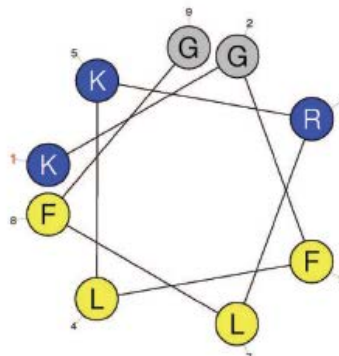
```

1 MALLDFFLSRKk-NTANIAKERLQIIVAERRr-SDAEPHYLPQLRKDILEVICKYVQIDPEMVTVQLEQKdDISILELNVTLPEAEEL-K 88
1 MALLDFFLSRKk-STANIAKERLQIIVAERRr-SDAEPHYLPQLRKDILEVICKYVQIDPEMVTVQLEQKdDISILELNVTLPEAEES-K 88
1 MALLDFFLSRKk-PTANIAKERLQIIVAERRr-GDSEPHYLPDLKRDILAVICKYIQIDPEMLHVQFEQKgdDISVLELNVTLPEETEETPK 89
1 MSLLFFFRPQKk-TSASVAKERLQIIVAERRsqNDPAPSYLPQLKEDILKVIKYYVAIDPSMVLSFEHKGdDISVLELNVKLPDDEK--- 87
1 MGLIDFLRNKT--KTAETAQRNRLQIIIAQERt-QRGGPDYLPPLQRELELVICKYVKIDADAVKVDLIKDG-ANDVLDISVALPDDSER-- 85
1 MSIFSIIR-KQ--KSAPLARERLQVLLAHERasSG--TDLVAVLREELSVIAKHVQIDNDRVHVKMDRDE-HVSILEIDVEIPLGAH-LR 84
1 MALLDFFLSRNk-NTANVAKERLQIIVAERqk-YNNEPDYFPQLKREILSVICKYVNIENMVTVQLDQKneDISILELNIILPD----- 83
1 MSLEDFFKKNG---SAATATDRLLKLLAKERt-LN--LPYMEEMRKEI IAVIQYTKSS-D-IHFKTLDNSqSVETIEVEIILPR----- 77
1 MSLEIFLFRGKq-KTATVARDRLQIIIAQERaqEGQTPDYLPPLRKLMEVLSKYVNVSLDNIRISQEKQD-GMDVLELNIITLPEQKKV-- 87
1 MSLLDFFRSRKsqNSASIAKERLQIIVAHERq-QRAQPDYLPQLQKDLLEVIRKYVPIDQEQIQVELENQG-NCSILELNIITLPEQKKV-- 84
1 MSIFRFFS-KQ--TSAPTARERLQVLLAHERasVG-QSDLVAVLREEL IAVIAKHVQVDRDKVNVMTMERGE-HVTTLEVDIEIPMKAG-VR 85
3 LELIERLFSRSgkNSGEDARRRLKLVIANDR--SGLSPEMMEEMREIVEVVSRYVEIDPGESEFSLESdq-RMTALIANLPVRRVRRTKA 90

```



MinE



MinD

Although the *minE*^{I24N} mutation was able to suppress *minE*^{F7E} and *minE*^{3LE}, it should not suppress a MinE mutant that has a defect in the MinD binding surface. For example, the *minE*^{I24N} mutation was unable to suppress the *minE*^{A18T} mutation (Fig. 15D), which alters a residue near the middle of the putative helix thought to come into direct contact with MinD. This result indicates A18 is part of the binding surface.

Structure of the MinD-MinE^{I24N} complex

As one approach to explore the structural basis of the MinD-MinE interaction we purified MinE^{I24N} with a C-terminal His tag and tested interaction with MinD. It migrated slightly faster than WT MinE on SDS-PAGE and the MALDI spectrum revealed that MinE^{I24N-h} was cleaved between amino acids 11 and 12 (designated MinE^{I24N*-h}). Several of the other MinE^{I24} mutants, MinE^{I24S} and the double mutant MinE^{I24T/N16K}, also underwent cleavage and, in all cases this occurred following cell lysis. The truncated MinE^{I24N*-h} retained activity since it was able to stimulate ATP hydrolysis by MinD, although at ~50% of the activity of full length MinE (Fig. 22A).

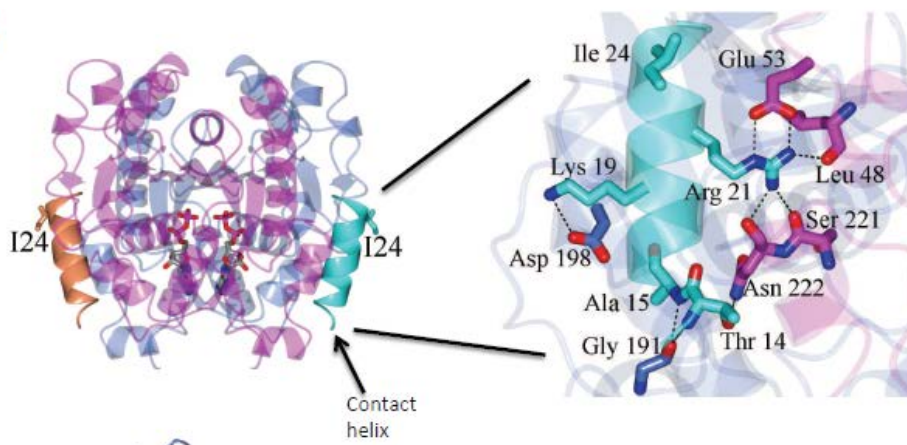
We tested if MinE^{I24N-h*} could form a complex with MinD in the absence of phospholipid vesicles by assaying retention of MinD on a His-tag affinity column. MinDD10^{D40A} (a nonhydrolytic mutant that lacks its C-terminal amphipathic helix that also functions as a MTS) was as retained on the column in the presence of MinE^{I24N-h*} in an ATP-dependent fashion (Fig. 22B). In fact, the retention of MinDD10^{D40A} on the column was greater in the presence of MinE^{I24N*-h} than with MinE-h. These results demonstrate that MinE^{I24N-h*} interacts with MinD even though it is missing the first 11 residues of MinE.

Our initial attempts to crystallize a MinD-MinE complex utilized MinDD10^{D40A} and WT MinE. However, adding ATP to a mixture containing these two proteins resulted in visible aggregation (perhaps due to release of the cryptic MTS of MinE). In contrast, aggregation was not observed when ATP was added to a mixture of MinDD10^{D40A} and MinE^{I24N*}-h and crystals were obtained that diffracted to 4.3 Å resolution (Table 6). The low resolution resulted from the high solvent content of the crystals (~70%) and attempts to improve resolution by dehydration or additive screening were not successful. It was previously shown that a MinE¹⁻³¹ peptide binds MinD, but as we have shown here the first 11 residues of MinE are not essential. Therefore, we sought to obtain crystals of MinDD10^{D40A} with a synthetic peptide consisting of residues MinE¹²⁻³¹. Crystals were obtained that diffracted to 2.6 Å resolution (Table 6). The structure was solved by using MinDD10^{D40A} as a search model (W. Wu et al., 2011b). Residues 13-26 of the MinE peptide, which includes most of the residues that correspond to the b1 strand of MinE, were visible in the structure as an α -helix, one present on each side of the MinD dimer interface (Fig. 21A and 23A; designated the contact helix). In the structure, the invariant R21 residue of MinE, required for stimulation of the MinD ATPase, forms hydrogen bonds with the side chain of E53 and backbone atoms of residues N222, S221 and L48 of MinD.

Also, K19 forms a hydrogen bond with the side chain of D198. All 5 of these MinD residues are necessary for MinE binding (W. Wu, Park, Holyoak, & Lutkenhaus, 2011a). In addition, T14 of MinE forms a hydrogen bond with the side chain of residue N222. Since T14 had not previously been examined, we analyzed a *minET14A* mutation. It was unable to rescue a Δ *min* strain from expression of MinC/MinD indicating that T14 is important for the MinD-MinE interaction (data not shown). In addition, the I24 residue of MinE was on the side of the helix away from MinD as

Fig. 21 Structure of the MinD-MinE complex. Panel (A) contains the complex between MinD Δ 10^{D40A} and MinE¹²⁻³¹ (only residues 13-26 are visible). The structure shows a MinE peptide (contact helix; colored cyan and orange) bound to each side of a MinD dimer (magenta and blue: ADP in red). On the right is a blowup of the MinE contact helix bound to MinD. It is rotated 90°. Hydrogen bonds are indicated by dashed lines. The I24 residue is on the side of the helix away from MinD. Panel (B) shows the structure of the complex between MinD Δ 10^{D40A} and MinE^{I24N*-h} (both dimers). In the crystal the dimers alternate to make a continuous helix (Fig. S5C). In the orientation on the left the membrane binding surface of MinD is beneath MinD so that the N-terminus of the contact helix (residue 13) is directed into the plane of the figure. In the structure on the right the MinD-MinE complex is rotated 90° so the orientation with respect to the membrane can be observed. The MTSs of MinD and MinE are depicted with dotted lines.

A)



B)

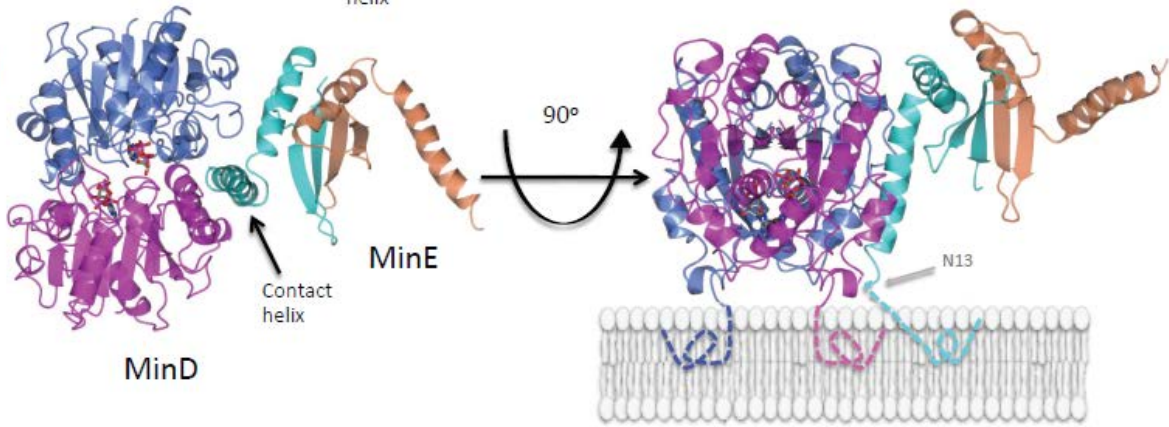


Fig. 22 Demonstration that MinE^{I24N}-h* interacts with MinD is related to Figure 21.

A) MinE^{I24N}-h* stimulates the ATPase activity of MinD. The effect of MinE^{I24N}-h* on the

B) ATPase activity of MinD was determined by measuring the release of inorganic

phosphate. The concentration of MinD, MinE and MinE^{I24N}-h* was 3 μM. B) His-tagged

MinE interacts with MinD in an ATP dependent manner. MinE-h or MinE^{I24N}-h* was

incubated with MinDΔ10^{D40A} (ATP hydrolytic mutant of MinD also missing the carboxy

terminal 10 residues) in the presence of ADP or ATP and run over a his-tag affinity

column. The bound proteins were eluted with imidazole and analyzed by SDS-PAGE.

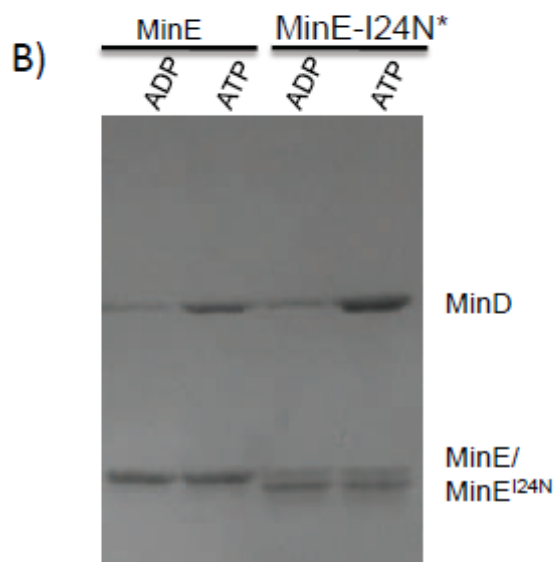
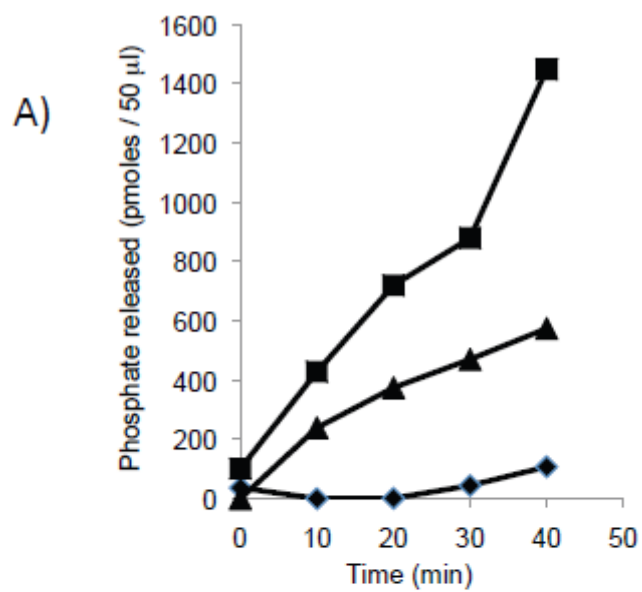


Fig. 23 The fit of MinE to the electron density map in the MinD-MinE peptide and MinD-MinE complexes is related to Table 6. A) The 2Fo-Fc electron density map contoured at 1σ following refinement is depicted. The MinE peptide corresponds to residues Asn 13 to Val 26. B) The electron density for the region between MinD dimers is shown along with the MinE structure to display the fit of the structure to the electron density. Two different views are shown. The subunits in the MinD dimer are colored blue and magenta. The subunits of MinE are colored orange and cyan. C) Two MinD dimers flanking a MinE dimer are depicted. One dimer is rotated 90° with respect to the other so both dimers could not be in contact with the membrane at the same time. The contact helices of MinE and the C-termini of MinD are in bolder colors. The position of the C-termini of MinD and the N-termini of MinE are highlighted by blue balls. On the left molecule the three balls lie in a plane that is below the structure whereas on the right molecule the three balls lie in a plane that is rotated 90° with respect to the first plane.

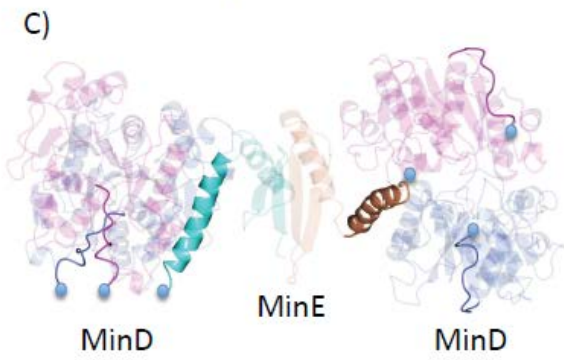
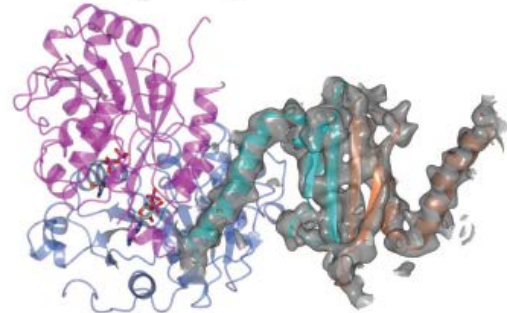
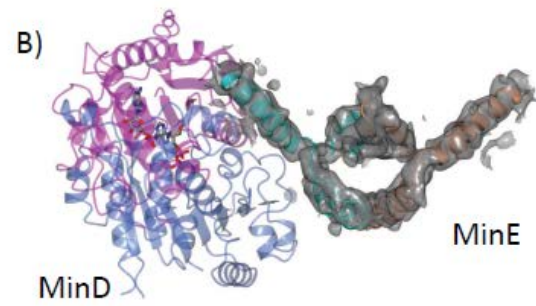
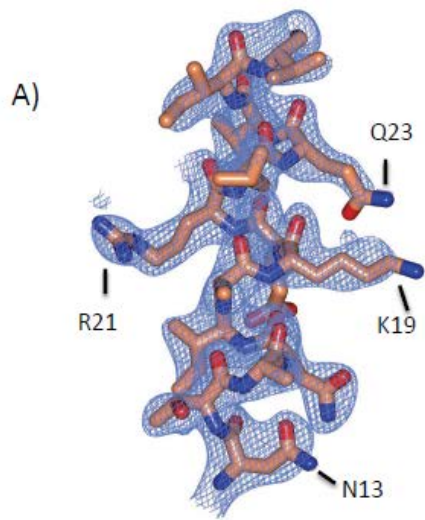


Table 6 Crystallographic Data for MinD-MinE Structures

| | MinD-MinE ¹²⁻³¹ | MinD-MinE ^{124N*-h} |
|--------------------------------------------------------|----------------------------------------------------------------------------|-------------------------------------------------|
| Data Collection | | |
| Unit-cell parameters (Å, °) | $a=64.29, b=71.80, c=76.64$ $\alpha=102.64, \beta=95.87, \gamma=111.72$ | $a=94.39, c=284.98$ $\alpha=\beta=\gamma=90$ |
| Space group | P1 | P4 ₃ 2 ₁ 2 |
| Resolution (Å) ¹ | 73.24-2.60 (2.74-2.60) | 50.0-4.30 (4.53-4.30) |
| Wavelength (Å) | 1.0000 | 1.0000 |
| Temperature (K) | 100 | 100 |
| Observed reflections | 129,007 | 121,143 |
| Unique reflections | 36,883 | 9,437 |
| Mean $\langle I/\sigma I \rangle$ ¹ | 7.1 (2.4) | 15.4 (5.5) |
| Completeness (%) ¹ | 98.5 (98.2) | 99.9 (100) |
| Multiplicity ¹ | 3.5 (3.5) | 12.8 (12.4) |
| R_{merge} (%) ^{1,2} | 15.3 (56.6) | 10.8 (52.3) |
| R_{meas} ⁴ | 18.2 (67.4) | 11.3 (54.5) |
| R_{pim} ⁴ | 9.7 (36.0) | 3.2 (15.3) |
| Refinement | | |
| Resolution (Å) | 43.42-2.60 | 48.71-4.30 |
| Reflections (working/test) | 35,023 / 1,825 | 8,925 / 455 |
| $R_{\text{factor}} / R_{\text{free}}$ (%) ³ | 20.1 / 24.3 | 29.4 / 31.1 |
| No. of atoms (protein / ADP / water) | 8,182 / 108 / 177 | 4,919 / 54 / 0 |
| Model Quality | | |
| R.m.s deviations | | |
| Bond lengths (Å) | 0.011 | 0.009 |
| Bond angles (°) | 1.356 | 1.07 |
| Average B factor (Å ²) | | |
| All Atoms | 30.6 | 135.0 |
| MinD | 30.5 | 135.0 |
| MinE | 36.3 | 135.0 |
| ADP | 21.6 | 135.0 |
| Water | 25.3 | - |
| Coordinate error (Å) | 0.41 | 1.630 |
| Ramachandran Plot | | |
| Favored (%) | 98.2 | 94.9 |
| Allowed (%) | 1.0 | 2.6 |

1) Values in parenthesis are for the highest resolution shell.

2) $R_{\text{merge}} = \sum_{hkl} \sum_i |I_i(hkl) - \langle I(hkl) \rangle| / \sum_{hkl} \sum_i I_i(hkl)$, where $I_i(hkl)$ is the intensity measured for the i th reflection and $\langle I(hkl) \rangle$ is the average intensity of all reflections with indices hkl .

3) $R_{\text{factor}} = \sum_{hkl} ||F_{\text{obs}}(hkl)| - |F_{\text{calc}}(hkl)|| / \sum_{hkl} |F_{\text{obs}}(hkl)|$; R_{free} is calculated in an identical manner using 5% of randomly selected reflections that were not included in the refinement

4) R_{meas} = redundancy-independent (multiplicity-weighted) R_{merge} (Evans, 2006).

R_{pim} = precision-indicating (multiplicity-weighted) R_{merge} (Weiss, 2001).

Expected (Figure 21A). The structure of the MinDD10^{D40A}-MinE^{I24N}-h* complex was solved by molecular replacement using the structure of MinDD10^{D40A}-MinE^{I2-31} as a search model. The difference electron density map was consistent with an α -helix extending beyond residue residue 26 of MinE that was connected by a turn to a second helix (corresponding to a1 of MinE) that was near the midpoint of a second MinD dimer. Thus, it appeared that a MinE dimer was bridging two MinD dimers. A model of the trypsin resistant fragment of MinE (PDB:1EV0, residues 39-53) was superimposed on the difference density and the b-sheet regions were fit to the corresponding electron density and the model further refined (Fig. 21B and 23B; MinE is also shown in Fig. 14C). The asymmetric unit contains one MinD and one MinE dimer. In the crystal the dimers form a continuous helix along the 4₃ screw axis. Therefore, an alternate arrangement of the asymmetric unit could be represented as a single MinE dimer positioned between two MinD dimers that are related by the crystallographic symmetry operator ($y+1/2, -x+1/2, z+1/4$). In other words, a single MinE dimer is positioned between two MinD dimers related by the aforementioned symmetry operator (Fig.21C).

Together the structures reveal several important features of the MinD-MinE interaction. The first is that the structure of MinE in the complex is consistent with a 4 stranded b-sheet but not with a 6 stranded b-sheet. Second, the b1 strand of MinE is present in an a helix (designated the 'contact' helix) that is at the MinD dimer interface, consistent with mutagenesis that identified MinD and MinE residues important for binding (Ghasriani et al., 2010; Hu & Lutkenhaus, 2001; L. Ma et al., 2004; W. Wu et al., 2011b). Thus, the b1 strand (residues 21-29), containing part of the anti-MinCD domain, is stabilized as a helix upon binding to MinD. Third, MinE bridges two MinD dimers leading to a continuous helix of alternating MinD dimers and MinE dimers. Since each MinD dimer is rotated 90° with respect to the previous one, only every fourth MinD dimer

would be in contact with the membrane (Fig. 21B and 23C). It is not clear that the continuous helix is physiologically relevant (see discussion). Fourth, the N-terminus of the contact helix of MinE^{I24N*-h} (residue 13) in the complex is oriented towards the membrane. As a result the MTS (not present in the crystal structure and indicated by dotted line in Fig. 21B) is on the same face of the complex as the MinD amphipathic helices and therefore is in position to interact with the membrane.

Discussion

Based upon the results presented here and the available structures of free MinE a model emerges for the interaction between MinE and MinD. In this model MinE switches between a ‘cryptic’ cytoplasmic conformation that is freely diffusible and an ‘active’ conformation bound to MinD and the membrane. The active conformation is achieved by MinE sensing membrane bound MinD whereas conversion to the cryptic conformation occurs following stimulation of the MinD ATPase and release from the membrane. Essential to this model is the dual role of residues ~21-29 of MinE; as the b1 strand sequestered at the MinE dimer interface and as the contact helix involved in binding MinD (Fig. 14B-D).

In the model MinE senses a MinD dimer at the membrane and undergoes a conformational change that releases the MTSs and the b1 strands with the C-terminal domain collapsing to a 4 stranded b-sheet (Fig. 21B and 14C). The b1-strand near MinD, along with additional N-terminal residues (~12-20), is stabilized as an a helix (the contact helix) upon binding MinD. Importantly, the orientation of the contact helix bound to MinD positions the MTS of MinE near the membrane (Fig. 21B). The released b1 strand not immediately in contact with a MinD dimer is tethered to the membrane by a contiguous MTS (Fig. 24). Following stimulation of the MinD

ATPase, MinD is released from the membrane and MinE either ‘snaps back’ to the 6-stranded β -sheet structure and dissociates from the membrane or is handed off to another MinD dimer (Fig. 24 and discussion below).

Residue I24 occupies a unique position in MinE since it can be altered to release the β 1 strand but is not required for MinD binding. The I24N substitution reduced the β strand content of MinE²¹⁻⁸⁸ and we propose that this substitution in full-length MinE releases the β 1 strand so that it is available for interaction with MinD. This effect of the *minE*^{I24N} mutation to ‘open up’ the MinE structure allows it to suppress some of the mutations in *minD* (*M193L*, *D198R*, *N22A* and *G224C*) and *minE* (*L3E* and *F7E*) that prevent interaction. Thus, the residues of MinD and MinE identified by these mutations are likely involved in the ‘sensing step’ that triggers the conversion of MinE from the 6 to the 4 β -stranded structure. On the other hand, mutations not suppressed by the *minE*^{I24N} mutation, such as *minE*^{A18T} and *minD*^{E53K}, likely identify residues directly involved in binding. This latter possibility is confirmed by the structure of the complex.

MinE residues important for stimulating the MinD ATPase (and also for binding) include R21, L22 and A18. Residue R21 forms a hydrogen bond with E53 of MinD and the backbone of residues N222, S221 and L48, all of which were recently shown to be important for MinE binding (W. Wu et al., 2011b). In addition, residues L22 and A18 abut MinD whereas residues I24 and E20, which are not important for binding, are on the face of the contact helix away from MinD (Fig. 21A). Although MinE stimulates the MinD ATPase, the mechanism is not clear. One possibility suggested for another WACA family member (ParF) - that a conserved arginine in its partner (ParG) functions as an arginine finger (Barilla, Carmelo, & Hayes, 2007)– can be ruled out. The conserved arginine, R21, in MinE interacts with MinD residue E53 and is not near the

catalytic site (Fig. 21B). MinE likely stimulates the ATPase of MinD by inducing subtle changes in the switch regions of MinD similar to what is observed in the nitrogenase complex (Schindelin et al., 1997).

One possible mechanism for the MinD-dependent conversion of MinE from the 6 to the 4 b-stranded structure is that the two structures are in equilibrium and that MinD binding to the 4 stranded structure pulls the equilibrium in this direction. However, we think this is unlikely since the 4-stranded structure (such as MinE^{I24N}) binds to the membrane independent of MinD. If the two structures were in equilibrium in WT MinE, one would expect WT MinE to go to the membrane independent of MinD (the binding to the membrane by the 4 stranded structure would pull the equilibrium in that direction).

Although the MTS contains highly conserved hydrophobic residues (Fig. 20), no function has been ascribed to this segment of MinE. Our study indicates it is a cryptic MTS that can be unmasked by mutation or through interaction with MinD. A previous study argued that positively charged residues were involved in direct MinE-membrane interaction since eliminating 3 charged residues (C1 mutant - positions 10-12) affected the interaction of MinE¹⁻³¹ with vesicles *in vitro* and Min oscillation *in vivo* (Hsieh et al., 2010). Although these residues could also contribute to membrane binding, they are also involved in 'sensing' MinD as altering these residues also affects the ability of MinE to displace MinC from MinD (Loose et al., 2011). In WT MinE the MTS is packed against the b-sheet and not available for interaction with the membrane (Fig. 14B). Therefore, it is not surprising that mutations that disrupt the 6-stranded b-sheet structure, such as *minE*^{I24N} and *minE*^{L22R}, release this MTS so that it is available to interact with the membrane. These mutations mimic the interaction with MinD to open up the MinE

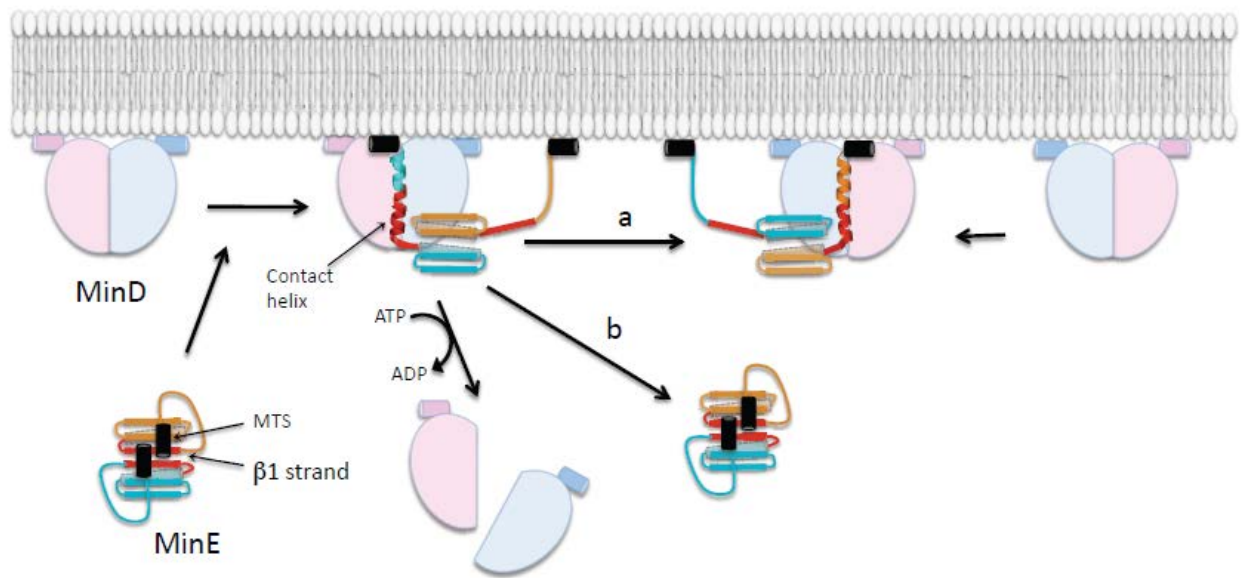
structure. In contrast, the *minE*^{I25R} mutation induces membrane binding, not by disrupting the β -sheet structure, but by disrupting the hydrophobic interaction that tethers the MTS to the β -sheet (Fig. 14B).

Although all 4 of the *minE* charge mutations (*minE*^{L3E}, *minE*^{L4E}, *minE*^{F6E} and *minE*^{F7E}) prevented MinE mutants (I25R and I24N) from going to the membrane, their effect on the ability of MinE to counter MinC/MinD varies. One possible explanation for this difference is the position of the corresponding amino acids in the MTS. Residues L3 and F7 interact with residue I25 to tether the MTS to the β -sheet whereas L4 and F6 do not (Ghasriani et al., 2010). Thus, substituting a charged residue for L3 or F7 would release the MTS and the loop formed by residues 8-20 would no longer be constrained, which is likely to be important for sensing. Residues L3 and F7 could be the most important of the hydrophobic residues for membrane binding but their additional involvement in sensing MinD makes this difficult to determine. Nonetheless, a role for the interaction of MinE with the membrane is indicated by the effect of the *minE*^{F6E} and *minE*^{L4E} mutations on cell morphology. Even though these mutations do not significantly affect MinD binding, strains with these mutations have a heterogeneous size distribution indicating that membrane binding by MinE contributes to spatial regulation. This is consistent with the phenotype previously observed with MinE⁶⁻⁸⁸, which suppresses the inhibitory activity of MinD/MinC but produces a phenotype resembling what we observe with *minE*^{F6E} and *minE*^{L4E} (Pichoff et al., 1995).

Importance of the MinE dimer – Tarzan of the jungle

Previous work indicated that the dimerization of MinE is important for its anti-MinC/MinD activity (Pichoff et al., 1995; Zhao et al., 1995). The basis for this conclusion is the observation

Fig. 24 Tarzan of the Jungle model for the interaction between MinD and MinE. In this model MinE encounters MinD bound to the membrane and the MTSs (black segments) and the β 1 strands (red) of MinE are released from the 6 stranded β -sheet structure resulting in formation of a 4-stranded β -sheet structure. One of the released β 1 strands along with N-terminal flanking residues form an β -helix that is stabilized by binding to MinD while the other is tethered to the membrane through its linked MTS. The fate of MinE depends on two competing reactions (indicated by 'a' and 'b') following the dissociation of MinD due to ATPase stimulation. Either it is handed off to another MinD (a) or dissociates from the membrane as it snaps back to the 6 β -stranded structure (b). A higher density of MinD on the membrane favors the former.



that heterodimers formed between WT MinE and MinE²²⁻⁸⁸ have reduced activity (Zhang et al., 1998). Formation of these heterodimers does not alter the total concentration of anti-MinCD domains in the cell, but simply limits each MinE dimer to one anti-MinCD domain. This monomerization of the anti-MinCD domains is sufficient to reduce their activity so at physiological levels they no longer counteract MinC/MinD and cells fail to divide.

The MinE C-terminal domain is necessary for spatial regulation of division. It has three known functions: sequestering and dimerizing the anti-MinCD domains and restraining the MTS so it does not interact with the membrane. As proposed here, MinE encountering a MinD dimer at the membrane releases the MTSs and the b1 strands, one of which becomes the contact a helix and binds to the encountered MinD dimer with the immediately adjacent MTS interacting with the membrane. The other released anti-MinCD domain is probably a nascent helix tethered to the membrane through its linked MTS (Fig.24).

It is possible that a MinE dimer bridges two membrane bound MinD dimers as observed in the crystal, however, the two MinD dimers are rotated 90° with respect to each other due to the angle of the MinE arms (Fig. 22B). If the junction between the contact helix and a1 is flexible, this is possible. We favor a “Tarzan traveling on vines through the jungle” model, with MinE as Tarzan and MinD as the vine (Fig. 24). Like Tarzan, MinE has two arms and swings from MinD (the vine) to MinD. In the model MinE bound to MinD has two alternatives following stimulation of the MinD ATPase and its release from the membrane. MinE, either dissociates from the membrane as it reverts back to the cryptic form, or before this happens, an anti-MinCD domain grasps a second MinD dimer. It is possible that MinE has an intermediate, transient membrane associated state free of MinD. In the Tarzan analogy, once he grabs the vine it has a finite

lifetime before it falls from the trees and he has to grab another vine or he suffers the same fate and has to start over. A high, local density of MinD on the membrane favors a successful ‘handoff’ whereas a lower density favors MinE ‘snapping’ back to the 6 stranded structure and being released from the membrane. The rates of these two competing reactions dictate the fate of the MinE (Fig. 24, A & B).

A recent report examining the Min system *in vitro* (Loose et al., 2011) found that the residence time for MinE in a traveling wave was longer than for MinD. It is likely that the ability of MinE to ‘swing from one MinD to the next’ explains the longer MinE residence times. It is also clear in this model why MinE tracks membrane bound MinD and moves towards regions of higher MinD density. Finally, our findings here about the MinD-MinE system are likely to be applicable to other members of the WACA family.

Experimental Procedures

Bacterial strains and growth conditions

E. coli strains JS964 (MC1061 *malP::lacI^q Δmin::kan*) and its isogenic parental strain JS219 (*minCDE⁺*) have previously been described (Pichoff et al., 1995). LB (Luria-Bertani) medium containing 0.5% NaCl and relevant antibiotics at 37°C was used for most experiments unless otherwise indicated. BTH101Δ*min* (F⁻ *cya-99, araD139, galE15, galK16, rpsL1 (Str^r), hsdR2, mcrA1, mcrB1 Δmin::kan*) was used for bacterial 2-hybrid system (Karimova, Pidoux, Ullmann, & Ladant, 1998).

Bacterial two-hybrid analysis

A *cya*-null strain BTH101Δ*min::kan* was transformed with plasmids pCT25-MinD and pUT18-MinE, respectively carrying wild-type or mutant *minD* and *minE* alleles, and grown overnight at 37°C on LB plates containing 0.2% glucose, 20 μg/ml chloramphenicol and 100 μg/ml ampicilin. For a plate-based assay, colonies from the LB plate were diluted in 300 μl volume of LB broth and spotted onto fresh LB plates supplemented with 20 μg/ml chloramphenicol, 100 μg/ml ampicilin, 40 μg/ml 5-bromo-4-chloro-3-indoyl-β-D-galactopyranoside (X-Gal), and 0.5 mM IPTG. Observation was usually made after 14-18 hours of incubation at 30°C.

Plasmids

Plasmids new to this study expressed MinE in which part of the N-terminus was replaced with a his-tag and were constructed as follows. *minE* fragments were obtained by PCR using pSEB104CDE as a template and were ligated into EcoRI / XbaI-treated pQE80L (Qiagen) to generate pQE80L-MinE²¹⁻⁸⁸, pQE80L-MinE²²⁻⁸⁸, pQE80L-MinE²³⁻⁸⁸, and pQE80L MinE³⁶⁻⁸⁸. A derivative of pQE80L-MinE²¹⁻⁸⁸ carrying the I24N substitution was made by site-directed mutagenesis. Plasmid pSEB104CD (P_{BAD}::minC minD), pSEB104CDE (P_{BAD}::minC minD minE) and pJB216 (P_{lac}::minE) were described earlier (H. Zhou & Lutkenhaus, 2005). Plasmids used to monitor the localization of MinE were pJK100 (P_{trc} minDE-GFP) and pJK110 (P_{trc} minE-GFP), which are derivatives of pDSW208 and were described earlier (H. Zhou & Lutkenhaus, 2005). Mutations in various genes on these plasmids were introduced by using the QuickChange site-directed mutagenesis kit according to the manufacturer's instruction (Stratagene). Plasmids for overexpression of various MinD proteins were derivatives of pZH115 (pJF118EH [P_{tac}::minD]) and pZH115-10 [P_{tac}::minDΔ10]), which were described earlier (Hu & Lutkenhaus, 2001; Hu et al., 2003). Additional *minD* mutations were introduced into these plasmids by site-directed mutagenesis. The plasmids for the bacterial 2-hybrid system are pKT25 and pUT18 (Karimova et al., 1998). A derivative of pKT25 carrying resistance to chloramphenicol was described recently [pCT25 (Cm^R)] as were derivatives that carried the *minD* and *minE* genes (W. Wu et al., 2011b).

Gel filtration and circular dichroism (CD) Spectroscopy

Protein samples (500 ul volume) at a final concentration of 1 ug/ml were diluted in buffer C (25 mM HEPES-NaOH [pH7.0], 250 mM NaCl, 1 mM EDTA, 5 mM DTT) before being subjected to an AKA-fast protein liquid chromatography equipped with SuperdexTM75HR 10/30 column

(GE Healthcare) with a flow rate of 0.5 ml/min. For CD analysis, MinE²¹⁻⁸⁸ and MinE^{21-88-124N} samples at a concentration of 570 μ M were prepared by 100-fold dilution in 10 mM sodium phosphate buffer (pH 7.5). Far-UV CD spectra were recorded on a Jasco - spectropolarimeter with a 1 mm path length at 20 °C. Spectra were an average of 10 scans over the wavelength from 190 nm to 250 nm. The secondary structure content of each sample was obtained using the K2d prediction program (Andrade et al., 1993).

Formaldehyde Crosslinking

Formaldehyde at the final concentration of 0.317 mM was introduced into the MinE samples diluted in 1x ATPase Buffer (25 mM Tris-HCl [pH 7.5], 50 mM KCl, 5 mM MgCl₂). The reaction was incubated at 37 °C for 20-30 min before being terminated by addition of 2x SDS sample loading buffer (125 mM Tris-HCl [pH 6.8], 20% glycerol, 4% SDS, 0.005% bromophenol blue). The samples were analyzed by SDS-PAGE.

Microscopy

Strain JS964 (Δ *min*)/pSEB104CDE and JS964(Δ *min*)/pSEB104CDE-24 were grown overnight at 37°C in LB medium containing 0.1% arabinose and 100 μ g/ml spectinomycin. The next day, cells were diluted and cultured under the same conditions described above to an OD₅₆₀ of 0.4-0.5. The phenotypes of cells were characterized using a Nikon microscope equipped with a 100 X objective. To determine subcellular localization of MinE proteins, cultures of JS964 (Δ *min*)/pJK110P_{lac}::*minE*^{I24N}-GFP, JS964(Δ *min*)/pJK100 (P_{lac}::*minD minE-GFP*), and JS964(Δ *min*)/pDSW208 (P_{lac}::*minD minE*^{I24N}-GFP) in exponential phase were incubated with

10 μ M IPTG for 1 hour at 37°C in LB. The images were recorded at 15 second intervals using a cooled CCD camera and processed using Metamorph and Adobe Photoshop.

MinD ATPase Assay

The hydrolysis of ATP was measured using the ATPase colorimetric assay kit that monitors the release of inorganic phosphate (P_i) (Innova Biosciences). The assay was performed according to the manufacturer's instructions with a minor modification to scale down reaction volumes. MinD (3 μ M) and MinE (3 μ M) were mixed in reaction buffer (25 mM Tris-HCl, pH7.5, 50 mM KCl, 5 mM MgCl₂). In some reactions the concentration of MinE was varied. After adding ATP (1 mM) and multilamellar vesicles (MLVs) (200 ng/ μ l), the reaction mixture was incubated at room temperature and samples taken at indicated times. Once the reaction was quenched, the OD₅₉₅ was recorded and the enzymatic activity was quantified based on the formula provided by the manufacturer.

Random mutagenesis of MinE

PCR reaction using pSEB104CDE ($P_{ara}::minC minD minE$) as a template was carried out with two primers: (F) 5' (BamHI) GAATGGATCCGTTGGCATTACTCGATTTCTTTCTC3' and (R) 5' (KpnI) GCATGGTACCCTTATTTTCAGCTCTTCTGCTTC3'. An optimal mutation rate (0.3-1 base/kb) was obtained with GeneMorph II Random Mutagenesis kit (Stratagene). The PCR product was then digested with BamHI and KpnI for cloning into the pUT18 vector. The library of *minE* containing plasmids was co-transformed with each of pCT25^{minD} mutants into

BTH101 Δ *min* strain and incubated at 30 °C on a plate containing chloramphenicol and ampicillin. Plasmids were isolated from colonies that produced blue color and were sequenced with a primer specifically designed for pUT18 vector.

Overexpression and purification of MinE and MinD proteins

JS964 (Δ *min*)/pJB216-MinE¹⁻⁸⁸, JS964 (Δ *min*)/pJB216-MinE^{1-88(I24N)}, JS964 (Δ *min*)/pQE80L-MinE²¹⁻⁸⁸, and JS964 (Δ *min*)/pQE80L-MinE^{21-88(I24N)} were grown at 37 °C in LB medium to an OD₅₄₀ of approximately 0.4. IPTG was then added to the culture at a final concentration of 1 mM. After 3 hours of incubation with IPTG, cells were harvested by centrifugation and stored frozen at -80 °C. Cells were thawed on ice after suspension in buffer A (50 mM Tris-HCl, pH7.5, 100 mM NaCl, 10 mM imidazole). Cells were lysed by three passages through a French press at 16,000 psi and the supernatant was obtained after centrifugation at 12,000 x g for 30 min. at 4°C. The supernatant was applied to a nickel affinity column (Qiagen) and proteins were eluted with buffer B (50 mM Tris-HCl [pH 7.5], 500 mM NaCl, 250 mM imidazole). The eluted protein samples were pooled and dialyzed against buffer C (25 mM HEPES-NaOH [pH7.0], 250 mM NaCl, 1 mM EDTA, 5 mM DTT) prior to final storage at -80 °C. MinD Δ 10 and MinD Δ 10^{D40A} were purified as recently described (W. Wu et al., 2011b).

Crystallization and Structure determination

The growth of crystals and the determination of the structures by X-ray crystallography are described in full in the Extended Experimental Procedures. In brief, crystals of MinD Δ 10^{D40A}

and MinE^{I24}-h* diffracted to 4.3 Å resolution and crystals of MinDΔ10^{D40A} and a synthetic peptide of MinE^{I2-31} diffracted to 2.6 Å resolution. The accession codes are 3R9I for MinD-MinE^{I2-31} and 3R9J for MinD-MinE^{I24N*-h}.

Crystallization and Data Collection

All Crystallization screening was conducted in Compact Jr. (Emerald biosystems) sitting drop vapor diffusion plates at 20 °C using 0.5 μL of protein and using 0.5 μL of crystallization solution equilibrated against 100 μL of the latter. Data were at the Advanced Photon Source IMCA-CAT beamline 17ID using a Dectris Pilatus 6M pixel array detector. Purified MinDΔ10^{D40A} in 20 mM NaCl, 10 mM Hepes [pH 7.0], 10% glycerol, 2 mM DTT and MinE^{I24}-h* in 250 mM NaCl, 25 mM Hepes [pH 7.0], 1 mM EDTA, 10% glycerol, 2 mM DTT were used for crystallization screening. The MinD-MinE^{I24N}-h* complex was prepared as follows: 100 μL of MinD (17.3 mg/mL), 42.9 μL of MinE (15.4 μg/mL), 50 μL of 5X ATPase buffer (125 mM Tris pH 7.5, 250 mM KCl, 25 mM MgCl₂), 12.5 μL ATP (100 μM), 1.25 μL DTT (1M) were mixed with water to a final volume of 250 μL and incubated on ice. This produced a mixture consisting of 6.9 mg/mL (0.24 mM) MinD and 2.6 mg/mL MinE (0.24 mM) in 50 mM KCl, 25mM Tris [pH 7.0], 5 mM ATP, 5 mM DTT, 5 mM MgCl₂. Original crystals were obtained from the Wizard 1 screen condition #41 (Emerald biosystems, 30% (w/v) PEG-3000, 100 mM CHES pH 9.5) using 0.5 μL of protein and using 0.5 μL of crystallization solution equilibrated against 100 μL of the latter at 20°C. Prismatic crystals were obtained within 24 hours. Refinement screening was conducted using the Additive Screen (Hampton Research) and the samples used for data collection were obtained from 30% (w/v) PEG-3000, 100 mM CHES

[pH 9.5], 10 mM EDTA. Single crystals were transferred to a drop containing 80% crystallization solution and 20% DMSO before freezing in liquid nitrogen for data collection. To obtain crystals of the MinD-MinE peptide, MinD Δ 10^{D40A} was concentrated to 10 mg/mL in 50 mM KCl, 25 mM Tris [pH 7.5], 5mM DTT, 5mM MgCl₂ and a 25 mM stock solution of a MinE peptide comprising residues 12 to 31 was prepared in the same buffer. The MinE¹²⁻³¹ peptide had the sequence NH₂-KNTANIAKERLQIIVAERRR-CO₂H (obtained from Genescript [$>98\%$ purity]). The MinD-MinE¹²⁻³¹ complex was prepared by mixing MinD (0.32 mM), MinE¹²⁻³¹ (0.7 mM) and 2.5 mM ATP. Crystallization screening was conducted as above and crystals displaying a needle morphology were obtained in approximately 3 days from the Wizard 4 screen condition #29 (Emerald biosystems, 20% (w/v) PEG 3350 100 mM citrate [pH 4.0], 200 mM sodium citrate) using 0.5 μ L of protein and 0.5 μ L of crystallization solution equilibrated against 100 μ L of the latter. Single crystals were transferred to a drop containing 80% crystallization solution and 20% glycerol before freezing in liquid nitrogen for data collection.

Structure Solution and Refinement

All intensities were integrated and scaled using the XDS and Scala (Evans, 2006) packages respectively. The Laue class was checked for each data set using Pointless (Evans, 2006) which indicated that the crystals belonged to the triclinic space group *P1* for MinD-MinE¹²⁻³¹ and Laue class *P4/mmm* and likely and likely space groups *P4₁2₁2* or *P4₃2₁2* for the MinD-MinE^{I24N*-h}. The Matthew's coefficient (Matthews, 1968) ($V_m=2.8$, solvent content=55%) indicated that there were two MinD dimers in the asymmetric unit for the MinD-MinE¹²⁻³¹ crystals and a single dimer of MinD and MinE in the asymmetric unit for MinD-MinE^{I24N*-h}.

MinD-MinE¹²⁻³¹

Coordinates from a previously determined structure of a MinD dimer (PDB: 3QL9) were used as the search model for molecular replacement with Molrep (Vagin & Teplyakov, 2010), which yielded a correlation coefficient of 0.404 after positioning the two dimers. Following initial refinement prominent difference electron density (Fo-Fc) greater than 3Å was observed at the dimer interfaces, which was consistent with an α -helical structure at the MinD dimer interface corresponding to residues 13-26 of the MinE peptide (designated the contact helix). In addition, electron density (Fo-Fc) consistent with ADP molecules was observed in the ATP binding pocket of each MinD subunit. MinE peptide residues 13-26 were manually fit to the electron density with Coot (Emsley & Cowtan, 2004) and the structure refined with Phenix (P. D. Adams et al., 2010) using NCS restraints between the MinD and MinE peptide molecules. Structure validation was carried out using Molprobity (Chen et al., 2010).

MinD-MinE^{I24N*-h}

Coordinates from the MinD-MinE¹²⁻³¹ structure were used as the search model for molecular replacement with Molrep (Vagin & Teplyakov, 2010). Searching with a single MinD dimer in the space group $P4_32_12$ yielded a solution with a correlation coefficient of 59.6%. Molecular replacement in the enantiomorphous space group $P4_12_12$ using the dimer as the search model yielded a correlation coefficient of 47.8%. Therefore, subsequent refinement was conducted in space group $P4_12_12$. Difference electron density (Fo-Fc) consistent with an α -helical structure that continued from the C-terminal end of the MinE¹²⁻³¹ peptide was observed. This second α -helix was directed towards the mid-point between a second MinD dimer related by the

crystallographic symmetry operator ($y+1/2, -x+1/2, z+1/4$). The difference electron density in this region was consistent with a 4-stranded β -sheet structure. Additional helical density continued from this region towards a MinD dimer related by the symmetry operator provided above. Therefore, it appeared that a MinE dimer was bridging two MinD dimers. The second helix, extending from the C-terminus of the MinE¹²⁻³¹ peptide, and the 4-stranded β -sheet structure were fit to the observed electron density maps using a previously determined MinE structure (PDB: 1EV0) as a guide. Structure refinement and manual model building were performed with Buster (Blanc et al., 2004) and Coot (Emsley & Cowtan, 2004) respectively. For structure refinement, tight geometry restraints and NCS restraints were applied. A reference model composed of the MinD-MinE¹²⁻³¹ structure and the previously determined MinE structure (PDB: 1EV0) was used during refinement to maintain secondary structure elements. β -factors for all residues were set to the Wilson b -factor, estimated by Buster, during refinement. Structure validation was carried out using Molprobity (Chen et al., 2010).

Chapter IV

Asymmetric binding of MinE stimulates MinD ATPase activity

Abstract

The operation of the Min oscillator, composed of MinD and MinE, requires energy in the form of ATP hydrolysis. MinD dimerizes and binds to the membrane in the presence of ATP. The membrane-bound MinD recruits MinE which stimulates ATP hydrolysis causing the release of MinD from the membrane. Despite the progress made in understanding Min protein dynamics, the underlying chemistry of the MinE-dependent MinD ATPase activation still remains ill-defined. To get a sense of how MinE stimulates the MinD ATPase, we have compared the dimeric structure of MinD with that of the MinD-MinE complex to determine residues affected by MinE binding. Our analysis shows that MinE induces some conformational changes in the ATP binding pocket and in the side chains at the MinD-MinE binding interface. The dimerization of the MinD-ATP gives rise to two symmetrical binding sites, both of which are occupied by MinE in the crystal structure. To test if MinD ATPase activation requires MinE binding to both sites, we measured the ATPase activity of a heterodimer that retains only one intact binding site for MinE^{CD}. Our results indicate that the binding of MinE to one side of the MinD-ATP dimeric interface is sufficient for hydrolysis of both ATPs bound to the MinD heterodimer, indicating that ATP catalysis involves asymmetric activation.

Introduction

The placement of the cytokinetic machinery at midcell is crucial to equipartition of cellular components, especially the genetic material, into the two daughter cells. In most prokaryotes the Z ring, which consists of polymers of the tubulin homologue FtsZ attached to the surface of the cytoplasmic membrane, provides a scaffold for the cytokinetic machinery (Erickson et al., 2010; Goehring & Beckwith, 2005; Lutkenhaus, 2007; Margolin, 2005). In *E. coli*, the Min system consisting of MinC, MinD, and MinE, plays an important role in spatial regulation of cytokinesis by preventing Z ring assembly at the poles of the cell ensuring that it takes place only at midcell (de Boer et al., 1989; P. A. de Boer et al., 1992; Hu et al., 1999; Hu et al., 2003; Pichoff & Lutkenhaus, 2001). This spatial regulation of Z ring formation is achieved by a periodic oscillation of the three Min proteins between the poles of the cell (Fu et al., 2001; Hu & Lutkenhaus, 1999; Raskin & de Boer, 1999a, 1999b). MinC and MinD function as an inhibitor of Z ring assembly that is positioned by the action of MinE.

MinD is a member of the deviant walker A cytomotive ATPase (WACA) family that binds cooperatively to the cytoplasmic membrane (de Boer et al., 1991; Lackner et al., 2003; Michie & Lowe, 2006; Mileykovskaya et al., 2003). MinC is a cytoplasmic protein that is a dimer and is recruited to the cytoplasmic membrane by MinD where it effectively exerts an inhibitory action on the Z ring (P. A. de Boer et al., 1992; Hu & Lutkenhaus, 2000; Hu et al., 1999; Johnson et al., 2004). MinE is a small protein that interacts with MinD to induce the oscillation. It consists of 88 amino acids that comprises two functionally distinct domains. The N-terminal domain (MinE^{CD}, residue 1-31), designated the anti-MinCD domain, displaces MinC from MinD and stimulates the MinD ATPase, resulting in the detachment of MinD from the membrane (Hu & Lutkenhaus, 2001; Lackner et al., 2003; Pichoff et al., 1995; Zhao et al., 1995). The C-terminal region,

referred to as the topological specificity domain (MinE^{TSD}, residues 32-88), is necessary to spatially regulate MinC and MinD (King et al., 2000; Shih et al., 2002; Zhang et al., 1998). It is responsible for the dimerization of MinE and sequesters part of the MinE^{CD} and masks a cryptic membrane binding motif located in MinE^{CD} (Ghasriani et al., 2010; Kang et al., 2010; Park et al., 2011).

During the pole-to-pole oscillation cycle, MinD occupies one polar zone that stretches from the pole to midcell. This zone is flanked by a ring-like structure of MinE (the MinE ring) that proceeds towards the pole and drives MinD off the membrane (Fu et al., 2001; Hale et al., 2001; Raskin & de Boer, 1997). As the MinD polar zone shrinks toward the pole, a new MinD polar zone forms at the opposite pole that will be in turn flanked by a MinE ring near midcell and the oscillatory cycle perpetuates (Lutkenhaus, 2007; Raskin & de Boer, 1999b). As a result of the oscillation, the inhibitory MinCD complexes are directed away from the midcell and toward the poles, which allows the Z ring to assemble at the midcell site.

At the physiological concentration of the Min proteins, the principal parameter governing the frequency of the oscillation is the MinE-dependent catalysis rate of the MinD ATPase where the membrane binding of MinD is an indispensable step (Hu & Lutkenhaus, 2001). The C-terminal 10 amino acids of MinD constitute a membrane targeting sequence (MTS) that becomes an amphipathic helix that embeds in the phospholipid membrane (Hu & Lutkenhaus, 2003; Szeto et al., 2003; Szeto et al., 2002; H. Zhou & Lutkenhaus, 2003). The fact that MinD devoid of the MTS cannot be not activated by MinE (Lutkenhaus J, unpublished) suggests that the membrane

binding of the C-terminal MTS causes conformational changes in MinD that make it competent to undergo ATP hydrolysis upon MinE binding. Unexpectedly, a recent study shows that the first 10 amino acids of MinE are sequestered by MinE^{TSD} and function as an MTS when released by certain *minE* mutations (Park et al., 2011). This MTS is also released upon MinD binding. It was proposed that the MTS may contribute to the enhanced retention of MinE on the membrane, thereby allowing MinE to move between MinD dimers, which appears crucial for the Min oscillation (Park et al., 2011).

The WACA family proteins share three motifs that mediate nucleotide coordination and hydrolysis: a deviant version of the Walker A motif, switch I, and switch II. In MinD the deviant walker A motif, also referred to as the P-loop, contains a signature lysine (K11) that forms hydrogen bonds with the α and γ -phosphate of ATP bound to opposite monomer (Leipe et al., 2002; Lutkenhaus & Sundaramoorthy, 2003; Michie & Lowe, 2006). This interaction is pivotal for ATP-dependent MinD dimerization (Hayashi et al., 2001; W. Wu et al., 2011b; H. Zhou et al., 2005) and to energetically predispose the γ -phosphate to hydrolysis by neutralizing the repulsive force between electronegative oxygen atoms (Frech et al., 1994; Hayashi et al., 2001; Maegley, Admiraal, & Herschlag, 1996). The carboxylate oxygen of the catalytic aspartate (D40) in the switch I motif functions as a general base and polarizes a water molecule for attack of the β - γ phosphate bond (Leonard et al., 2005; Schindelin et al., 1997). The aspartate residue in the switch II motif (D120), also called the walker B motif, interacts with magnesium directly or indirectly via water and therefore aids in ATP binding and hydrolysis (Hayashi et al., 2001; W. Wu et al., 2011b).

In vitro a MinE peptide corresponding to part of MinE^{CD} (residues 1-27) cooperatively stimulates the MinD ATPase with a Hill coefficient of over 3 (Ghasriani et al., 2010). A little shorter peptide (residues 1-22) is also fully able to activate the MinD ATPase but has 5 fold lower affinity for MinD (Ghasriani et al., 2010). Our recent study demonstrated that MinE lacking the first 11 amino acids can stimulate the MinD ATPase, indicating that residues critical for the enzymatic activation lie within 12-22 and that the residues located outside of 12-22 in the MinE^{CD} probably augment the interaction with MinD (Ghasriani et al., 2010; Park et al., 2011). Systemic substitutions in the MinE¹⁻²⁷ peptide indicated that 3 positions (A18, R21, L22) are critical for MinD activation (Ghasriani et al., 2010). This result is consistent with previous genetic analysis which identified two residues (A18, L22) as critical for MinD binding. These residues are located on the same face of the α helical structure of MinE^{CD} that is adjacent to MinD (L. Y. Ma et al., 2003). From all studies combined, it appears that three residues (A18, R21, L22) are essential for the activation of MinD ATPase while other residues (T14, A15, K19) involved in MinD binding are less critical.

The crystal structure revealed extensive hydrogen bonding between R21 and conserved MinD residues located on one monomer. These include the side chain of E53 and the backbone atoms of L48, S221 and N222 (Park et al., 2011). This implies a rather indirect but still very important role for R21, a residue conserved in all MinEs, in ATP hydrolysis. Although MinE binds at the MinD dimer interface, 8 out of 13 MinD residues involved in MinE binding are on the monomer contacted by R21 (W. Wu et al., 2011b). Moreover, those residues involved in binding that are located on the other monomer, D192, M193, and D198, appear to be less critical since mutations altering those residues can be bypassed by MinE mutations that release MinE^{CD} from the MinE

dimer interface (Park et al., 2011). Due to the asymmetry, MinE binding at the MinD dimeric interface should transmit different signals to each MinD monomer.

In this study, we examined the impact of MinE binding on the structural alterations of MinD to determine how MinE stimulates the MinD ATPase. To this end, we compared the structures of free MinD and MinD in complex with a MinE peptide corresponding to the critical part of MinE^{CD}. In addition, using a MinD heterodimer composed of the wild-type and a mutant MinD protein that cannot bind MinE, we asked whether stimulation of the MinD ATPase requires the interaction of MinE on both sides of the dimeric interface. Answers obtained will provide an insight into the dynamics of WACA family of proteins.

Results

Comparison of the MinD^{D40A}Δ10 and the MinD^{D40A}Δ10-MinE structures

To obtain information about the chemical basis of the MinE activation of the MinD ATPase, we have compared the structure of MinD^{D40A}Δ10 dimer (PDB 3Q9L) with that of MinD^{D40A}Δ10 dimer complexed with MinE¹²⁻³¹ (PDB 3R9I). The MinD dimer contains ATP, however, in the MinD-MinE complex the ATP has been hydrolyzed to ADP. It appears, however, that MinD in the complex is still in the “ATP conformation” since the K11 residue still forms hydrogen bonds with the phosphates of the nucleotide and the overall structure is largely superimposable on the structure of the free MinD.

Although the two structures share a striking similarity, as we have already anticipated in chapter III, several structural alterations were detected in the nucleotide binding pocket that includes the

switch I and a region proximal to the switch II (Fig.25). The conserved E146 rotates away from a contact with the ribose of ATP in the MinD structure to form a new hydrogen bond with S149 and a contact with S221 in the MinD-MinE peptide complex. The latter contact may stabilize the interaction of the R21 of MinE with S221 (Fig.26). However, the significance of this motion for ATP hydrolysis is not clear. Also, from comparison of the structures several residues have to undergo conformational changes to accommodate MinE. Two arginine residues (R51 and R54) have to move so that E53 can move into place and form hydrogen bonds with R21 of MinE (Fig.27). Lastly, I41 undergoes a rotation away from the nucleotide, which may be due to the loss of the γ phosphate (Fig. 25). In summary, the structures are largely similar and the differences observed in MinD are due to changes that allow MinE binding. The basis for ATP hydrolysis is not clear.

MinE activation of the MinD heterodimer ATPase

To test whether MinE activation of MinD ATPase requires MinE binding to the both sides of a MinD-ATP dimer, we used the scheme depicted in Fig.28. In this approach MinD heterodimers are generated by incubating wild type MinD protein, MinD^{WT}, with an excess of the MinD double mutant, MinD^{E53A/N222A}, that is unable to bind MinE. As previously shown, either mutation (E53A or N222A) is sufficient to prevent MinE interaction although neither mutation affects interaction with MinC (W. Wu et al., 2011b). To ensure that MinD did not interact with MinE, we used a double mutant MinD^{E53A/N222A}. Consistent with our expectation, the ATPase activity of the double mutant was minimally stimulated by MinE (Fig.29). In contrast, the ATPase activity of the MinD^{WT} was stimulated as shown previously (Hu & Lutkenhaus, 2001). To our surprise, the incubation of 4 μ M MinD^{WT} with 4 μ M MinD^{E53A/N222A} resulted in a 2 fold

increase in the rate of ATP hydrolysis over that observed with just 4 μM MinD^{WT} . This result is consistent with MinD^{WT} and $\text{MinD}^{\text{E53A/N222A}}$ forming a heterodimer and the ATP bound by each subunit in the heterodimer undergoing hydrolysis (Fig. 29). Consistent with this, the extent of stimulation is similar to what is observed with 8 μM MinD^{WT} .

To confirm this finding, we examined the effect of increasing the concentration of $\text{MinD}^{\text{E53A/N222A}}$ in a reaction with the concentration of MinD^{WT} fixed at 2 μM . If our interpretation is correct, further addition of the mutant protein should not have an effect and the stimulation should be limited by the concentration of MinD^{WT} . Consistent with this, the addition of a two or three fold excess of $\text{MinD}^{\text{E53A/N222A}}$ did stimulate the overall rate of ATP hydrolysis more than two fold (Fig. 30). This observation indicates that the total enzyme activity is limited by the amount of MinD^{WT} available in the reaction. This result is also consistent with all of the MinD^{WT} subunits present in heterodimers and that both subunits of the heterodimers are fully activated by MinE.

ATP hydrolysis is not required for the coupled MinD activation

The above results demonstrated that MinE bound to one side of a MinD dimer was sufficient to stimulate ATP hydrolysis by both subunits. Although MinE binds at the dimeric interface of MinD, the interaction of MinE with the two subunits is asymmetric. For example, R21 of MinE only forms hydrogen bonds with residues located on one of the subunits (Fig.28 and discussion). It is likely that the interaction of R21 of MinE with residues L48, E53, S221 and N222 of MinD^{WT} (Fig.27) initiates structural alterations leading to ATP hydrolysis by MinD^{WT} , which is

sequentially coupled to the hydrolysis of ATP by the MinD^{E53A/N222A} subunit (see discussion). Hence, to examine whether the coupled activation of MinD^{E53A/N222A} requires ATP hydrolysis by MinD^{WT}, we incubated an excess of the catalytic mutant MinD^{D40A} with MinD^{E53A/N222A} in the reaction. In the control we observed that the MinD^{D40A} homodimer, like MinD^{E53A/N222A} homodimer, was poorly stimulated by MinE (Fig.31), Although both of these mutants are poorly stimulated by MinE, MinD^{D40A} binds MinE (used in the crystal structure). The ATPase activity of the MinD^{D40A}-MinD^{E53A/N222A} heterodimer was stimulated by MinE to the same extent as MinD^{WT} homodimer. The observation that ATPase was stimulated confirms dimerization, since neither mutant is stimulated. Our interpretation is that the R21 residue of MinE binds to the MinD^{D40A} subunit ultimately leading to ATP hydrolysis by the MinD^{E53A/N222A} subunit. This suggests that the MinD^{D40A} subunit within the heterodimer undergoes the same conformational change that occurs in MinD^{WT} that is necessary for the activation of MinD^{E53A/N222A} (Fig.27).

The activation of a MinD subunit bound to R21 of MinE independent of the other subunit

In connection with the previous experiment we wanted to test if the stimulation of the MinD^{WT} ATPase activity can in turn be affected by the MinD^{E53A/N222A} activity. For this purpose, MinD^{WT} was incubated with an excess amount of a catalytic deficient version of the MinD^{E53A/N222A} mutant, MinD^{D40A/E53A/N222A}, to generate the MinD^{WT}-MinD^{D40A/E53A/N222A} heterodimer. Although MinD^{D40A/E53A/N222A} is to some extent defective in membrane binding in the presence of ATP (data not shown), the activity of the MinD^{WT}-MinD^{D40A/E53A/N222A} heterodimer was similar to that of the MinD^{WT} homodimer (Fig. 32). This result suggests that MinE first causes the hydrolysis of ATP bound to MinD^{WT} prior to the futile attempt to activate the MinD^{D40A/E53A/N222A} mutant

Fig. 25 Comparison of the ATP binding region for MinD-MinE (12-31) peptide complex (magenta) and the MinD dimer (cyan). Regions of difference are highlighted. Especially, I41 underwent a drastic shift in position in MinD-MinE (12-31) peptide complex. The ADP (magenta) and ATP (cyan) molecules are shown on the right side of the figure for reference.

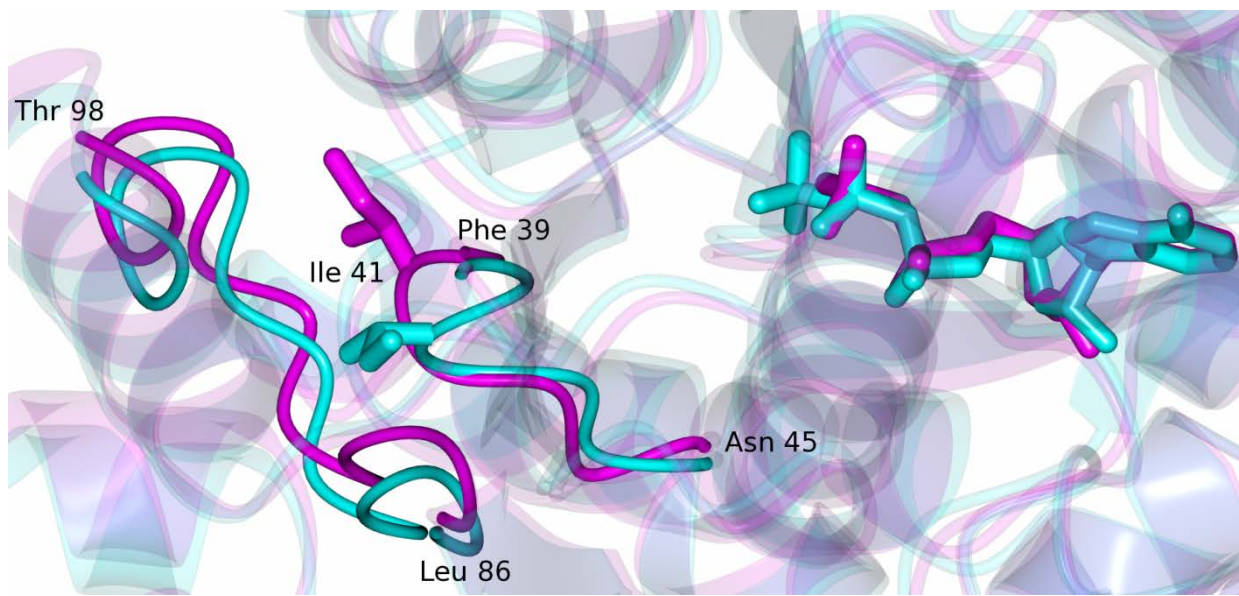


Fig. 26 Comparison of the ATP binding region for MinD-MinE (12-31) peptide complex (magenta) and the MinD dimer (cyan) at residue Glu 146. In the MinD dimer, Glu 146 forms hydrogen bonds with an ATP molecule (green). However, in the MinD-MinE (12-31) peptide complex, Glu 146 rotates away from the ADP molecule (blue) and forms a hydrogen bond with Ser 149 and a close contact of 3.8Å with Ser 221 which in turn forms a hydrogen bond with Arg 21 of MinE.

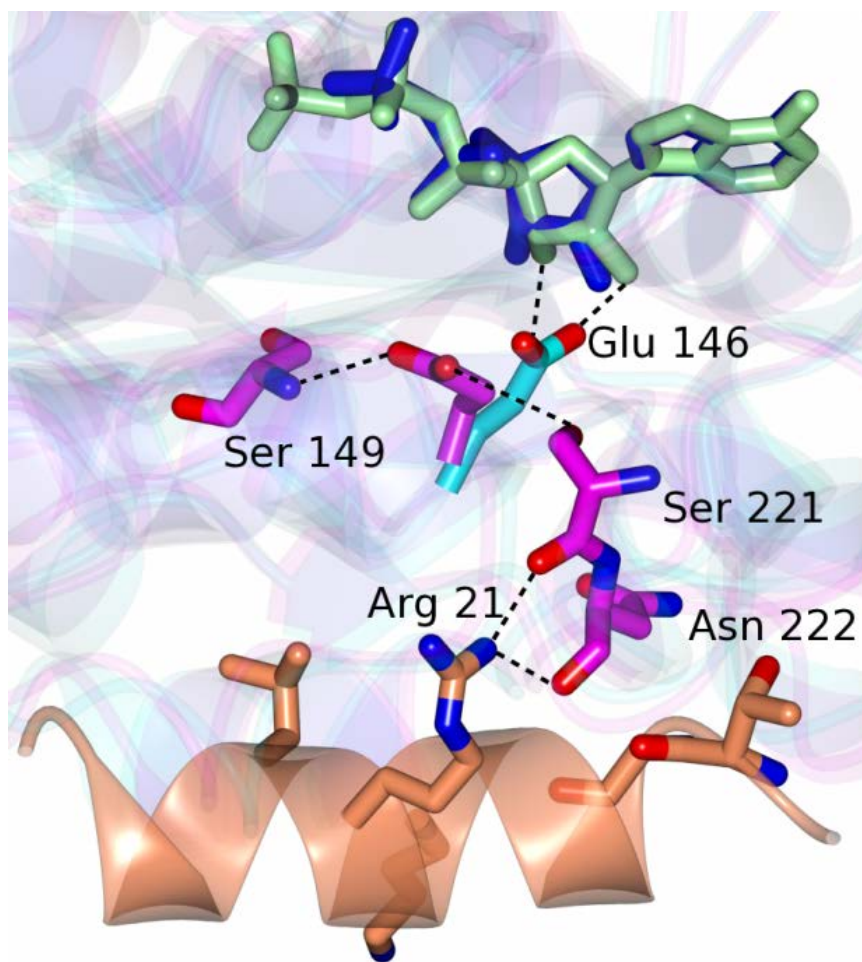


Fig. 27 Hydrogen bonding interactions between a MinD dimer and MinE peptide molecule at the dimer interface. MinD residues undergoing positional shift in the MinD-MinE (12-31) peptide complex (magenta) and the MinD dimer (cyan) are shown. Hydrogen bonding interactions are represented as dashed lines.

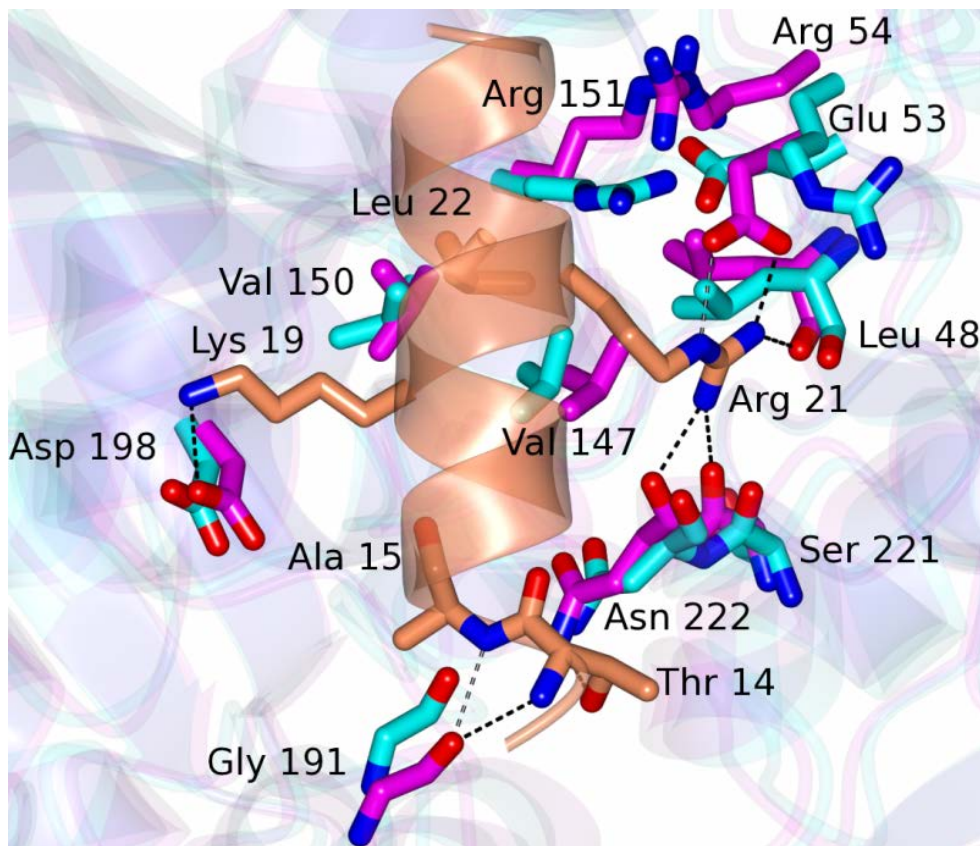


Fig. 28 Overall scheme for the generation of a MinD heterodimer composed of MinD^{WT}-MinD^{E53A/N222A}. (A) The round shape indicates ADP-bound MinD and the square shape indicates MinD bound to ATP. The cross symbol represents the two substitutions due to the double mutations (E53A/N222A). (B) Both MinD^{WT} and MinD^{E53A/N222A} bound to ADP or in the absence of any nucleotides exist as monomers. (C) The addition of ATP to the reaction containing MinD^{E53A/N222A} and MinD^{WT} produces MinD heterodimers and MinD^{E53A/N222A} homodimers. (D) MinE in green can bind to the MinD interface that does not contain the two substitutions. The arrow represents R21 that make hydrogen bonds with MinD.

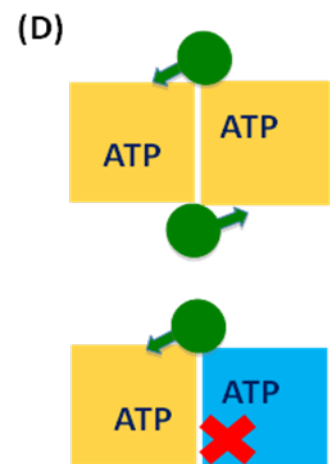
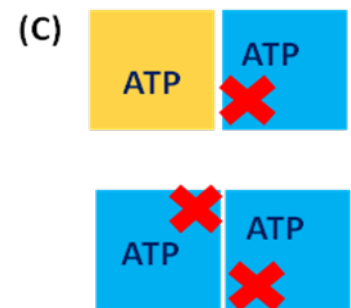
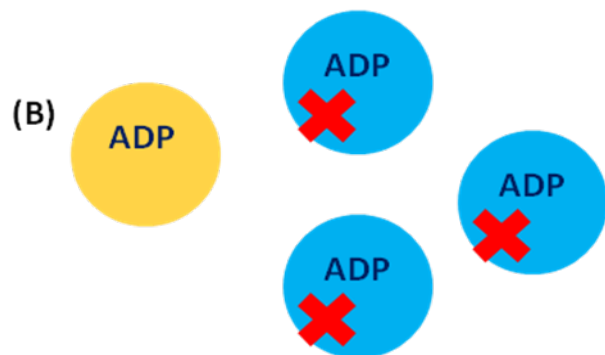
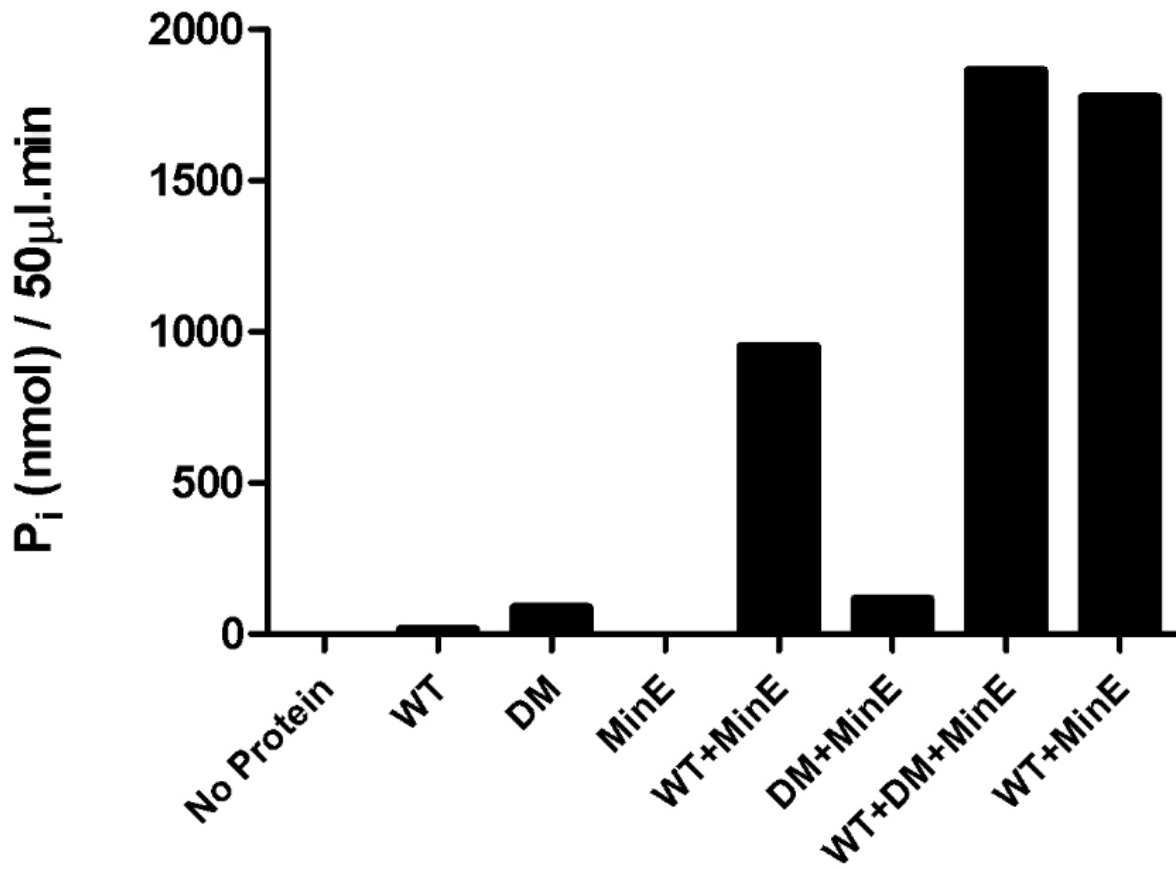


Fig.29 MinD^{WT} and MinD^{E53A/N222A} form a heterodimer that is activated by MinE to hydrolyze ATP. The heterodimer was generated by incubating MinD^{WT} (4 μM) and the MinD^{E53A/N222A} mutant (4 μM) in the presence of MinE (4 μM) and multilamellar vesicles (MLV, 400 ng/ul). The rightmost column represents a reaction where 8 μM of MinD, instead of 4 μM, was incubated with MinE (4 μM). The WT and DM refer to wild type (MinD^{WT}) and double mutant (MinD^{E53A/N222A}) protein, respectively.



and that the ATP hydrolysis of MinD^{WT} occurs independent of the conformational changes in the MinD^{D40A/E53A/N222A} mutant.

Discussion

The remarkable pole-to-pole oscillation of Min proteins makes sure that the Z ring is positioned at midcell. Both the *in vivo* and *in vitro* evidence suggests that the rate of the enzymatic reaction, the MinE-stimulated MinD ATPase, primarily dictates the frequency of the standing wave-like oscillation. In this study, we explored the MinD ATPase activation by MinE by employing a comparative analysis of the structures of free MinD with that of MinD bound with MinE^{CD}. In addition, we found that the MinD ATPase activation is achieved by MinE^{CD} binding to one side of the MinD-ATP dimeric interface, so called asymmetric activation. The incorporation of this finding would be important in devising a more detailed Min oscillation model in the future.

The nature of the MinD^{D40A} Δ10 structure

One of the most intriguing issues is what the structure of MinD^{D40A} Δ10 represents in terms of the ATPase cycle. Previous studies have found that MinD is able to recruit MinC or MinE to the membrane in the presence of ATPγS although MinE is preferred (Hu et al., 2002; Hu et al., 2003; Lackner et al., 2003). As mentioned in the introduction, the deletion of the C-terminal MTS of MinD promotes dimerization. However, the membrane insertion of the MTS appears to induce additional structural changes in MinD since MinD^{WT} Δ10 can dimerize *in vitro* and bind to MinC but is unable to bind to the membrane or MinE (Lutkenhaus J, unpublished). In contrast, the MinD^{D40A} Δ10 dimer binds MinE but the ability to bind MinC is compromised (Park et al., 2011). Thus, the structure of the MinD^{D40A} Δ10 dimer appears

Fig. 30 Activity of a MinD heterodimer composed of MinD^{WT} and MinD^{E53A/N222A} is not affected by an excess of MinD^{E53A/N222A} mutant protein in the reaction. The WT and DM refer to wild type (MinD^{WT}) and double mutant (MinD^{E53A/N222A}) protein, respectively.

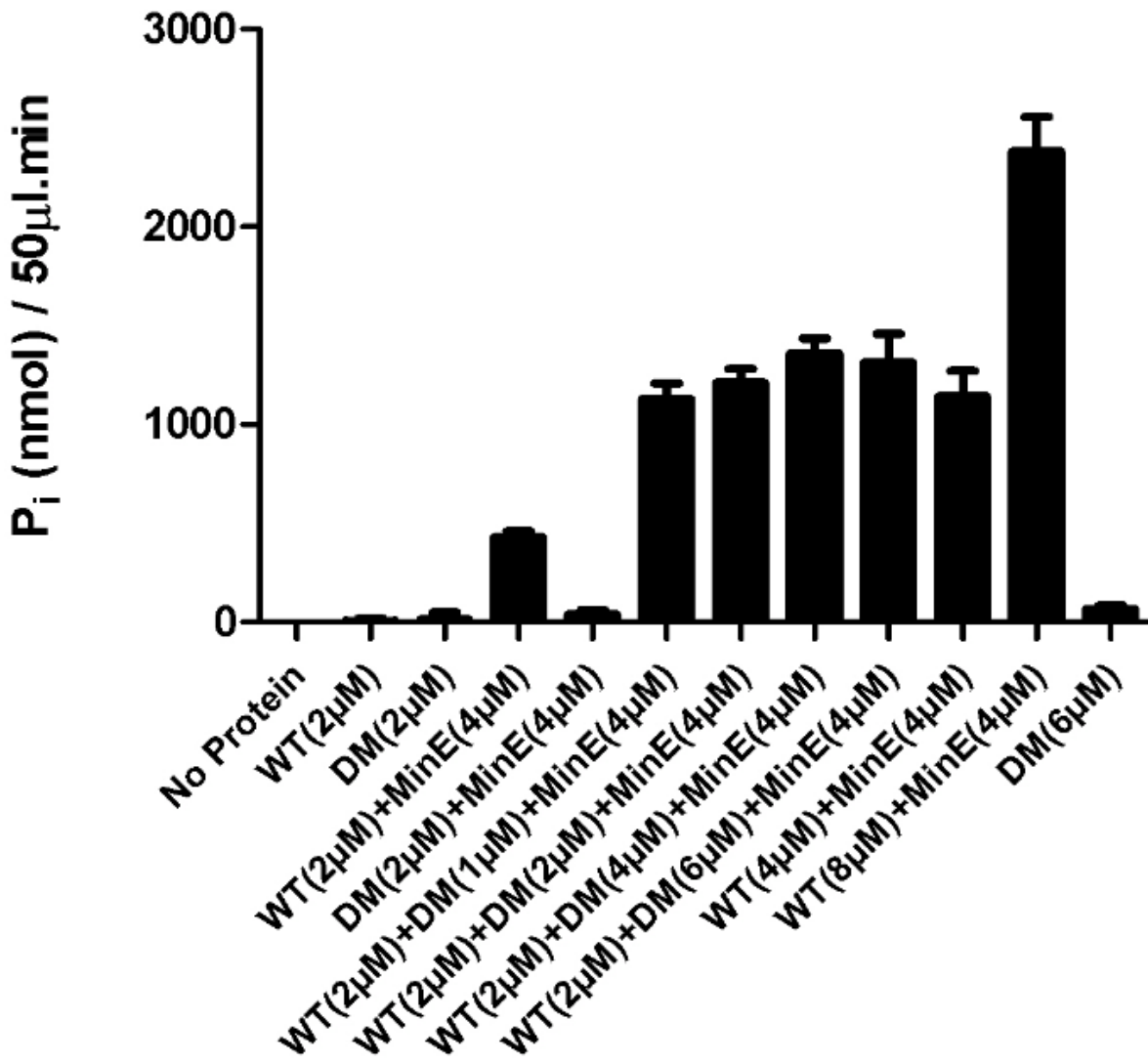


Fig. 31 MinE stimulates the MinD^{D40A}-MinD^{E53A/N222A} heterodimer. The WT, D40A and DM refer to wild type (MinD^{WT}), catalytic-deficient mutant (MinD^{D40A}) and double mutant (MinD^{E53A/N222A}) protein, respectively.

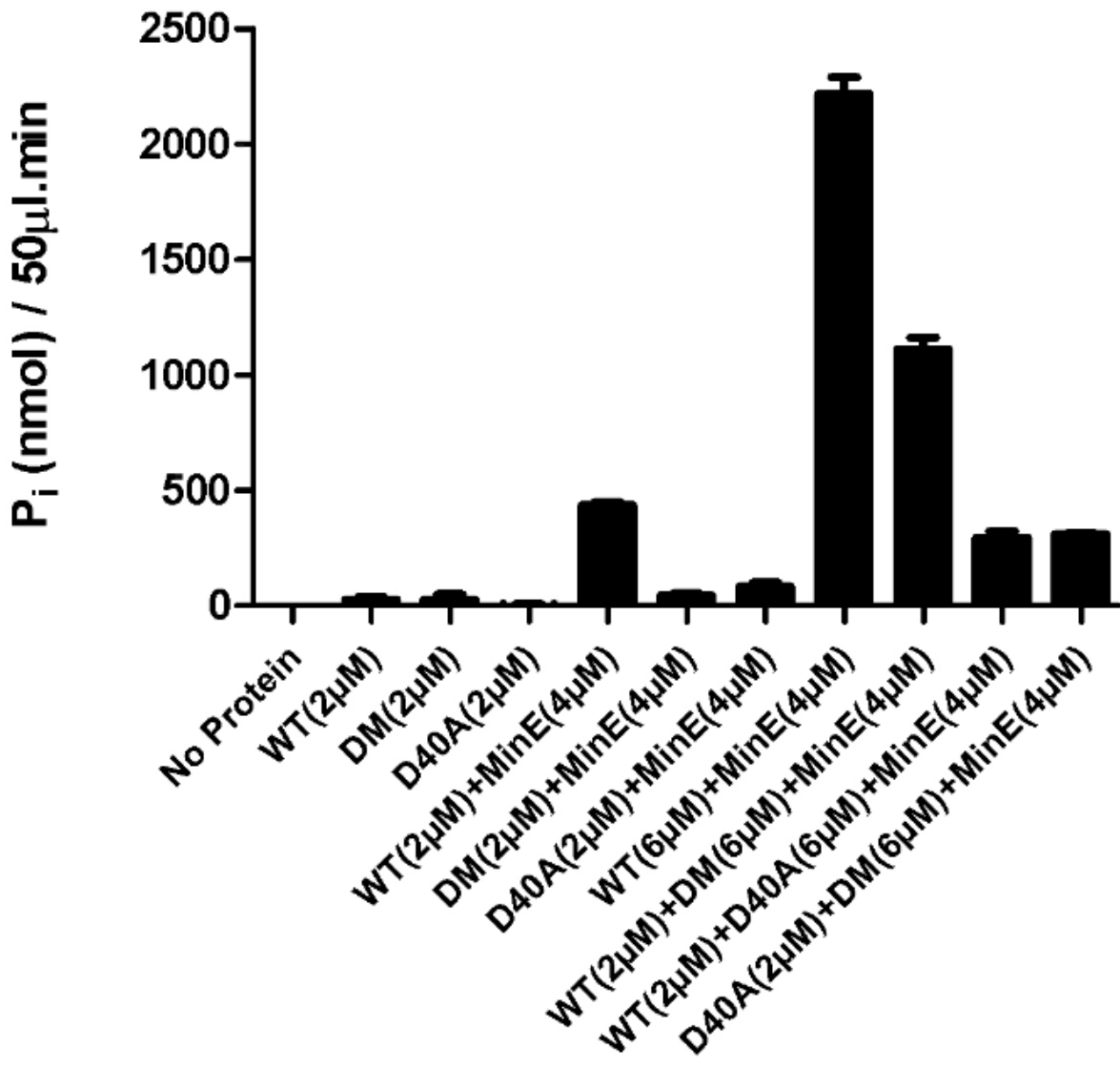
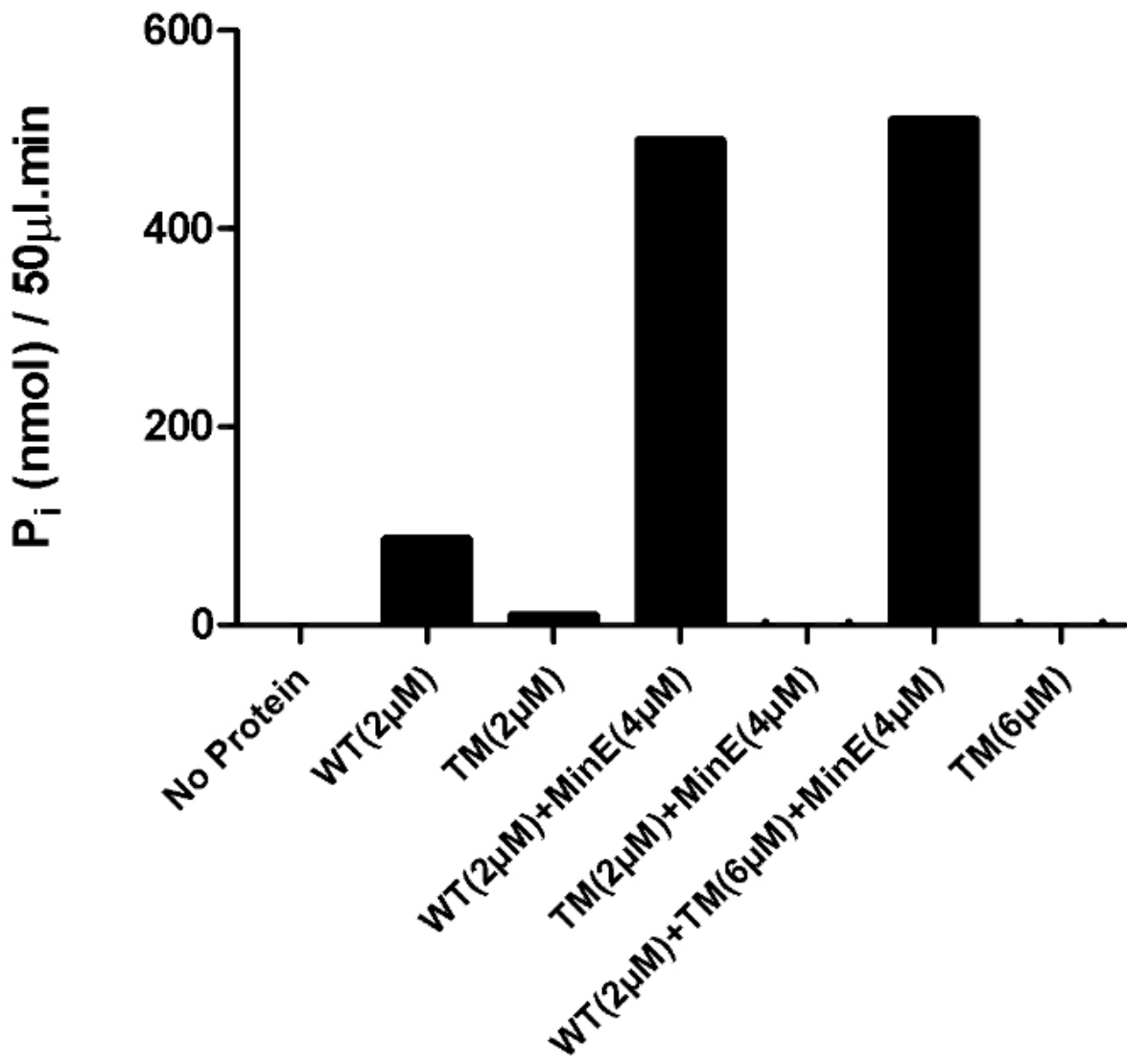


Fig.32 ATP bound to MinD^{WT} dimerized with MinD^{D40A/E53A/N222A} undergoes hydrolysis independent of the activation of MinD^{D40A/E53A/N222A} ATPase. The WT and TM refer to wild type (MinD^{WT}) and triple mutant (MinD^{D40A/E53A/N222A}) protein, respectively.



similar to that of MinD^{WT} as it exists on the membrane. The reduced MinC binding could be due to a local effect of the D40A mutation since mutations affecting residues near D40 such as G42A, L43D, and R44G abrogate MinC binding without affecting dimerization (W. Wu et al., 2011b; H. Zhou & Lutkenhaus, 2004). Since the presence of the D40A mutation in MinD^{WT}Δ10 restores the ability to bind to MinE, the structural alterations caused by the D40A mutation may be similar to that induced by the insertion of the MTS into the membrane (Hu & Lutkenhaus, 2001). Hence, we propose that structure of the MinD^{D40A}Δ10-ATP dimer is similar to that of dimeric MinD^{WT} on the membrane, which is why it is competent to interact with MinE.

The MinD^{D40A} Δ10 complexed with MinE peptide

The structures of MinD^{D40A}Δ10 free of MinE and MinD^{D40A}Δ10 in complex with MinE (12-31) peptide were compared to see if some insight into how MinE activates the MinD ATPase could be obtained. The dimeric structure of MinD^{D40A}Δ10 bound with MinE¹²⁻³¹ peptide displays some changes compared to the structure of MinD^{D40A}Δ10 free of MinE. First, the MinE binding interface of MinD consists of four regions, mostly loops and helices, which upon MinE binding undergo concerted motions involving side chains of several MinD residues that seem to stabilize MinE^{CD} bound to MinD (Fig. 27). Upon MinE binding, for example, E146 loses the interaction with the ribose of ATP to form a new hydrogen bond with S221 (Fig.26). Second, via yet unidentified pathways the MinE^{CD} binding causes noticeable changes in the ATP binding pocket in the switch I and the proximal region of the switch II (Fig. 25). These alterations were predicted in our previous study described in the chapter III. For ATP hydrolysis to occur in MinD, two conditions should be met. One is the polarization of water for nucleophilic attack of the γ phosphate of ATP and the other is neutralization of a negative charge produced by the

leaving γ phosphate (Frech et al., 1994; Maegley et al., 1996). Since in the $\text{MinD}^{\text{D40A}}\Delta 10$ structure the signature lysines (K11), a functional counterpart of an arginine finger that lowers the energy barrier for the ATP hydrolysis, interacts with γ phosphate of ATP, we anticipated that MinE binding affects switch regions to polarize a water molecule (Park et al., 2011).

Our analysis could not identify the precise mechanism by which MinE induces the hydrolysis of ATP, however, it is highly likely that structural changes in the switch regions polarizes the water that attacks the γ phosphate of ATP. This speculation is based on rather solid evidence. First, consistent with a previous study where the $\text{MinD}^{\text{E146A}}$ activated MinC but could not bind MinE, the E146 residue is involved in both ATP and MinE binding. Second, the $\text{MinD}^{\text{D40A}}$ mutant can induce the hydrolysis of ATP bound to the $\text{MinD}^{\text{E53A/N222A}}$ subunit when the heterodimer composed of the two MinD mutants is stimulated with MinE, suggesting that the $\text{MinD}^{\text{D40A}}$ mutant undergoes the same conformational changes as MinD^{WT} does.

Our comparative analysis was hampered by some intrinsic limitations as follows. First, both the dimeric interfaces of the $\text{MinD}^{\text{D40A}}\Delta 10$ and MinE interaction are occupied by the MinE^{12-31} peptides. Given our observation that the binding of the MinE^{CD} to one side of the MinD is sufficient to trigger the hydrolysis of both ATPs in a MinD dimer, we may not capture the asymmetric conformational changes taking place during the activation of MinD ATPase. Second, the ATP in the $\text{MinD}^{\text{D40A}}\Delta 10$ complexed with MinE^{12-31} was already hydrolyzed, which raises a possibility that the complex structure is not what we really want. However, this is unlikely, since the position of the K11 is similar in the two structures and MinE^{12-31} interacts with the MinD residues which we had previously identified by genetic analysis. Presumably the ATP hydrolysis occurred in the crystal and the ATP conformation was retained.

A Model for the MinE activation of the MinD ATPase

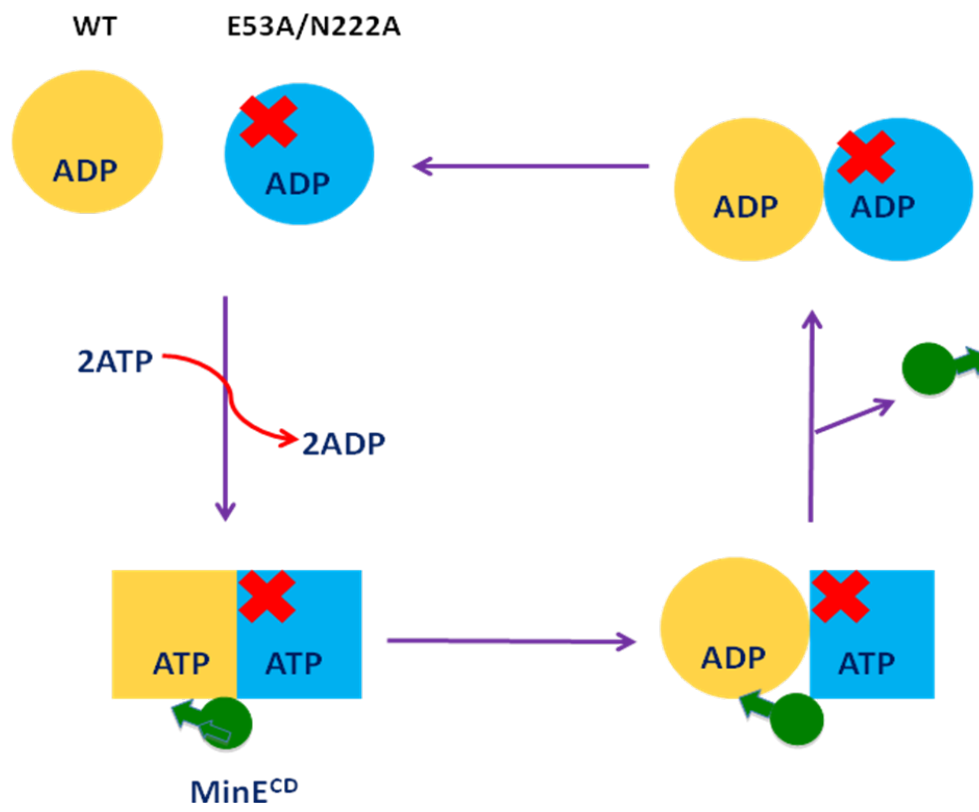
In this study we investigated whether the MinD ATPase activation requires the binding of MinE^{CD} to both sides of a MinD dimer. To this end, we generated a MinD^{WT}-MinD^{E53A/N222A} heterodimer that can accommodate only one MinE^{CD} (Fig. 28). The addition of excess amounts of the MinD^{E53A/N222A} mutant in reactions with a fixed concentration of MinD^{WT} led to a twofold increase in the rate of ATP hydrolysis compared to the MinD^{WT} homodimer. Since the MinD^{E53A/N222A} mutant homodimer does not respond to MinE, the results suggest that heterodimerization is occurring and that both ATPs bound to the MinD^{WT}-MinD^{E53A/N222A} heterodimer are hydrolyzed (Fig. 29 & Fig.30). Further experimental support for heterodimerization came from mixing MinD^{E53A/N222A} with MinD^{D40A}. Neither of these mutants can be stimulated by MinE, however, the reaction containing both mutants displayed MinE-dependent MinD ATPase activity. In this case, the amount of the activity was consistent with only one of the two subunits being activated (Fig. 31).

This finding implies that the conformational changes in a MinD dimer leading to the hydrolysis of the two ATP molecules is asymmetric and sequential where the interaction of R21 of MinE with L48, E53, S221, and N222 might be pivotal (Fig. 27 & Fig. 33). The possibility that the binding of MinE^{CD} to the intact dimeric interface induces the simultaneous hydrolysis of both ATPs in the MinD heterodimer is remote since the MinD residues in the intact dimeric interface coming from each subunit uniquely interact with different residues of the MinE¹²⁻³¹ peptide (Park et al., 2011) (Fig.27 & Fig.28). It is hard to perceive that the unique interaction occurring between MinE¹²⁻³¹ and each of the two MinD subunits could evoke the same end point, the hydrolysis of ATP.

Accordingly, we propose a two step activation model where the binding of the highly conserved R21 initiates a conformational change in the MinD^{WT} monomer resulting in ATP hydrolysis that leads ultimately to the activation of the ATPase activity of the other subunit (Fig.27 & Fig. 33). Residues T14 and K19 make backbone hydrogen bonds and residues I17 and L22 make hydrophobic interactions with the MinD^{E53A/N222A} mutant, respectively, which might prime the MinD^{E53A/N222A} subunit for the activation by the MinD^{WT} subunit (Fig. 27). In line with this idea, we have shown that what is important is not ATP hydrolysis per se but the structural changes occurring due to MinE^{CD} binding to MinD^{WT} since it is evident that the catalytic deficient MinD^{D40A} mutant is also able to activate the MinD^{E53A/N222A} mutant subunit upon MinE binding. The result suggests that the ATP bound to MinD^{WT} was hydrolyzed by the MinE^{CD} when it was dimerized with MinD^{D40A/E53A/N222A} but the ATP bound to the mutant subunit was not.

In the Tarzan in the jungle model presented in chapter III, we assumed that MinE contacting one side of a MinD dimer was sufficient to stimulate ATP hydrolysis. This assumption is verified here. At present the significance of the asymmetric activation of the MinD ATPase in MinE ring formation and Min oscillation is hard to comprehend. However, it is conceivable that our finding might have profound implications on both concerted motion and period of the Min oscillator on the membrane. Moreover, sufficiency of one MinE^{CD} in activating MinD attests that the Min oscillator is labile by nature, which might explain a precondition of Min wave in vitro, the spontaneous breakdown of homogeneity on the membrane surface (Ivanov & Mizuuchi, 2010; Loose et al., 2011; Loose et al., 2008).

Fig. 33 A sequential model for MinE activation of heterodimeric MinD ATPase. MinE binding to the intact dimeric interface causes conformational changes in MinD^{WT} resulting in hydrolysis of ATP bound to MinD^{WT}, which in turn activates MinD^{E53A/N222A} to hydrolyze ATP bound to MinD^{E53A/N222A}. The D40A mutation does not affect the necessary conformational changes required to activate the neighboring subunit since MinD^{D40A} can also activate MinD^{E53A/N222A}. The round and square shapes represent MinD bound with ADP and ATP, respectively. The cross symbol indicates the double mutant (E53A/N222A). The green symbol with the arrow indicates MinE. The arrow indicates the direction of the activation pathway initiated by MinE^{CD} bound to MinD^{WT}.



The activation of the ATPase of the MinD-related proteins such as SoJ, NifH, and ArsA is stimulated by their respective cognate activator. A series of structural studies on ArsA from *E. coli* whose enzymatic activity is allosterically triggered by metallic cation Sb (III) suggest that two ATP molecules bound to two distinctive nucleotide binding sites are sequentially hydrolyzed (Jiang et al., 2005; T. Zhou, Radaev, Rosen, & Gatti, 2000; T. Zhou, Shen, Liu, & Rosen, 2002). Relevance of those findings has nonetheless been questioned due to the omission of ArsB, the pump with which ArsA interacts to extrude the Sb(III) ions. NifH, iron-sulfur protein derived from *Azotobacter vinelandii*, interacts with MoFe-protein to form a nitrogenase complex that catalyzes N₂ reduction-fixation using ATP as an energy source (Seefeldt, Hoffman, & Dean, 2009). The homodimeric Fe-protein retaining single [4Fe-4S] cluster is at reduced state when each monomer is bound with ATP. Upon binding to a dimeric MoFe-protein, the two ATP are hydrolyzed concomitant with one electron transfer to the MoFe-Co center of MoFe-protein (Seefeldt et al., 2009). Although the coupled mechanism of ATP hydrolysis and electron transfer is still elusive, the symmetric contact of those two proteins on a very limited interface may be an indication that the two ATP bound to the Fe-protein undergo simultaneous hydrolysis (Schindelin et al., 1997). The SoJ dimer mediating chromosome segregation in *B. subtilis* is activated by SpoJ. Based on the high identity in the primary structures between SoJ and MinD, it is believed that ATP hydrolysis in a SoJ dimer is also asymmetric.

Experimental procedures

Structural Comparison

The crystal structure of the MinD dimer (PDB 3Q9L) was compared with structure of the MinD-MinE (12-31) peptide complex (PDB 3R9L). Superposition of the two structures was conducted using the program Superpose (Krissinel & Henrick, 2004) via the CCP4 interface (Potterton, Briggs, Turkenburg, & Dodson, 2003). For the superposition, chains A and B of the MinD dimer (residues 2-258) were fit to the corresponding residues in the MinD-MinE (12-31) peptide complex. The RMSD deviation between C-alpha atoms was found to be 0.924 Å with a maximum displacement observed at Ile 41 of chain B. An additional superposition was conducted in which all atoms of chain A and B (residues 2-258) were compared. An RMSA deviation of 1.223 Å was observed between all atoms.

Multilamellar Vesicle (MLV) Preparation

E. coli phospholipids in chloroform were purchased from Avanti Polar Lipids (Alabaster, Ala). To prepare MLV, the *E. coli* phospholipids were vigorously mixed and the chloroform was evaporated under constant flow of nitrogen gas. The dried *E. coli* phospholipid powder was thereafter suspended in Buffer A (25 mM Tris-HCl, pH 7.5, 50 mM KCl) at 10 µg/uL and incubated at 65 °C for 2 hours with occasional vortexing. All aliquots of the MLV were stored frozen at -80 °C.

MinD Purification

MinD^{D40A}Δ10 was purified from JS964 (*Δmin*) containing pZH115-40. Cells were collected from 1 liter cultures grown in LB with ampicillin (100 μg/ml), resuspended in buffer A (25 mM Tris-HCl [pH 7.5]), 20 mM NaCl, 1mM EDTA, 2 mM DTT and 10 % glycerol) and lysed with a French press. The clarified lysate was loaded on a DEAE column and MinD^{D40A}Δ10 eluted with a 60-120 mM NaCl gradient in buffer A. The peak fractions were pooled and run over a HiLoad Superdex 200 column in buffer B (10 mM HEPES-NaOH, pH7.0, 20 mM NaCl, 10% glycerol). The peak fractions were collected and concentrated with a Vivaspin 20 (MW cutoff of 10 kDa) to ~10 mg/ml. The purification of full length wild-type and mutant MinD proteins was carried out using the same method described above except for the NaCl gradient. For the full-length version of MinD proteins, a 20-120 mM NaCl gradient in Buffer A was used for the elution from a DEAE column.

MinE Purification

For MinE-HISx6 purification, JS964 (*Δmin*) cells containing pJB216-HISx6 were grown at 37 °C in LB medium to an OD₅₄₀ of approximately 0.4. IPTG was then added to the culture at a final concentration of 1mM. After 3 hours of incubation with IPTG, the cells were harvested by centrifugation and stored frozen at -80 °C. The cells were thawed on ice after suspension in buffer A (50 mM Tris-HCl, pH7.5, 100 mM NaCl, 10 mM imidazole). The cells were lysed by three passages through a French press at 16,000 psi and the supernatant was obtained after centrifugation at 12,000 x g for 30 min. at 4 °C. The supernatant was applied to a nickel affinity column (Qiagen) and proteins were eluted with buffer B (50 mM Tris-HCl, pH 7.5, 500 mM

NaCl, 250 mM imidazole). The eluted protein samples were pooled and dialyzed against buffer (25 mM HEPES-NaOH, pH7.0, 250 mM NaCl, 1 mM EDTA, 5 mM DTT) prior to final storage at -80 °C.

The Measurement of MinD ATPase Activity

The hydrolysis of ATP was measured using the ATPase colorimetric assay kit that monitors the release of inorganic phosphate (P_i) (Innova Biosciences). The assay was performed according to the manufacturer's instructions with a minor modification to scale down reaction volumes. MinD (2-4 μ M) and MinE (4 μ M) were mixed in reaction buffer (25 mM Tris-HCl, pH7.5, 50 mM KCl, 5 mM $MgCl_2$). In some reactions the concentration of MinE was varied. After adding ATP (1 mM) and multilamellar vesicles (MLVs) (200 ng/ μ l), the reaction mixture was incubated at room temperature and samples taken at indicated times. Once the reaction was quenched, the OD_{595} was recorded and the total enzymatic activity was quantified.

Chapter V

Discussion

The fascinating Min oscillation in *Escherichia coli* that ensures division at midcell has been under intense investigation for more than a decade. In spite of significant progress in our understanding of the biochemical basis of the Min protein dynamics, few structural details were available to support previous findings and to provide the basis of the interactions between Min proteins. In this dissertation, the interactions between MinD and the two other Min proteins, MinC and MinE, have been explored in the context of the MinD structure that we solved. The combination of genetic and structural studies has provided new details of the MinD-MinE and MinD-MinC interactions and has led to a model suggesting how the behavior of MinD-MinE is coupled.

Our contribution to the understanding of the Min system detailed in the first part of this dissertation can be summarized as follows. First, the structure of *Escherichia coli* MinD bound to ATP was determined to be a dimer. Second, the binding sites for MinC and MinE on the MinD structure were comprehensively assigned. Third, the significance of MinD dimerization for the interaction with MinC and MinE was expounded. Lastly, the structure of MinD allowed us to assign the orientation of MinD on the membrane.

The *E. coli* MinD^{D40A}Δ10, a soluble and catalytic deficient mutant form of MinD, was crystallized as a nucleotide sandwich dimer (Fig.34A) in which the signature lysine (K11), a characteristic hallmark of the deviant walker A family, forms a salt bridge with the α and γ -

phosphates of ATP bound to the opposite monomer (Fig.34B). The importance of this interaction is supported by the finding that the K11A mutant does not dimerize and cannot activate MinC (Hayashi et al., 2001; H. Zhou et al., 2005). The result is also consistent with the dimeric structures of deviant walker A motif-containing proteins such as NifH and Soj which are also glued together via the signature lysine residues (Leonard et al., 2005; Schindelin et al., 1997).

The MinCD complex that blocks polar Z ring formation consists of a MinD dimer bound to two ATP molecules and a MinC dimer where the C-terminal domain is involved in both the constitutive dimerization and MinD binding (Lutkenhaus, 2007; Rothfield et al., 2005; H. Zhou & Lutkenhaus, 2005). A previous study identified six residues (S148, D154, L157, G158, I159, A161) as critical for MinC binding, all located in $\alpha 7$ helix (L. Ma et al., 2004). Three of the six residues (S148, D154, I159) are also important for MinE binding, which led to the suggestion that MinC and MinE compete for an overlapping site. In this study, however, it was assumed that *E.coli* MinD is a monomer and did not reflect the accumulating evidence that *E.coli* MinD and MinD-related proteins bound to ATP exist as dimers (Hu et al., 2003; J. Szeto et al., 2001; Szeto et al., 2003). In addition, the ATP-dependent binding of MinC and MinE was not explained.

Our study based on the structure of dimeric *E.coli* MinD^{D40A} $\Delta 10$ bound to ATP (Fig.34A) identified an additional eleven residues (L43, R44, V57, Y58, V61, N62, Q90, T91, R92, K94, R151) involved in MinC binding, where five residues (V56, Y58, V61, N62, K94) are also important for MinE binding. As depicted in Chapter II, this finding confirms that MinC binding site overlaps with the site for MinE binding. Furthermore, the result revealed that the MinC binding site is located at the dimeric interface and is only intact when MinD dimerizes. In summary, our extensive mutational analysis is relevant in that it not only verified the finding of

the previous study but also revealed that MinD dimerization brings all the residues involved in MinC binding together at the dimeric surface.

The residues important for MinC binding can be classified into two categories. One includes residues specific for MinC binding since altering these residues does not affect MinE binding or MinD dimerization. The second category includes residues such as Y58 and V61 since altering these residues affects interaction with both MinC and MinE without affecting MinD dimerization. As discussed above, this latter result is consistent with the previous study suggesting that MinC and MinE compete for overlapping sites on MinD (L. Ma et al., 2004). Interestingly, four residues at the vertex of the triangular beta helix of the MinC C-terminal domain are reported to be critical for MinD interaction (Ramirez-Arcos et al., 2004; H. Zhou & Lutkenhaus, 2005) (Fig. 3 in chapter I). This raises the possibility that a MinC dimer might bind to each side of a MinD dimer if the local concentration of MinC is high.

The comparison of the monomeric *P. furiosus* MinD bound with ADP (Hayashi et al., 2001) and our dimeric *E. coli* MinD bound with ATP (W. Wu et al., 2011b) revealed that the MinD dimerization involves the disruption of the interaction between D152 in the $\alpha 7$ helix and the signature lysine (K11) (Fig. 34B). Hence, the old model that MinE competes with D152 for K11 so that K11 is released to promote hydrolysis of ATP (L. Ma et al., 2004) can be rejected. Instead, the D152-K11 linkage is disrupted by ATP binding since the K11 interacts with ATP (Fig. 34B). Also, the MinD^{D152A} mutant where K11 is free to bind ATP does not show an enhanced ATP hydrolysis rate and it can still interact with MinE (H. Zhou et al., 2005), suggesting that D152 is not critical for MinE binding. The MinD^{D40A} Δ 10 structure, together with the result that K11A

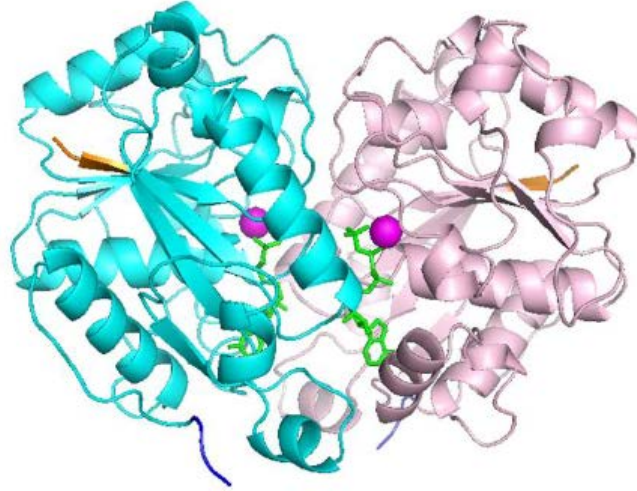
cannot dimerize, indicates that the signature lysine plays a critical role in ATP-dependent dimerization.

In contrast to the limited size of the MinC binding site, our mutation analysis revealed that the residues important for MinE binding are more extensively distributed at the MinD dimeric interface. Through our study we identified 18 residues important for MinE binding, 13 of which are specifically involved in the interaction with MinE. Our analysis shows that mutations of some residues such as E53 and N222 produced a much more pronounced defect in MinE binding than the residues in the α 7 helix identified in the previous study. This result unequivocally highlights three key points. First, the role of the α 7 helix in MinE binding is less significant. Second, the binding site for MinE is more extensive than for MinC. Third, the MinE binding site, like that of MinC, is only fully constituted upon dimerization.

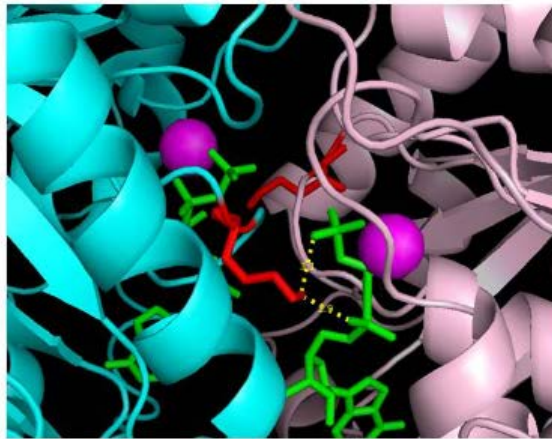
Even though both a previous genetic analysis and our study provided evidence that MinC and MinE share an overlapping binding site on MinD as a mechanistic basis for MinC displacement by MinE (L. Ma et al., 2004; W. Wu et al., 2011b), it is uncertain how MinE can dislodge MinC from the surface of a MinD dimer. One possibility is that MinE binding to MinD involves a two-step process. In this model, once MinE binds to the residues specifically important for MinE (specific site), MinE encroaches on the site where MinC is bound (overlapping site), thereby weakening the MinC binding on MinD. The latter process might involve a local conformational change of MinD or a direct repulsive interaction between MinC and MinE. The other scenario is that, instead of a direct competition for the overlapping site, MinE may indirectly cause the MinC displacement from a MinD dimer. In this case, MinE binding to one

Fig. 34 Structure of *E. coli* MinD^{D40A} Δ 10 (PDB: 3Q9L). (A) ATP and magnesium ions are green and pink color, respectively. Three residues at the N-terminal and C-terminal ends are highlighted in orange and blue color, respectively. 10 amino acids from the C-terminal tail are membrane targeting sequences (MTS) that mediate reversible membrane binding and are not present. (B) K11 (red) of a MinD monomer (cyan) forms a salt bridge (yellow dashed line) with oxygen atoms of α and γ phosphate of ATP (green). Distance between K11 and oxygens are less than 3 Å.

A



B



side of a MinD dimeric interface unoccupied by MinC induces conformational changes that lead to the displacement of MinC bound to the other side of a MinD dimeric interface. Since MinC concentration in vivo is ten fold lower than that of MinD (Loose et al., 2011; T. H. Szeto et al., 2001), it is highly unlikely that a MinD dimer would have MinC bound to both sides of the dimeric interface.

For the second part of this dissertation, the contribution of our study to the advancement of the understanding of the Min system is significant for the following reasons. Our study resolved the conundrum posed by the various MinE structures: the 4 β -stranded structure of the trypsin-treated *E. coli* MinE (EcMinE) and the 6 β -stranded structure of *H. pylori* (HpMinE) and *N. gonorrhoeae* MinE (NgMinE). Our evidence indicates that full length EcMinE is also a 6 β -stranded structure but undergoes a structural rearrangement upon sensing MinD to take an active 4 β -stranded configuration. Next, our finding that the N-terminal region of MinE, the MinE^{CD}, is structurally versatile validates unequivocally the idea that MinE^{CD} interacts with MinD as an α helix. In addition, the mechanism and physiological implication of MinE membrane localization induced by MinD was revealed. Lastly, our Tarzan of the jungle model will be very instrumental in devising a new generation of models for the MinE ring and Min oscillation.

For over a decade the prevailing view of MinE was that a dimer of EcMinE consisted of two autonomous domains, the N-terminal MinE^{CD} (residues 1-31) and the C-terminal MinE^{TSD} (residues 32-88) (King et al., 1999; King et al., 2000; L. Y. Ma et al., 2003; Pichoff et al., 1995; Shih et al., 2002; Zhang et al., 1998; Zhao et al., 1995). In this view, MinE^{CD} attached to the MinE^{TSD} would be converted from a nascent α helix into a stable α helix upon MinD binding. The basis of this hypothesis stemmed from the observation that the MinE peptide (residues 1-22)

is prone to form an α helix (King et al., 1999), that a fragment resistant to trypsin digestion and corresponding to the MinE^{TSD} (residues 36-88) was in a 4 β stranded configuration (King et al., 2000), and that a mutational analysis covering the residues 8-31 of the MinE^{CD} was compatible with an α helix where one face of the α helical MinE^{CD} interacts with MinD (L. Y. Ma et al., 2003).

Overall, our study revealed that MinE undergoes a drastic conformational change from a 6 β -stranded to a 4 β -stranded structure upon sensing MinD that also releases a cryptic membrane targeting sequence. First, we have shown that our MinD mutants that do not interact with MinE are of two types. One type such as MinD^{M193L} can be rescued by hydrophilic substitutions at position I24 of MinE (such as I24N). The second type such as MinD^{E53K} cannot be suppressed by the I24N. These latter mutants alter residues that comprise the MinD and MinE binding interface as found in the MinDE complex structure. This suggests that MinD^{M193L} retains an intact binding site for MinE and is defective in converting the 6 β -stranded structure of MinE to the 4 β -stranded structure. Likewise, MinE mutants unable to interact with MinD are classified into two types. One includes certain MinE mutants such as L3E and F7E that are rescued by I24N suggesting they are deficient in undergoing the transition. Mutants such as A18T belonging to the second type are not rescued by I24N. The effect of the I24N mutation is revealed by its effect on a truncated MinE²¹⁻⁸⁸. It disrupted its ability to form a heterodimer with full-length MinE and inhibit cell division. Furthermore, circular dichroism of MinE²¹⁻⁸⁸ and MinE^{21-88 I24N} strongly indicates that the I24N mutation disrupts the β 1 strand. In addition, we found that the N-terminal region composed of the first 9~10 residues of MinE is a membrane targeting sequence (MTS) sequestered by the C-terminal domain of MinE. It is released by some *minE* mutations as well as by interaction with MinD. Furthermore, mutations in the MTS failed to generate a wild type

phenotype at the physiological level of MinCDE expression indicative of the involvement of the MTS in the selection of the midcell division site. Lastly, the crystal structures of MinDE complexes revealed that the part of the MinE^{CD} derived from the β 1 region exists as a α helix bound at the MinD dimeric interface.

During Min wave propagation in vitro, which resembles Min oscillation in vivo, MinE is known to have a longer retention time on the membrane than MinD (Loose et al., 2011), which indicates that a MinE molecule might interact with more than one MinD dimer. This finding is consistent with our Tarzan of the jungle model that proposes MinE can persistently chase MinD on the membrane by jumping from one MinD to another. So, our study uncovered an important element critical for Min oscillation.

One of the most provocative findings is that the binding of MinD could cause MinE to bind directly to the membrane. Our study demonstrated that the first 9-10 amino acids of MinE constitutes a MTS that becomes unleashed by the MinD-induced conversion of MinE from the 4 β stranded to the 6 β stranded configuration. Our model also explains why certain MinE mutants such as L22D and I25R are targeted to the membrane independent of MinD (L. Y. Ma et al., 2003) and why MinE N-terminal domain alone fused with GFP (MinE^{CD}-GFP) is localized to the membrane (L. Y. Ma et al., 2003; Raskin & de Boer, 1997; Rowland et al., 2000). Whereas L22D and the I24N cause formation of the 4 β stranded structure, the I25R mutation does not unravel β 1 but prevents the tethering of the MTS to the β sheet. The MTS is very dynamic based on the NMR study (Ghasriani et al., 2010) and it is plausible that a small fraction of total MinE in a cell might localize to the membrane but is not microscopically detectable. Therefore, the

prevention of the tethering of the MTS to the β sheet by the I25R mutation must have profoundly shifted the equilibrium in favor of membrane binding.

There are two possible models to account for the interaction between MinD and MinE. One is induced fit, where MinD stimulates the structural conversion of MinE. The other is conformational selection. We proposed a sensing or an induced fit model for the MinD and MinE interaction. In this model, MinE molecules in a cell exist as the compact 6 β stranded conformation but undergo the release of the MTS and the β 1 strand upon sensing MinD as depicted in chapter III. It is possible that the loop (residues 11-18) linking the MTS to the β 1 strand serves as a sensor of MinD. Although the T14A and A15C mutations are unlikely to disrupt the loop, they are rescued by I24N. This finding suggests that T14 and A15 could be directly involved in sensing MinD. In contrast, mutations in the MTS such as L3E and F7E, which are also suppressed by I24N, are deficient since the MTS is no longer tethered.

Alternatively, it is conceivable that those MinD mutants such as M193L and G224C that we believe are defective in MinE sensing might be characterized by an overall loss of affinity to MinE. In support of this possibility, the suppression of MinD^{M193}-MinC activity requires overexpression of MinE^{I24N}, which indicates that the simple release of β 1 is not enough. What is more, we have never been able to observe the suppression of the MinD^{M193L} by the overexpression of the MinE^{CD} alone. In this respect, a revised so-called conformation selection model emerges where the latent 6 β stranded and active 4 β stranded structures are in equilibrium and the MinD dimer on the membrane selectively recruits the active form. In this scenario, one appealing reason why we cannot microscopically detect the 4 β stranded form on the membrane is that the equilibrium highly favors the 6 β latent form. In other words, the membrane binding of

the 4 β active form in the absence of MinD is energetically unfavorable so that there is only a transient and minor retention of the 4 β form on the membrane, which is difficult to detect in the presence of an ample pool of cytoplasmic 6 β form.

Arguing against the conformational selection scheme, and in favor of our original model, is the possibility that the I24N mutation does not completely release β 1 from MinE. Alternatively, the release of β 1 from MinE^{I24N} destroys the loop configuration (residues 11-18) which is needed for MinD sensing. Thus, the overexpression of MinE^{I24N} in rescuing MinD^{M193L} can be justifiable if either of the two cases is true. Hence, future studies are needed to resolve the conflicting issues above and provide a clear answer on which model is correct.

In the third part of this dissertation, information about the MinE-induced MinD ATPase activation was sought by comparing the structure of the free MinD^{D40A} Δ 10-ATP dimer with that complexed with the MinE¹²⁻³¹ peptide. MinD does not undergo many conformational changes upon binding MinE¹²⁻³¹. Several MinD residues located around the MinD-MinE^{CD} binding interface undergo a series of flexible motions to better accommodate MinE. The binding of MinE¹²⁻³¹ caused E146 to no longer hydrogen bond with ATP but to interact with S221, a critical residue for interacting with R21 of MinE. The stabilization of S221 by E146 seems to be crucial since MinE cannot bind to MinD^{E146A} even though it dimerizes (H. Zhou et al., 2005). Also, residue I41 is drastically rotated in the complex, but the implications of this change and the alteration of E146 to ATP hydrolysis is vague. In summary, our comparative analysis revealed some changes in MinD affecting the switch regions although the implications are not clear.

An alternative idea concerning the task of MinE in activating MinD ATPase is that MinE is acting like a nucleotide exchange factor. In this model, ATP hydrolysis is triggered upon dimerization of MinD-ATP on the membrane, but ADP and P_i are not released and MinD is not capable of dissociating from the membrane. MinE binding to this complex breaks inter-monomeric interactions in the MinD dimer causing release from the membrane and dissociation of ADP. As addressed before, the signature (K11) mediates MinD dimerization by interacting with ATP in the opposite monomer (Fig.1B). In this regard, implicit assumptions are that binding of the MTS of MinD to the membrane induces alterations of switch regions to hydrolyze ATP and that MinE binding to dimeric MinD-ADP+ P_i causes K11 to interact with residues in $\alpha 7$ helix such as E146, S148, and D152. These residues were shown to form hydrogen bonds with K11 in the monomeric MinD-ADP (Hayashi et al., 2001). The evidence supporting this model is the MinD^{D152A} mutant which can localize to the membrane in vitro even in the presence of ADP (H. Zhou et al., 2005). This result raises the possibility that a MinD dimer bound with ADP+ P_i is stable on the membrane, thus requiring MinE to dissociate into monomers and detach from the membrane. In MinD^{D152A}, however, K11 cannot bind to D152, which means that K11 is forced to interact with ADP and MinD^{D152A} is thereby prone to dimerization. So, the study with MinD^{D152A} might bear little biological relevance. In NifH bound with ADP, the signature lysine residue (K11) is distant from ADP (Schindelin et al., 1997), consistent with the idea that MinD bound to ADP exists as a monomer. On the other hand, in the structure of ArsA-ADP, signature lysines (K31, K340) still interact with β phosphates (T. Zhou et al., 2000). Hence, future studies should clarify what MinE exactly does for MinD.

In the crystal structure of dimeric NifH-ADPAIF₄ complexed with MoFe-protein dimer, no direct contact between the ATP-binding loops of NifH and MoFe-protein exists. In analogy with the

MinD-MinE¹²⁻³¹ complex, residues of NifH such as D129 and C132 present in the switch II region underwent alterations in the complex (Schindelin et al., 1997). By the same token, however, the nature of the communication between the nucleotide binding pocket and the surface interacting with MoFe-protein is obscure although the MoFe-protein is believed to stabilize an intermediate step among reaction coordinates leading to ATP hydrolysis.

So far various crystal structures of ArsA dimer bound with ADP, ATP, and nucleotide mimics have been determined (T. Zhou et al., 2000, 2001). These studies indicate that ArsA is structurally closely related to ABC (ATP-binding cassette) transporters that transport a wide range of substrates across cellular membrane. In ArsA metal binding leads to an asymmetric ATP hydrolysis in two structurally distinct sites, which is in turn coupled to the activation of ArsB, a pump that catalyzes efflux of the metal ions. Binding of allosteric activator, MoFe-protein and MinE, respectively, to NifH and MinD stimulates ATP hydrolysis, however, the pathway of the stimulation (for example, from MinD-MinE binding interface to ATP binding pocket) is elusive. In contrast, in ArsA two stretches of residues are believed to directly transmit metal binding signal to ATP-binding pocket, resulting in approximation of an in-line water to γ phosphate of ATP.

We demonstrated that MinE^{CD} binding to one side of the MinD-ATP dimeric interface suffices to activate the MinD ATPase using a heterodimer composed of MinD^{WT}-MinD^{E53A/N222A}. The stimulation appears to rely on asymmetric and sequential conformational changes from the MinD monomer to which R21 of MinE binds to the other MinD monomer. Intriguingly, MinE R21 interacting with MinD^{D40A} also induced ATP hydrolysis in a heterodimer with MinD^{E53A/N222A}, suggesting that MinD^{D40A} can undergo the same conformational alterations as MinD^{WT}. This

observation further indicates that the structural alterations catalogued in MinD^{D40A}Δ10-MinE¹²⁻³¹ complex in chapter IV might not be artifactual. Our model depicted in Fig.9 was further supported by the evidence that MinD^{WT} heterodimerized with MinD^{D40A/E53A/N222A} hydrolyzes ATP upon MinE binding. This result implies that MinD^{WT} subunit hydrolyzes ATP even though MinD^{D40A/E53A/N222A} cannot carry out ATP hydrolysis. In this experiment, it is likely that MinD^{WT} activated the triple mutant but the presence of catalytic-deficient D40A must have prevented ATP hydrolysis in the triple mutant. Unless the pathway of the transfer of the conformational changes from one MinD to the other MinD in a heterodimer dimer is determined, it is will be difficult to determine if ATP hydrolysis in the MinD to which the R21 of MinE binds can take place truly independent of the activation of the other MinD.

It is not clear how the finding in chapter IV can be integrated into the future Min oscillation models. The simple implication that we can conjure at this juncture is that sensitivity of the MinD ATPase activation to MinE might be a critical factor in dictating the characteristic period of the oscillation observed in vivo (Fu et al., 2001; Hale et al., 2001; Raskin & de Boer, 1999b). Moreover, our finding might account for simultaneous and complete detachment of MinD molecules on the membrane at the edge of polar zone in vivo (Raskin & de Boer, 1999b) and at the peak of MinE wave in vitro (Ivanov & Mizuuchi, 2010; Loose et al., 2011; Loose et al., 2008). The significance of our asymmetric activation model in MinE ring formation itself cannot be grasped at present, but the sequential stimulation mechanism is well-positioned to explain how a cognate activator stimulates the ATPase activity of WACA family that is supposed to form polymers on surface of substrates such as DNA and membrane (Hu et al., 2002; Ivanov & Mizuuchi, 2010; Leonard et al., 2005; Suefuji et al., 2002). Accessibility of a cognate activator to

polymerized proteins of the WACA family is expected to be limited by steric hindrance such that binding of an activator to both sides of a dimeric protein of WACA family may not be possible.

There are many questions about the Min system that are not answered. The structure of the MinE ring at the edge of the MinD polar zone has not been characterized. Also, the contribution of the MTS of MinE to the displacement of MinC from the MinCD complex is not clear. A detailed mechanism for MinE stimulation of the MinD ATPase activation is not known and the exact mechanism by which MinE displaces MinC from the MinCD complex has not been elucidated. Nevertheless, our overall contributions to the better comprehension of the Min system will overshadow those lingering issues when it is considered that we proved that the entire MinE protein, not the C-terminal fragment (residues 32-88), can be regarded as the MinE^{TSD}, that the membrane targeting and the MTS of MinE could be intricate parts of the Min oscillation, and that to formulate more sensible theoretical models the Tarzan of the jungle model should be incorporated into the new schemes.

Bibliography

- Aarsman, M. E., Piette, A., Fraipont, C., Vinkenvleugel, T. M., Nguyen-Disteche, M., & den Blaauwen, T. (2005). Maturation of the Escherichia coli divisome occurs in two steps. *Mol Microbiol*, 55(6), 1631-1645. doi: 10.1111/j.1365-2958.2005.04502.x
- Adams, D. W., & Errington, J. (2009). Bacterial cell division: assembly, maintenance and disassembly of the Z ring. *Nat Rev Microbiol*, 7(9), 642-653. doi: 10.1038/nrmicro2198
- Adams, P. D., Afonine, P. V., Bunkoczi, G., Chen, V. B., Davis, I. W., Echols, N., . . . Zwart, P. H. (2010). PHENIX: a comprehensive Python-based system for macromolecular structure solution. *Acta Crystallogr D Biol Crystallogr*, 66(Pt 2), 213-221. doi: 10.1107/s0907444909052925
- Addinall, S. G., Cao, C., & Lutkenhaus, J. (1997). FtsN, a late recruit to the septum in Escherichia coli. *Mol Microbiol*, 25(2), 303-309.
- Adler, H. I., Fisher, W. D., Cohen, A., & Hardigree, A. A. (1967). MINIATURE escherichia coli CELLS DEFICIENT IN DNA. *Proc Natl Acad Sci U S A*, 57(2), 321-326.
- Aldridge, C., Maple, J., & Moller, S. G. (2005). The molecular biology of plastid division in higher plants. *J Exp Bot*, 56(414), 1061-1077. doi: 10.1093/jxb/eri118
- Andrade, M. A., Chacon, P., Merelo, J. J., & Moran, F. (1993). Evaluation of secondary structure of proteins from UV circular dichroism spectra using an unsupervised learning neural network. *Protein Eng*, 6(4), 383-390.

- Arjunan, S. N., & Tomita, M. (2010). A new multicompartmental reaction-diffusion modeling method links transient membrane attachment of E. coli MinE to E-ring formation. *Syst Synth Biol*, 4(1), 35-53. doi: 10.1007/s11693-009-9047-2
- Atlung, T., & Hansen, F. G. (1993). Three distinct chromosome replication states are induced by increasing concentrations of DnaA protein in Escherichia coli. *J Bacteriol*, 175(20), 6537-6545.
- Barilla, D., Carmelo, E., & Hayes, F. (2007). The tail of the ParG DNA segregation protein remodels ParF polymers and enhances ATP hydrolysis via an arginine finger-like motif. *Proc Natl Acad Sci U S A*, 104(6), 1811-1816. doi: 10.1073/pnas.0607216104
- Bernhardt, T. G., & de Boer, P. A. (2003). The Escherichia coli amidase AmiC is a periplasmic septal ring component exported via the twin-arginine transport pathway. *Mol Microbiol*, 48(5), 1171-1182.
- Bernhardt, T. G., & de Boer, P. A. (2005). SlmA, a nucleoid-associated, FtsZ binding protein required for blocking septal ring assembly over Chromosomes in E. coli. *Mol Cell*, 18(5), 555-564. doi: 10.1016/j.molcel.2005.04.012
- Bi, E., & Lutkenhaus, J. (1990). Interaction between the min locus and ftsZ. *J Bacteriol*, 172(10), 5610-5616.
- Bi, E., & Lutkenhaus, J. (1993). Cell division inhibitors Sula and MinCD prevent formation of the FtsZ ring. *J Bacteriol*, 175(4), 1118-1125.
- Bi, E. F., & Lutkenhaus, J. (1991). FtsZ ring structure associated with division in Escherichia coli. *Nature*, 354(6349), 161-164. doi: 10.1038/354161a0

- Bigot, S., Sivanathan, V., Possoz, C., Barre, F. X., & Cornet, F. (2007). FtsK, a literate chromosome segregation machine. *Mol Microbiol*, *64*(6), 1434-1441. doi: 10.1111/j.1365-2958.2007.05755.x
- Blanc, E., Roversi, P., Vornrhein, C., Flensburg, C., Lea, S. M., & Bricogne, G. (2004). Refinement of severely incomplete structures with maximum likelihood in BUSTER-TNT. *Acta Crystallogr D Biol Crystallogr*, *60*(Pt 12 Pt 1), 2210-2221. doi: 10.1107/s0907444904016427
- Boye, E., & Nordstrom, K. (2003). Coupling the cell cycle to cell growth. *EMBO Rep*, *4*(8), 757-760. doi: 10.1038/sj.embor.embor895
- Bramhill, D., & Thompson, C. M. (1994). GTP-dependent polymerization of Escherichia coli FtsZ protein to form tubules. *Proc Natl Acad Sci U S A*, *91*(13), 5813-5817.
- Bramkamp, M., & van Baarle, S. (2009). Division site selection in rod-shaped bacteria. *Curr Opin Microbiol*, *12*(6), 683-688. doi: 10.1016/j.mib.2009.10.002
- Buddelmeijer, N., & Beckwith, J. (2004). A complex of the Escherichia coli cell division proteins FtsL, FtsB and FtsQ forms independently of its localization to the septal region. *Mol Microbiol*, *52*(5), 1315-1327. doi: 10.1111/j.1365-2958.2004.04044.x
- Chen, V. B., Arendall, W. B., 3rd, Headd, J. J., Keedy, D. A., Immormino, R. M., Kapral, G. J., . . . Richardson, D. C. (2010). MolProbity: all-atom structure validation for macromolecular crystallography. *Acta Crystallogr D Biol Crystallogr*, *66*(Pt 1), 12-21. doi: 10.1107/s0907444909042073
- Cho, H., McManus, H. R., Dove, S. L., & Bernhardt, T. G. (2011). Nucleoid occlusion factor SlmA is a DNA-activated FtsZ polymerization antagonist. *Proc Natl Acad Sci U S A*, *108*(9), 3773-3778. doi: 10.1073/pnas.1018674108

- Cooper, S., & Helmstetter, C. E. (1968). Chromosome replication and the division cycle of *Escherichia coli* B/r. *J Mol Biol*, *31*(3), 519-540.
- Corbin, B. D., Wang, Y., Beuria, T. K., & Margolin, W. (2007). Interaction between cell division proteins FtsE and FtsZ. *J Bacteriol*, *189*(8), 3026-3035. doi: 10.1128/jb.01581-06
- Corbin, B. D., Yu, X. C., & Margolin, W. (2002). Exploring intracellular space: function of the Min system in round-shaped *Escherichia coli*. *EMBO J*, *21*(8), 1998-2008. doi: 10.1093/emboj/21.8.1998
- Cordell, S. C., Anderson, R. E., & Lowe, J. (2001). Crystal structure of the bacterial cell division inhibitor MinC. *EMBO J*, *20*(10), 2454-2461. doi: 10.1093/emboj/20.10.2454
- Cordell, S. C., & Lowe, J. (2001). Crystal structure of the bacterial cell division regulator MinD. *FEBS Lett*, *492*(1-2), 160-165.
- Cytrynbaum, E. N., & Marshall, B. D. (2007). A multistranded polymer model explains MinDE dynamics in *E. coli* cell division. *Biophys J*, *93*(4), 1134-1150. doi: 10.1529/biophysj.106.097162
- Dai, K., Mukherjee, A., Xu, Y., & Lutkenhaus, J. (1994). Mutations in *ftsZ* that confer resistance to Sula affect the interaction of FtsZ with GTP. *J Bacteriol*, *176*(1), 130-136.
- Dajkovic, A., Lan, G., Sun, S. X., Wirtz, D., & Lutkenhaus, J. (2008). MinC spatially controls bacterial cytokinesis by antagonizing the scaffolding function of FtsZ. *Curr Biol*, *18*(4), 235-244. doi: 10.1016/j.cub.2008.01.042
- Dajkovic, A., Mukherjee, A., & Lutkenhaus, J. (2008). Investigation of regulation of FtsZ assembly by Sula and development of a model for FtsZ polymerization. *J Bacteriol*, *190*(7), 2513-2526. doi: 10.1128/jb.01612-07

- Daniel, R. A., Harry, E. J., & Errington, J. (2000). Role of penicillin-binding protein PBP 2B in assembly and functioning of the division machinery of *Bacillus subtilis*. *Mol Microbiol*, 35(2), 299-311.
- de Boer, P., Crossley, R., & Rothfield, L. (1992). The essential bacterial cell-division protein FtsZ is a GTPase. *Nature*, 359(6392), 254-256. doi: 10.1038/359254a0
- de Boer, P. A. (2010). Advances in understanding *E. coli* cell fission. *Curr Opin Microbiol*, 13(6), 730-737. doi: 10.1016/j.mib.2010.09.015
- de Boer, P. A., Crossley, R. E., Hand, A. R., & Rothfield, L. I. (1991). The MinD protein is a membrane ATPase required for the correct placement of the *Escherichia coli* division site. *EMBO J*, 10(13), 4371-4380.
- de Boer, P. A., Crossley, R. E., & Rothfield, L. I. (1988). Isolation and properties of minB, a complex genetic locus involved in correct placement of the division site in *Escherichia coli*. *J Bacteriol*, 170(5), 2106-2112.
- de Boer, P. A., Crossley, R. E., & Rothfield, L. I. (1989). A division inhibitor and a topological specificity factor coded for by the minicell locus determine proper placement of the division septum in *E. coli*. *Cell*, 56(4), 641-649.
- de Boer, P. A., Crossley, R. E., & Rothfield, L. I. (1990). Central role for the *Escherichia coli* minC gene product in two different cell division-inhibition systems. *Proc Natl Acad Sci U S A*, 87(3), 1129-1133.
- de Boer, P. A., Crossley, R. E., & Rothfield, L. I. (1992). Roles of MinC and MinD in the site-specific septation block mediated by the MinCDE system of *Escherichia coli*. *J Bacteriol*, 174(1), 63-70.

- de Leeuw, E., Graham, B., Phillips, G. J., ten Hagen-Jongman, C. M., Oudega, B., & Luirink, J. (1999). Molecular characterization of *Escherichia coli* FtsE and FtsX. *Mol Microbiol*, *31*(3), 983-993.
- den Blaauwen, T., de Pedro, M. A., Nguyen-Disteche, M., & Ayala, J. A. (2008). Morphogenesis of rod-shaped sacculi. *FEMS Microbiol Rev*, *32*(2), 321-344. doi: 10.1111/j.1574-6976.2007.00090.x
- Derouaux, A., Wolf, B., Fraipont, C., Breukink, E., Nguyen-Disteche, M., & Terrak, M. (2008). The monofunctional glycosyltransferase of *Escherichia coli* localizes to the cell division site and interacts with penicillin-binding protein 3, FtsW, and FtsN. *J Bacteriol*, *190*(5), 1831-1834. doi: 10.1128/jb.01377-07
- Derr, J., Hopper, J. T., Sain, A., & Rutenberg, A. D. (2009). Self-organization of the MinE protein ring in subcellular Min oscillations. *Phys Rev E Stat Nonlin Soft Matter Phys*, *80*(1 Pt 1), 011922.
- Donachie, W. D. (1968). Relationship between cell size and time of initiation of DNA replication. *Nature*, *219*(5158), 1077-1079.
- Donachie, W. D., & Blakely, G. W. (2003). Coupling the initiation of chromosome replication to cell size in *Escherichia coli*. *Curr Opin Microbiol*, *6*(2), 146-150.
- Drew, D. A., Osborn, M. J., & Rothfield, L. I. (2005). A polymerization-depolymerization model that accurately generates the self-sustained oscillatory system involved in bacterial division site placement. *Proc Natl Acad Sci U S A*, *102*(17), 6114-6118. doi: 10.1073/pnas.0502037102

- Dubarry, N., Possoz, C., & Barre, F. X. (2010). Multiple regions along the Escherichia coli FtsK protein are implicated in cell division. *Mol Microbiol*, 78(5), 1088-1100. doi: 10.1111/j.1365-2958.2010.07412.x
- Ebersbach, G., Galli, E., Moller-Jensen, J., Lowe, J., & Gerdes, K. (2008). Novel coiled-coil cell division factor ZapB stimulates Z ring assembly and cell division. *Mol Microbiol*, 68(3), 720-735. doi: 10.1111/j.1365-2958.2008.06190.x
- Elledge, S. J. (1996). Cell cycle checkpoints: preventing an identity crisis. *Science*, 274(5293), 1664-1672.
- Emsley, P., & Cowtan, K. (2004). Coot: model-building tools for molecular graphics. *Acta Crystallogr D Biol Crystallogr*, 60(Pt 12 Pt 1), 2126-2132. doi: 10.1107/s0907444904019158
- Erickson, H. P. (1995). FtsZ, a prokaryotic homolog of tubulin? *Cell*, 80(3), 367-370.
- Erickson, H. P., Anderson, D. E., & Osawa, M. (2010). FtsZ in bacterial cytokinesis: cytoskeleton and force generator all in one. *Microbiol Mol Biol Rev*, 74(4), 504-528. doi: 10.1128/mubr.00021-10
- Erickson, H. P., Taylor, D. W., Taylor, K. A., & Bramhill, D. (1996). Bacterial cell division protein FtsZ assembles into protofilament sheets and minirings, structural homologs of tubulin polymers. *Proc Natl Acad Sci U S A*, 93(1), 519-523.
- Evans, P. (2006). Scaling and assessment of data quality. *Acta Crystallogr D Biol Crystallogr*, 62(Pt 1), 72-82. doi: 10.1107/s0907444905036693
- Fange, D., & Elf, J. (2006). Noise-induced Min phenotypes in E. coli. *PLoS Comput Biol*, 2(6), e80. doi: 10.1371/journal.pcbi.0020080

- Frech, M., Darden, T. A., Pedersen, L. G., Foley, C. K., Charifson, P. S., Anderson, M. W., & Wittinghofer, A. (1994). Role of glutamine-61 in the hydrolysis of GTP by p21H-ras: an experimental and theoretical study. *Biochemistry*, *33*(11), 3237-3244.
- Fu, X., Shih, Y. L., Zhang, Y., & Rothfield, L. I. (2001). The MinE ring required for proper placement of the division site is a mobile structure that changes its cellular location during the Escherichia coli division cycle. *Proc Natl Acad Sci U S A*, *98*(3), 980-985. doi: 10.1073/pnas.031549298
- Gamba, P., Veening, J. W., Saunders, N. J., Hamoen, L. W., & Daniel, R. A. (2009). Two-step assembly dynamics of the Bacillus subtilis divisome. *J Bacteriol*, *191*(13), 4186-4194. doi: 10.1128/jb.01758-08
- Gerding, M. A., Liu, B., Bendezu, F. O., Hale, C. A., Bernhardt, T. G., & de Boer, P. A. (2009). Self-enhanced accumulation of FtsN at Division Sites and Roles for Other Proteins with a SPOR domain (DamX, DedD, and RlpA) in Escherichia coli cell constriction. *J Bacteriol*, *191*(24), 7383-7401. doi: 10.1128/jb.00811-09
- Gerding, M. A., Ogata, Y., Pecora, N. D., Niki, H., & de Boer, P. A. (2007). The trans-envelope Tol-Pal complex is part of the cell division machinery and required for proper outer-membrane invagination during cell constriction in E. coli. *Mol Microbiol*, *63*(4), 1008-1025. doi: 10.1111/j.1365-2958.2006.05571.x
- Ghasriani, H., Ducat, T., Hart, C. T., Hafizi, F., Chang, N., Al-Baldawi, A., . . . Goto, N. K. (2010). Appropriation of the MinD protein-interaction motif by the dimeric interface of the bacterial cell division regulator MinE. *Proc Natl Acad Sci U S A*, *107*(43), 18416-18421. doi: 10.1073/pnas.1007141107

- Goehring, N. W., & Beckwith, J. (2005). Diverse paths to midcell: assembly of the bacterial cell division machinery. *Curr Biol*, *15*(13), R514-526. doi: 10.1016/j.cub.2005.06.038
- Gonzalez, J. M., Jimenez, M., Velez, M., Mingorance, J., Andreu, J. M., Vicente, M., & Rivas, G. (2003). Essential cell division protein FtsZ assembles into one monomer-thick ribbons under conditions resembling the crowded intracellular environment. *J Biol Chem*, *278*(39), 37664-37671. doi: 10.1074/jbc.M305230200
- Gueiros-Filho, F. J., & Losick, R. (2002). A widely conserved bacterial cell division protein that promotes assembly of the tubulin-like protein FtsZ. *Genes Dev*, *16*(19), 2544-2556. doi: 10.1101/gad.1014102
- Hale, C. A., Meinhardt, H., & de Boer, P. A. (2001). Dynamic localization cycle of the cell division regulator MinE in Escherichia coli. *EMBO J*, *20*(7), 1563-1572. doi: 10.1093/emboj/20.7.1563
- Hale, C. A., Rhee, A. C., & de Boer, P. A. (2000). ZipA-induced bundling of FtsZ polymers mediated by an interaction between C-terminal domains. *J Bacteriol*, *182*(18), 5153-5166.
- Hale, C. A., Shiomi, D., Liu, B., Bernhardt, T. G., Margolin, W., Niki, H., & de Boer, P. A. (2011). Identification of Escherichia coli ZapC (YcbW) as a component of the division apparatus that binds and bundles FtsZ polymers. *J Bacteriol*, *193*(6), 1393-1404. doi: 10.1128/jb.01245-10
- Harry, E., Monahan, L., & Thompson, L. (2006). Bacterial cell division: the mechanism and its precision. *Int Rev Cytol*, *253*, 27-94. doi: 10.1016/s0074-7696(06)53002-5

- Harry, E. J., Rodwell, J., & Wake, R. G. (1999). Co-ordinating DNA replication with cell division in bacteria: a link between the early stages of a round of replication and mid-cell Z ring assembly. *Mol Microbiol*, *33*(1), 33-40.
- Hayashi, I., Oyama, T., & Morikawa, K. (2001). Structural and functional studies of MinD ATPase: implications for the molecular recognition of the bacterial cell division apparatus. *EMBO J*, *20*(8), 1819-1828. doi: 10.1093/emboj/20.8.1819
- Heidrich, C., Templin, M. F., Ursinus, A., Merdanovic, M., Berger, J., Schwarz, H., . . . Holtje, J. V. (2001). Involvement of N-acetylmuramyl-L-alanine amidases in cell separation and antibiotic-induced autolysis of Escherichia coli. *Mol Microbiol*, *41*(1), 167-178.
- Henriques, A. O., Glaser, P., Piggot, P. J., & Moran, C. P., Jr. (1998). Control of cell shape and elongation by the rodA gene in Bacillus subtilis. *Mol Microbiol*, *28*(2), 235-247.
- Hester, C. M., & Lutkenhaus, J. (2007). Soj (ParA) DNA binding is mediated by conserved arginines and is essential for plasmid segregation. *Proc Natl Acad Sci U S A*, *104*(51), 20326-20331. doi: 10.1073/pnas.0705196105
- Holyoak, T., Fenn, T. D., Wilson, M. A., Moulin, A. G., Ringe, D., & Petsko, G. A. (2003). Malonate: a versatile cryoprotectant and stabilizing solution for salt-grown macromolecular crystals. *Acta Crystallogr D Biol Crystallogr*, *59*(Pt 12), 2356-2358.
- Howard, M., & Kruse, K. (2005). Cellular organization by self-organization: mechanisms and models for Min protein dynamics. *J Cell Biol*, *168*(4), 533-536. doi: 10.1083/jcb.200411122
- Howard, M., & Rutenberg, A. D. (2003). Pattern formation inside bacteria: fluctuations due to the low copy number of proteins. *Phys Rev Lett*, *90*(12), 128102.

- Howard, M., Rutenberg, A. D., & de Vet, S. (2001). Dynamic compartmentalization of bacteria: accurate division in *E. coli*. *Phys Rev Lett*, *87*(27 Pt 1), 278102.
- Hsieh, C. W., Lin, T. Y., Lai, H. M., Lin, C. C., Hsieh, T. S., & Shih, Y. L. (2010). Direct MinE-membrane interaction contributes to the proper localization of MinDE in *E. coli*. *Mol Microbiol*, *75*(2), 499-512. doi: 10.1111/j.1365-2958.2009.07006.x
- Hu, Z., Gogol, E. P., & Lutkenhaus, J. (2002). Dynamic assembly of MinD on phospholipid vesicles regulated by ATP and MinE. *Proc Natl Acad Sci U S A*, *99*(10), 6761-6766. doi: 10.1073/pnas.102059099
- Hu, Z., & Lutkenhaus, J. (1999). Topological regulation of cell division in *Escherichia coli* involves rapid pole to pole oscillation of the division inhibitor MinC under the control of MinD and MinE. *Mol Microbiol*, *34*(1), 82-90.
- Hu, Z., & Lutkenhaus, J. (2000). Analysis of MinC reveals two independent domains involved in interaction with MinD and FtsZ. *J Bacteriol*, *182*(14), 3965-3971.
- Hu, Z., & Lutkenhaus, J. (2001). Topological regulation of cell division in *E. coli*. spatiotemporal oscillation of MinD requires stimulation of its ATPase by MinE and phospholipid. *Mol Cell*, *7*(6), 1337-1343.
- Hu, Z., & Lutkenhaus, J. (2003). A conserved sequence at the C-terminus of MinD is required for binding to the membrane and targeting MinC to the septum. *Mol Microbiol*, *47*(2), 345-355.
- Hu, Z., Mukherjee, A., Pichoff, S., & Lutkenhaus, J. (1999). The MinC component of the division site selection system in *Escherichia coli* interacts with FtsZ to prevent polymerization. *Proc Natl Acad Sci U S A*, *96*(26), 14819-14824.

- Hu, Z., Saez, C., & Lutkenhaus, J. (2003). Recruitment of MinC, an inhibitor of Z-ring formation, to the membrane in *Escherichia coli*: role of MinD and MinE. *J Bacteriol*, *185*(1), 196-203.
- Huang, K. C., Meir, Y., & Wingreen, N. S. (2003). Dynamic structures in *Escherichia coli*: spontaneous formation of MinE rings and MinD polar zones. *Proc Natl Acad Sci U S A*, *100*(22), 12724-12728. doi: 10.1073/pnas.2135445100
- Ivanov, V., & Mizuuchi, K. (2010). Multiple modes of interconverting dynamic pattern formation by bacterial cell division proteins. *Proc Natl Acad Sci U S A*, *107*(18), 8071-8078. doi: 10.1073/pnas.0911036107
- Jiang, Y., Bhattacharjee, H., Zhou, T., Rosen, B. P., Ambudkar, S. V., & Sauna, Z. E. (2005). Nonequivalence of the nucleotide binding domains of the ArsA ATPase. *J Biol Chem*, *280*(11), 9921-9926. doi: 10.1074/jbc.M413391200
- Johnson, J. E., Lackner, L. L., Hale, C. A., & de Boer, P. A. (2004). ZipA is required for targeting of DMinC/DicB, but not DMinC/MinD, complexes to septal ring assemblies in *Escherichia coli*. *J Bacteriol*, *186*(8), 2418-2429.
- Kang, G. B., Song, H. E., Kim, M. K., Youn, H. S., Lee, J. G., An, J. Y., . . . Eom, S. H. (2010). Crystal structure of *Helicobacter pylori* MinE, a cell division topological specificity factor. *Mol Microbiol*, *76*(5), 1222-1231. doi: 10.1111/j.1365-2958.2010.07160.x
- Karimova, G., Pidoux, J., Ullmann, A., & Ladant, D. (1998). A bacterial two-hybrid system based on a reconstituted signal transduction pathway. *Proc Natl Acad Sci U S A*, *95*(10), 5752-5756.
- Karimova, G., Ullmann, A., & Ladant, D. (2000). A bacterial two-hybrid system that exploits a cAMP signaling cascade in *Escherichia coli*. *Methods Enzymol*, *328*, 59-73.

- Kerr, R. A., Levine, H., Sejnowski, T. J., & Rappel, W. J. (2006). Division accuracy in a stochastic model of Min oscillations in *Escherichia coli*. *Proc Natl Acad Sci U S A*, *103*(2), 347-352. doi: 10.1073/pnas.0505825102
- King, G. F., Rowland, S. L., Pan, B., Mackay, J. P., Mullen, G. P., & Rothfield, L. I. (1999). The dimerization and topological specificity functions of MinE reside in a structurally autonomous C-terminal domain. *Mol Microbiol*, *31*(4), 1161-1169.
- King, G. F., Shih, Y. L., Maciejewski, M. W., Bains, N. P., Pan, B., Rowland, S. L., . . . Rothfield, L. I. (2000). Structural basis for the topological specificity function of MinE. *Nat Struct Biol*, *7*(11), 1013-1017. doi: 10.1038/80917
- Kondo, S., & Miura, T. (2010). Reaction-diffusion model as a framework for understanding biological pattern formation. *Science*, *329*(5999), 1616-1620. doi: 10.1126/science.1179047
- Koonin, E. V. (1993). A superfamily of ATPases with diverse functions containing either classical or deviant ATP-binding motif. *J Mol Biol*, *229*(4), 1165-1174. doi: 10.1006/jmbi.1993.1115
- Krissinel, E., & Henrick, K. (2004). Secondary-structure matching (SSM), a new tool for fast protein structure alignment in three dimensions. *Acta Crystallogr D Biol Crystallogr*, *60*(Pt 12 Pt 1), 2256-2268. doi: 10.1107/s0907444904026460
- Kruse, K. (2002). A dynamic model for determining the middle of *Escherichia coli*. *Biophys J*, *82*(2), 618-627. doi: 10.1016/s0006-3495(02)75426-x
- Kruse, K., Howard, M., & Margolin, W. (2007). An experimentalist's guide to computational modelling of the Min system. *Mol Microbiol*, *63*(5), 1279-1284. doi: 10.1111/j.1365-2958.2007.05607.x

- Lackner, L. L., Raskin, D. M., & de Boer, P. A. (2003). ATP-dependent interactions between *Escherichia coli* Min proteins and the phospholipid membrane in vitro. *J Bacteriol*, *185*(3), 735-749.
- Leipe, D. D., Wolf, Y. I., Koonin, E. V., & Aravind, L. (2002). Classification and evolution of P-loop GTPases and related ATPases. *J Mol Biol*, *317*(1), 41-72. doi: 10.1006/jmbi.2001.5378
- Leonard, T. A., Butler, P. J., & Lowe, J. (2005). Bacterial chromosome segregation: structure and DNA binding of the Soj dimer--a conserved biological switch. *EMBO J*, *24*(2), 270-282. doi: 10.1038/sj.emboj.7600530
- Lesterlin, C., Pages, C., Dubarry, N., Dasgupta, S., & Cornet, F. (2008). Asymmetry of chromosome Replichores renders the DNA translocase activity of FtsK essential for cell division and cell shape maintenance in *Escherichia coli*. *PLoS Genet*, *4*(12), e1000288. doi: 10.1371/journal.pgen.1000288
- Lobner-Olesen, A., Skarstad, K., Hansen, F. G., von Meyenburg, K., & Boye, E. (1989). The DnaA protein determines the initiation mass of *Escherichia coli* K-12. *Cell*, *57*(5), 881-889.
- Loose, M., Fischer-Friedrich, E., Herold, C., Kruse, K., & Schwille, P. (2011). Min protein patterns emerge from rapid rebinding and membrane interaction of MinE. *Nat Struct Mol Biol*, *18*(5), 577-583. doi: 10.1038/nsmb.2037
- Loose, M., Fischer-Friedrich, E., Ries, J., Kruse, K., & Schwille, P. (2008). Spatial regulators for bacterial cell division self-organize into surface waves in vitro. *Science*, *320*(5877), 789-792. doi: 10.1126/science.1154413

- Low, H. H., Moncrieffe, M. C., & Lowe, J. (2004). The crystal structure of ZapA and its modulation of FtsZ polymerisation. *J Mol Biol*, *341*(3), 839-852. doi: 10.1016/j.jmb.2004.05.031
- Lowe, J., & Amos, L. A. (1998). Crystal structure of the bacterial cell-division protein FtsZ. *Nature*, *391*(6663), 203-206. doi: 10.1038/34472
- Lowe, J., & Amos, L. A. (1999). Tubulin-like protofilaments in Ca²⁺-induced FtsZ sheets. *EMBO J*, *18*(9), 2364-2371. doi: 10.1093/emboj/18.9.2364
- Lowe, J., & Amos, L. A. (2000). Helical tubes of FtsZ from *Methanococcus jannaschii*. *Biol Chem*, *381*(9-10), 993-999. doi: 10.1515/bc.2000.122
- Lu, C., Reedy, M., & Erickson, H. P. (2000). Straight and curved conformations of FtsZ are regulated by GTP hydrolysis. *J Bacteriol*, *182*(1), 164-170.
- Lutkenhaus, J. (2007). Assembly dynamics of the bacterial MinCDE system and spatial regulation of the Z ring. *Annu Rev Biochem*, *76*, 539-562. doi: 10.1146/annurev.biochem.75.103004.142652
- Lutkenhaus, J. (2009). FtsN--trigger for septation. *J Bacteriol*, *191*(24), 7381-7382. doi: 10.1128/jb.01100-09
- Lutkenhaus, J., & Addinall, S. G. (1997). Bacterial cell division and the Z ring. *Annu Rev Biochem*, *66*, 93-116. doi: 10.1146/annurev.biochem.66.1.93
- Lutkenhaus, J., & Sundaramoorthy, M. (2003). MinD and role of the deviant Walker A motif, dimerization and membrane binding in oscillation. *Mol Microbiol*, *48*(2), 295-303.
- Ma, L., King, G. F., & Rothfield, L. (2004). Positioning of the MinE binding site on the MinD surface suggests a plausible mechanism for activation of the *Escherichia coli* MinD

- ATPase during division site selection. *Mol Microbiol*, 54(1), 99-108. doi: 10.1111/j.1365-2958.2004.04265.x
- Ma, L. Y., King, G., & Rothfield, L. (2003). Mapping the MinE site involved in interaction with the MinD division site selection protein of Escherichia coli. *J Bacteriol*, 185(16), 4948-4955.
- Maegley, K. A., Admiraal, S. J., & Herschlag, D. (1996). Ras-catalyzed hydrolysis of GTP: a new perspective from model studies. *Proc Natl Acad Sci U S A*, 93(16), 8160-8166.
- Margolin, W. (2005). FtsZ and the division of prokaryotic cells and organelles. *Nat Rev Mol Cell Biol*, 6(11), 862-871. doi: 10.1038/nrm1745
- Marston, A. L., Thomaides, H. B., Edwards, D. H., Sharpe, M. E., & Errington, J. (1998). Polar localization of the MinD protein of Bacillus subtilis and its role in selection of the mid-cell division site. *Genes Dev*, 12(21), 3419-3430.
- Matthews, B. W. (1968). Solvent content of protein crystals. *J Mol Biol*, 33(2), 491-497.
- Meacci, G., & Kruse, K. (2005). Min-oscillations in Escherichia coli induced by interactions of membrane-bound proteins. *Phys Biol*, 2(2), 89-97. doi: 10.1088/1478-3975/2/2/002
- Meinhardt, H., & de Boer, P. A. (2001). Pattern formation in Escherichia coli: a model for the pole-to-pole oscillations of Min proteins and the localization of the division site. *Proc Natl Acad Sci U S A*, 98(25), 14202-14207. doi: 10.1073/pnas.251216598
- Mercer, K. L., & Weiss, D. S. (2002). The Escherichia coli cell division protein FtsW is required to recruit its cognate transpeptidase, FtsI (PBP3), to the division site. *J Bacteriol*, 184(4), 904-912.
- Michie, K. A., & Lowe, J. (2006). Dynamic filaments of the bacterial cytoskeleton. *Annu Rev Biochem*, 75, 467-492. doi: 10.1146/annurev.biochem.75.103004.142452

- Mileykovskaya, E., Fishov, I., Fu, X., Corbin, B. D., Margolin, W., & Dowhan, W. (2003). Effects of phospholipid composition on MinD-membrane interactions in vitro and in vivo. *J Biol Chem*, 278(25), 22193-22198. doi: 10.1074/jbc.M302603200
- Moriya, S., Imai, Y., Hassan, A. K., & Ogasawara, N. (1999). Regulation of initiation of *Bacillus subtilis* chromosome replication. *Plasmid*, 41(1), 17-29. doi: 10.1006/plas.1998.1381
- Mukherjee, A., & Lutkenhaus, J. (1994). Guanine nucleotide-dependent assembly of FtsZ into filaments. *J Bacteriol*, 176(9), 2754-2758.
- Mukherjee, A., Saez, C., & Lutkenhaus, J. (2001). Assembly of an FtsZ mutant deficient in GTPase activity has implications for FtsZ assembly and the role of the Z ring in cell division. *J Bacteriol*, 183(24), 7190-7197. doi: 10.1128/jb.183.24.7190-7197.2001
- Mulder, E., & Woldringh, C. L. (1989). Actively replicating nucleoids influence positioning of division sites in *Escherichia coli* filaments forming cells lacking DNA. *J Bacteriol*, 171(8), 4303-4314.
- Muller, P., Ewers, C., Bertsche, U., Anstett, M., Kallis, T., Breukink, E., . . . Vollmer, W. (2007). The essential cell division protein FtsN interacts with the murein (peptidoglycan) synthase PBP1B in *Escherichia coli*. *J Biol Chem*, 282(50), 36394-36402. doi: 10.1074/jbc.M706390200
- Nogales, E., Downing, K. H., Amos, L. A., & Lowe, J. (1998). Tubulin and FtsZ form a distinct family of GTPases. *Nat Struct Biol*, 5(6), 451-458.
- Nordstrom, K., Bernander, R., & Dasgupta, S. (1991). The *Escherichia coli* cell cycle: one cycle or multiple independent processes that are co-ordinated? *Mol Microbiol*, 5(4), 769-774.

- Ogura, Y., Imai, Y., Ogasawara, N., & Moriya, S. (2001). Autoregulation of the dnaA-dnaN operon and effects of DnaA protein levels on replication initiation in *Bacillus subtilis*. *J Bacteriol*, *183*(13), 3833-3841. doi: 10.1128/jb.183.13.3833-3841.2001
- Oliva, M. A., Cordell, S. C., & Lowe, J. (2004). Structural insights into FtsZ protofilament formation. *Nat Struct Mol Biol*, *11*(12), 1243-1250. doi: 10.1038/nsmb855
- Oliva, M. A., Huecas, S., Palacios, J. M., Martin-Benito, J., Valpuesta, J. M., & Andreu, J. M. (2003). Assembly of archaeal cell division protein FtsZ and a GTPase-inactive mutant into double-stranded filaments. *J Biol Chem*, *278*(35), 33562-33570. doi: 10.1074/jbc.M303798200
- Osawa, M., Anderson, D. E., & Erickson, H. P. (2008). Reconstitution of contractile FtsZ rings in liposomes. *Science*, *320*(5877), 792-794. doi: 10.1126/science.1154520
- Painter, J., & Merritt, E. A. (2005). A molecular viewer for the analysis of TLS rigid-body motion in macromolecules. *Acta Cryst*, *D61*, 465-471.
- Painter, J., & Merritt, E. A. (2006a). Optimal description of a protein structure in terms of multiple groups undergoing TLS motion. *Acta Crystallographica Section D-Biological Crystallography*, *62*, 439-450.
- Painter, J., & Merritt, E. A. (2006b). TLSMD web server for the generation of multi-group TLS models. *Journal of Applied Crystallography*, *39*, 109-111.
- Park, K. T., Wu, W., Battaile, K. P., Lovell, S., Holyoak, T., & Lutkenhaus, J. (2011). The Min oscillator uses MinD-dependent conformational changes in MinE to spatially regulate cytokinesis. *Cell*, *146*(3), 396-407. doi: 10.1016/j.cell.2011.06.042

- Peters, N. T., Dinh, T., & Bernhardt, T. G. (2011). A fail-safe mechanism in the septal ring assembly pathway generated by the sequential recruitment of cell separation amidases and their activators. *J Bacteriol*, *193*(18), 4973-4983. doi: 10.1128/jb.00316-11
- Pichoff, S., & Lutkenhaus, J. (2001). Escherichia coli division inhibitor MinCD blocks septation by preventing Z-ring formation. *J Bacteriol*, *183*(22), 6630-6635. doi: 10.1128/jb.183.22.6630-6635.2001
- Pichoff, S., & Lutkenhaus, J. (2002). Unique and overlapping roles for ZipA and FtsA in septal ring assembly in Escherichia coli. *EMBO J*, *21*(4), 685-693.
- Pichoff, S., & Lutkenhaus, J. (2005). Tethering the Z ring to the membrane through a conserved membrane targeting sequence in FtsA. *Mol Microbiol*, *55*(6), 1722-1734. doi: 10.1111/j.1365-2958.2005.04522.x
- Pichoff, S., Vollrath, B., Touriol, C., & Bouche, J. P. (1995). Deletion analysis of gene minE which encodes the topological specificity factor of cell division in Escherichia coli. *Mol Microbiol*, *18*(2), 321-329.
- Potterton, E., Briggs, P., Turkenburg, M., & Dodson, E. (2003). A graphical user interface to the CCP4 program suite. *Acta Crystallogr D Biol Crystallogr*, *59*(Pt 7), 1131-1137.
- Priyadarshini, R., Popham, D. L., & Young, K. D. (2006). Daughter cell separation by penicillin-binding proteins and peptidoglycan amidases in Escherichia coli. *J Bacteriol*, *188*(15), 5345-5355. doi: 10.1128/jb.00476-06
- Ramirez-Arcos, S., Greco, V., Douglas, H., Tessier, D., Fan, D., Szeto, J., . . . Dillon, J. R. (2004). Conserved glycines in the C terminus of MinC proteins are implicated in their functionality as cell division inhibitors. *J Bacteriol*, *186*(9), 2841-2855.

- Ramirez-Arcos, S., Szeto, J., Dillon, J. A., & Margolin, W. (2002). Conservation of dynamic localization among MinD and MinE orthologues: oscillation of *Neisseria gonorrhoeae* proteins in *Escherichia coli*. *Mol Microbiol*, *46*(2), 493-504.
- Ramos, D., Ducat, T., Cheng, J., Eng, N. F., Dillon, J. A., & Goto, N. K. (2006). Conformation of the cell division regulator MinE: evidence for interactions between the topological specificity and anti-MinCD domains. *Biochemistry*, *45*(14), 4593-4601. doi: 10.1021/bi060022j
- Raskin, D. M., & de Boer, P. A. (1997). The MinE ring: an FtsZ-independent cell structure required for selection of the correct division site in *E. coli*. *Cell*, *91*(5), 685-694.
- Raskin, D. M., & de Boer, P. A. (1999a). MinDE-dependent pole-to-pole oscillation of division inhibitor MinC in *Escherichia coli*. *J Bacteriol*, *181*(20), 6419-6424.
- Raskin, D. M., & de Boer, P. A. (1999b). Rapid pole-to-pole oscillation of a protein required for directing division to the middle of *Escherichia coli*. *Proc Natl Acad Sci U S A*, *96*(9), 4971-4976.
- Ravier, M. A., Gilon, P., & Henquin, J. C. (1999). Oscillations of insulin secretion can be triggered by imposed oscillations of cytoplasmic Ca²⁺ or metabolism in normal mouse islets. *Diabetes*, *48*(12), 2374-2382.
- RayChaudhuri, D. (1999). ZipA is a MAP-Tau homolog and is essential for structural integrity of the cytokinetic FtsZ ring during bacterial cell division. *EMBO J*, *18*(9), 2372-2383. doi: 10.1093/emboj/18.9.2372
- Reeve, J. N., Mendelson, N. H., Coyne, S. I., Hallock, L. L., & Cole, R. M. (1973). Minicells of *Bacillus subtilis*. *J Bacteriol*, *114*(2), 860-873.

- Regamey, A., Harry, E. J., & Wake, R. G. (2000). Mid-cell Z ring assembly in the absence of entry into the elongation phase of the round of replication in bacteria: co-ordinating chromosome replication with cell division. *Mol Microbiol*, 38(3), 423-434.
- Ricard, M., & Hirota, Y. (1973). Process of cellular division in Escherichia coli: physiological study on thermosensitive mutants defective in cell division. *J Bacteriol*, 116(1), 314-322.
- Rothfield, L., Justice, S., & Garcia-Lara, J. (1999). Bacterial cell division. *Annu Rev Genet*, 33, 423-448. doi: 10.1146/annurev.genet.33.1.423
- Rothfield, L., Taghbalout, A., & Shih, Y. L. (2005). Spatial control of bacterial division-site placement. *Nat Rev Microbiol*, 3(12), 959-968. doi: 10.1038/nrmicro1290
- Rowland, S. L., Fu, X., Sayed, M. A., Zhang, Y., Cook, W. R., & Rothfield, L. I. (2000). Membrane redistribution of the Escherichia coli MinD protein induced by MinE. *J Bacteriol*, 182(3), 613-619.
- Ryan, K. R., & Shapiro, L. (2003). Temporal and spatial regulation in prokaryotic cell cycle progression and development. *Annu Rev Biochem*, 72, 367-394. doi: 10.1146/annurev.biochem.72.121801.161824
- Sakai, N., Yao, M., Itou, H., Watanabe, N., Yumoto, F., Tanokura, M., & Tanaka, I. (2001). The three-dimensional structure of septum site-determining protein MinD from Pyrococcus horikoshii OT3 in complex with Mg-ADP. *Structure*, 9(9), 817-826.
- Schaechter, M., Maaloe, O., & Kjeldgaard, N. O. (1958). Dependency on medium and temperature of cell size and chemical composition during balanced grown of Salmonella typhimurium. *J Gen Microbiol*, 19(3), 592-606.

- Scheffers, D. J., de Wit, J. G., den Blaauwen, T., & Driessen, A. J. (2001). Substitution of a conserved aspartate allows cation-induced polymerization of FtsZ. *FEBS Lett*, 494(1-2), 34-37.
- Schindelin, H., Kisker, C., Schlessman, J. L., Howard, J. B., & Rees, D. C. (1997). Structure of ADP x AIF4(-)-stabilized nitrogenase complex and its implications for signal transduction. *Nature*, 387(6631), 370-376. doi: 10.1038/387370a0
- Schmidt, K. L., Peterson, N. D., Kustus, R. J., Wissel, M. C., Graham, B., Phillips, G. J., & Weiss, D. S. (2004). A predicted ABC transporter, FtsEX, is needed for cell division in *Escherichia coli*. *J Bacteriol*, 186(3), 785-793.
- Seefeldt, L. C., Hoffman, B. M., & Dean, D. R. (2009). Mechanism of Mo-dependent nitrogenase. *Annu Rev Biochem*, 78, 701-722. doi: 10.1146/annurev.biochem.78.070907.103812
- Shen, B., & Lutkenhaus, J. (2009). The conserved C-terminal tail of FtsZ is required for the septal localization and division inhibitory activity of MinC(C)/MinD. *Mol Microbiol*, 72(2), 410-424.
- Shen, B., & Lutkenhaus, J. (2010). Examination of the interaction between FtsZ and MinCN in *E. coli* suggests how MinC disrupts Z rings. *Mol Microbiol*, 75(5), 1285-1298. doi: 10.1111/j.1365-2958.2010.07055.x
- Shih, Y. L., Fu, X., King, G. F., Le, T., & Rothfield, L. (2002). Division site placement in *E. coli*: mutations that prevent formation of the MinE ring lead to loss of the normal midcell arrest of growth of polar MinD membrane domains. *EMBO J*, 21(13), 3347-3357. doi: 10.1093/emboj/cdf323

- Shih, Y. L., Huang, K. F., Lai, H. M., Liao, J. H., Lee, C. S., Chang, C. M., . . . Lin, C. C. (2011). The N-terminal amphipathic helix of the topological specificity factor MinE is associated with shaping membrane curvature. *PLoS One*, 6(6), e21425. doi: 10.1371/journal.pone.0021425
- Suefuji, K., Valluzzi, R., & RayChaudhuri, D. (2002). Dynamic assembly of MinD into filament bundles modulated by ATP, phospholipids, and MinE. *Proc Natl Acad Sci U S A*, 99(26), 16776-16781. doi: 10.1073/pnas.262671699
- Sun, Q., Yu, X. C., & Margolin, W. (1998). Assembly of the FtsZ ring at the central division site in the absence of the chromosome. *Mol Microbiol*, 29(2), 491-503.
- Szeto, J., Ramirez-Arcos, S., Raymond, C., Hicks, L. D., Kay, C. M., & Dillon, J. A. (2001). Gonococcal MinD affects cell division in *Neisseria gonorrhoeae* and *Escherichia coli* and exhibits a novel self-interaction. *J Bacteriol*, 183(21), 6253-6264. doi: 10.1128/jb.183.21.6253-6264.2001
- Szeto, T. H., Rowland, S. L., Habrukowich, C. L., & King, G. F. (2003). The MinD membrane targeting sequence is a transplantable lipid-binding helix. *J Biol Chem*, 278(41), 40050-40056. doi: 10.1074/jbc.M306876200
- Szeto, T. H., Rowland, S. L., & King, G. F. (2001). The dimerization function of MinC resides in a structurally autonomous C-terminal domain. *J Bacteriol*, 183(22), 6684-6687. doi: 10.1128/jb.183.22.6684-6687.2001
- Szeto, T. H., Rowland, S. L., Rothfield, L. I., & King, G. F. (2002). Membrane localization of MinD is mediated by a C-terminal motif that is conserved across eubacteria, archaea, and chloroplasts. *Proc Natl Acad Sci U S A*, 99(24), 15693-15698. doi: 10.1073/pnas.232590599

- Taschner, P. E., Huls, P. G., Pas, E., & Woldringh, C. L. (1988). Division behavior and shape changes in isogenic *ftsZ*, *ftsQ*, *ftsA*, *pbpB*, and *ftsE* cell division mutants of *Escherichia coli* during temperature shift experiments. *J Bacteriol*, *170*(4), 1533-1540.
- Terwilliger, T. C. (2000). Maximum-likelihood density modification. *Acta Crystallogr D Biol Crystallogr*, *56*(Pt 8), 965-972.
- Terwilliger, T. C. (2003). Automated main-chain model building by template matching and iterative fragment extension. *Acta Crystallogr D Biol Crystallogr*, *59*(Pt 1), 38-44.
- Terwilliger, T. C., & Berendzen, J. (1999). Automated MAD and MIR structure solution. *Acta Crystallogr D Biol Crystallogr*, *55*(Pt 4), 849-861.
- Tonthat, N. K., Arold, S. T., Pickering, B. F., Van Dyke, M. W., Liang, S., Lu, Y., . . . Schumacher, M. A. (2011). Molecular mechanism by which the nucleoid occlusion factor, SImA, keeps cytokinesis in check. *EMBO J*, *30*(1), 154-164. doi: 10.1038/emboj.2010.288
- Tostevin, F., & Howard, M. (2006). A stochastic model of Min oscillations in *Escherichia coli* and Min protein segregation during cell division. *Phys Biol*, *3*(1), 1-12. doi: 10.1088/1478-3975/3/1/001
- Touhami, A., Jericho, M., & Rutenberg, A. D. (2006). Temperature dependence of MinD oscillation in *Escherichia coli*: running hot and fast. *J Bacteriol*, *188*(21), 7661-7667. doi: 10.1128/jb.00911-06
- Tsai, Y., Sawaya, M. R., & Yeates, T. O. (2009). Analysis of lattice-translocation disorder in the layered hexagonal structure of carboxysome shell protein CsoS1C. *Acta Crystallogr D Biol Crystallogr*, *65*(Pt 9), 980-988. doi: 10.1107/s0907444909025153

- Uehara, T., Parzych, K. R., Dinh, T., & Bernhardt, T. G. (2010). Daughter cell separation is controlled by cytokinetic ring-activated cell wall hydrolysis. *EMBO J*, 29(8), 1412-1422. doi: 10.1038/emboj.2010.36
- Ursinus, A., van den Ent, F., Brechtel, S., de Pedro, M., Holtje, J. V., Lowe, J., & Vollmer, W. (2004). Murein (peptidoglycan) binding property of the essential cell division protein FtsN from *Escherichia coli*. *J Bacteriol*, 186(20), 6728-6737. doi: 10.1128/jb.186.20.6728-6737.2004
- Vagin, A., & Teplyakov, A. (2010). Molecular replacement with MOLREP. *Acta Crystallogr D Biol Crystallogr*, 66(Pt 1), 22-25. doi: 10.1107/s0907444909042589
- Vaughan, S., Wickstead, B., Gull, K., & Addinall, S. G. (2004). Molecular evolution of FtsZ protein sequences encoded within the genomes of archaea, bacteria, and eukaryota. *J Mol Evol*, 58(1), 19-29. doi: 10.1007/s00239-003-2523-5
- Wang, J., Kamtekar, S., Berman, A. J., & Steitz, T. A. (2005). Correction of X-ray intensities from single crystals containing lattice-translocation defects. *Acta Crystallogr D Biol Crystallogr*, 61(Pt 1), 67-74. doi: 10.1107/s0907444904026721
- Wang, J., Rho, S. H., Park, H. H., & Eom, S. H. (2005). Correction of X-ray intensities from an HslV-HslU co-crystal containing lattice-translocation defects. *Acta Crystallogr D Biol Crystallogr*, 61(Pt 7), 932-941. doi: 10.1107/s0907444905009546
- Wang, J. D., & Levin, P. A. (2009). Metabolism, cell growth and the bacterial cell cycle. *Nat Rev Microbiol*, 7(11), 822-827. doi: 10.1038/nrmicro2202
- Ward, J. E., Jr., & Lutkenhaus, J. (1985). Overproduction of FtsZ induces minicell formation in *E. coli*. *Cell*, 42(3), 941-949.

- Weart, R. B., Lee, A. H., Chien, A. C., Haeusser, D. P., Hill, N. S., & Levin, P. A. (2007). A metabolic sensor governing cell size in bacteria. *Cell*, *130*(2), 335-347. doi: 10.1016/j.cell.2007.05.043
- Woldringh, C. L., Mulder, E., Huls, P. G., & Vischer, N. (1991). Toporegulation of bacterial division according to the nucleoid occlusion model. *Res Microbiol*, *142*(2-3), 309-320.
- Wu, L. J., & Errington, J. (2004). Coordination of cell division and chromosome segregation by a nucleoid occlusion protein in *Bacillus subtilis*. *Cell*, *117*(7), 915-925. doi: 10.1016/j.cell.2004.06.002
- Wu, W., Park, K. T., Holyoak, T., & Lutkenhaus, J. (2011a). Determination of the structure of the MinD-ATP complex reveals the orientation of MinD on the membrane and the relative location of the binding sites for MinE and MinC. *Mol Microbiol*. doi: 10.1111/j.1365-2958.2010.07536.x
- Wu, W., Park, K. T., Holyoak, T., & Lutkenhaus, J. (2011b). Determination of the structure of the MinD-ATP complex reveals the orientation of MinD on the membrane and the relative location of the binding sites for MinE and MinC. *Mol Microbiol*, *79*(6), 1515-1528. doi: 10.1111/j.1365-2958.2010.07536.x
- Yoshikawa, H., O'Sullivan, A., & Sueoka, N. (1964). SEQUENTIAL REPLICATION OF THE BACILLUS SUBTILIS CHROMOSOME. 3. REGULATION OF INITIATION. *Proc Natl Acad Sci U S A*, *52*, 973-980.
- Zhang, Y., Rowland, S., King, G., Braswell, E., & Rothfield, L. (1998). The relationship between hetero-oligomer formation and function of the topological specificity domain of the *Escherichia coli* MinE protein. *Mol Microbiol*, *30*(2), 265-273.

- Zhao, C. R., de Boer, P. A., & Rothfield, L. I. (1995). Proper placement of the Escherichia coli division site requires two functions that are associated with different domains of the MinE protein. *Proc Natl Acad Sci U S A*, 92(10), 4313-4317.
- Zhou, H., & Lutkenhaus, J. (2003). Membrane binding by MinD involves insertion of hydrophobic residues within the C-terminal amphipathic helix into the bilayer. *J Bacteriol*, 185(15), 4326-4335.
- Zhou, H., & Lutkenhaus, J. (2004). The switch I and II regions of MinD are required for binding and activating MinC. *J Bacteriol*, 186(5), 1546-1555.
- Zhou, H., & Lutkenhaus, J. (2005). MinC mutants deficient in MinD- and DicB-mediated cell division inhibition due to loss of interaction with MinD, DicB, or a septal component. *J Bacteriol*, 187(8), 2846-2857. doi: 10.1128/jb.187.8.2846-2857.2005
- Zhou, H., Schulze, R., Cox, S., Saez, C., Hu, Z., & Lutkenhaus, J. (2005). Analysis of MinD mutations reveals residues required for MinE stimulation of the MinD ATPase and residues required for MinC interaction. *J Bacteriol*, 187(2), 629-638. doi: 10.1128/jb.187.2.629-638.2005
- Zhou, T., Radaev, S., Rosen, B. P., & Gatti, D. L. (2000). Structure of the ArsA ATPase: the catalytic subunit of a heavy metal resistance pump. *EMBO J*, 19(17), 4838-4845. doi: 10.1093/emboj/19.17.4838
- Zhou, T., Radaev, S., Rosen, B. P., & Gatti, D. L. (2001). Conformational changes in four regions of the Escherichia coli ArsA ATPase link ATP hydrolysis to ion translocation. *J Biol Chem*, 276(32), 30414-30422. doi: 10.1074/jbc.M103671200
- Zhou, T., Shen, J., Liu, Y., & Rosen, B. P. (2002). Unisite and multisite catalysis in the ArsA ATPase. *J Biol Chem*, 277(26), 23815-23820. doi: 10.1074/jbc.M203432200